



Universidade Federal de Santa Catarina  
CFM-PGQMC

Behramand

**SYNTHESES AND CHARACTERIZATION OF LUMINESCENT  
COMPOUNDS CONTAINING 2,1,3-BENZOXADIAZOLE AND  
2,1,3 BENZO THIADIAZOLE AND THIOPHENE BASED  
LUMINESCENT LIQUID CRYSTALS**

This thesis is submitted to the Post-graduation program of the Federal University of Santa Catarina in partial fulfillment of the requirements for degree of the Doctor of Philosophy in Chemistry

Area: Organic Chemistry  
Research supervisor: Prof. Dr. Hugo Gallardo

**Florianópolis / SC-Brazil  
2013**

Ficha de identificação da obra elaborada pelo autor,  
através do Programa de Geração Automática da Biblioteca Universitária da UFSC.

Behramand, Behramand

Syntheses and Characterization of Luminescent Compounds  
Containing 2,1,3-Benzoxadiazole and 2,1,3-Benzothiadiazole  
and Thiophene Based Luminescent Liquid Crystals /  
Behramand Behramand ; orientador, Hugo Gallardo -  
Florianópolis, SC, 2013.

181 p.

Tese (doutorado) - Universidade Federal de Santa  
Catarina, Centro de Ciências Físicas e Matemáticas.  
Programa de Pós-Graduação em Química.

Inclui referências

1. Química. 2. Luminescence. 3. Liquid crystals. 4.  
2,1,3-benzoxadiazole, 2,1,3-benzothiadiazole, Thiophene.  
5. Sonogashira cross coupling. I. Gallardo, Hugo . II.  
Universidade Federal de Santa Catarina. Programa de Pós-  
Graduação em Química. III. Título.

Behramand

SYNTHESES AND CHARACTERIZATION OF LUMINESCENT  
COMPOUNDS CONTAINING 2,1,3-BENZOXADIAZOLE AND 2,1,3  
BENZOTHIADIAZOLE AND THIOPHENE BASED LUMINESCENT  
LIQUID CRYSTALS

This thesis has been evaluated by the Post-graduation program of the  
**Department of Chemistry at Federal University of Santa Catarina**  
and approved for obtaining the degree of  
**Doctor of Philosophy in Chemistry**  
Florianópolis, 8<sup>th</sup> March 2013

---

Prof. Dr. Almir Spinelli  
Coordinator of the Post-graduation Program in Chemistry  
Federal University of Santa Catarina-UFSC

**Examination Committee**

---

Prof. Dr. Hugo Gallardo  
(QMC-UFSC)  
Research Supervisor

---

Prof. Dr. Maria Graça Nascimento  
(QMC-UFSC)  
Member of the defense committee

---

Prof. Dr. Antonio Luiz Braga  
(QMC-UFSC)  
Member of the defense committee

---

Prof. Dr. Ivan H. Bechtold  
(UFSC)  
Member of the defense committee

---

Prof. Dr. Rodrigo Cristiano  
(DQ-UFPB)  
Member of the defense committee

---

Prof. Dr. Aloir Merlo  
(IQ-UFRGS)  
Member of the defense committee

**Dedicated to my parents and my family**

## ACKNOWLEDGEMENTS

"In the name of God, most gracious, most compassionate"

I would like to express my greatest gratitude and sincere thanks to my research advisor and mentor Prof. Dr. Hugo Gallardo for all his supervision during this work. With my very limited research experience, he took me as his graduate student and with his integrity, patience and guidance encouraged me throughout the years. Besides providing chemicals and instruments, he has always been available and accessible all the time to provide suggestions and ideas and helps in every way to make things work.

I am very grateful to the members of the defense committee Prof. Dr. Rodrigo Cristiano, Prof. Dr. Antonio Luiz Braga, Prof. Dr. Maria Graça Nascimento, Prof. Dr. Aloir Merlo and Prof. Dr. Ivan H. Bechtold for their precious contribution in improving this thesis.

It is beyond the words to express my gratitude to my laboratory fellows Gilmar, Deisi, André, Molin, Eduard, Marli and Luciano, Japa (formally as Patrícia kkkk), Hugo, Didi, Alana, Danilo, Neto, Coelho, Paolla, Renato, Ratto and friends from the other laboratories for all kind of support and keeping a very friendly and caring environment in the laboratory which make working enjoyable. All the moments spent together whether travelling for conferences, waiting in queue of the university restaurant, social gatherings and barbecue parties with pushing to the swimming pool in Prof. house was a great fun. I wish best of luck to all in academic and scientific endeavors and hope the friendship established in Brazil will last in years to come.

I am thankful to Prof. Haidi Fiedler, Prof. Faruk Nome, Prof. Edson Minatti and Prof. Iolanda Souza for free access to the optical electrochemical equipments and to Dr. Ismael Bellettini and Jorge A. Pedro for assistance in emission experiments. I am also thankful to Professors of the Chemistry department, the technical staff of the center of analysis and to Grace and Jadir of the Post-Graduation office for their cooperations.

I am also thankful to the Conselho Nacional de Desenvolvimento Científico e Tecnológico (CNPq) and the Academy of Sciences for the Developing world (TWAS) for financial support.

I am grateful to all my friends in Brazil, in other parts of the world and my friends and relatives back in Pakistan for their care and moral support.

At last but not least, I am extremely indebted to my parents and other family members for their love, understanding, and support. It was not easy being so far away from you all, but knowing deep and down, you are very proud of me.

Behramand, Florianopolis, Brazil.  
12th Feb. 2013.

## ABSTRACT

This thesis entitled as “*Synthesis and Characterization of Luminescent Compounds Containing 2,1,3-Benzoxadiazole and 2,1,3-Benzothiadiazole and Thiophene Based Luminescent Liquid Crystals*” presents the synthesis and characterization of two series of compounds. The first series consist of  $\pi$ -conjugated luminescent compounds containing 2,1,3-benzoxadiazole and 2,1,3 benzothiadiazole as the central units to which terminal carbocycles with varying number of alkoxy chains are connected *via*  $-C \equiv C-$  bonds. Their synthesis and structural characterizations are described in **section A** along with a discussion of the results obtained from their optical and electrochemical analysis. These compounds showed an intense and bright yellowish green fluorescence with relative quantum yields ( $\Phi_f$ ) of 27 to 32 % in their  $CHCl_3$  solutions. Identity of the central heterocycle and length of the directly attached alkoxy chains showed minute influence on both the absorption and emission behavior. However, the number of terminal alkoxy chains attached to the terminal carbocycles showed a moderate effect on the absorption. The Stokes shifts were determined to be reasonably high, with values ranging from 95 to 107 nm and with only a small region of coincidence between the absorption and emission. Electrochemical measurements exhibit single oxidation and reduction peaks in anodic and cathodic sweeps respectively. The HOMO and LUMO energy levels were assessed from the voltammetric data and the calculations showed that these compounds possess small energy band gaps between 1.91 and 2.57 eV.

The second series of compounds are described in **section B**. These compounds possess bent shaped molecular structures due to the presence of thiophene at their centers. As in the previous series, these compounds are also highly conjugated and the terminal carbocycles are connected to the central thiophene *via*  $-C \equiv C-$  bonds. These compounds were designed to exhibit liquid-crystalline and luminescent properties. They showed strong blue fluorescence with satisfactory quantum yields of 26 to 56 % relative to quinine sulfate. Some of the compounds of this series showed mesomorphism. The preliminary results suggest a general pattern that increasing the length of the rigid part of the molecule increase the tendency to form a mesophase. Another general conclusion that can be drawn from these results is that an increase in the molecular length also enhances the thermal stability of

the mesophases due to increased rigidity which facilitates a better orientational order and molecular packing in the mesophases.

**Key words:** Luminescence, Liquid crystals, Sonogashira cross coupling, 2,1,3-Benzoxadiazole, 2,1,3-Benzothiadiazole, Thiophene.

## RESUMO

Esta tese é intitulada "*Syntheses and Characterization of Luminescent Compounds Containing 2,1,3-Benzoxadiazole and 2,1,3-Benzothiadiazole and Thiophene Based Luminescent Liquid Crystals*" apresenta a síntese e caracterização de duas séries de compostos. A primeira série consiste na preparação de compostos luminescentes  $\pi$  conjugados contendo os núcleos 2,1,3-benzoxadiazol e 2,1,3-benzotiadiazol como as unidades centrais aos quais os anéis aromáticos terminais, com números variáveis de cadeias alcóxi, estão ligados *via* ligações triplas ( $-C\equiv C-$ ). A síntese e caracterização estrutural é descrita na **seção A**, juntamente com a discussão dos resultados obtidos a partir das análises ópticas e eletroquímicas. Estes compostos mostraram uma fluorescência verde amarelada intensa com rendimentos quânticos relativos ( $\Phi_f$ ) de 27 a 32% em suas soluções em  $CHCl_3$ . A natureza do heterociclo e comprimento das cadeias alcóxi diretamente ligadas a este mostraram pequena influência tanto na absorção quanto na emissão. No entanto, o número de cadeias alcóxi terminais ligadas aos anéis aromáticos apresentaram um efeito moderado sobre o comportamento da absorção. Os deslocamentos de Stokes foram razoavelmente elevados, com valores entre 95-107 nm, e com apenas uma pequena região de sobreposta entre a absorção e emissão. As medidas eletroquímicas apresentaram um pico de oxidação e um de redução em ciclos anódico e catódico, respectivamente. Os níveis de energia dos orbitais HOMO e do LUMO foram avaliados a partir dados voltamétricos e os cálculos mostraram que estes compostos possuem pequenos deslocamentos de bandas de energia, entre 1,91 e 2,57 eV.

A segunda série de compostos é descrita na **seção B**. Estes compostos possuem estruturas moleculares curvadas devido à presença do tiofeno nos seus centros. Tal como na série anterior, estes compostos também possuem alta conjugação e os anéis aromáticos terminais estão ligados ao tiofeno através de ligações triplas ( $-C\equiv C-$ ). Estes compostos foram planejados para apresentar propriedades líquido-cristalinas e luminescentes. Eles mostraram forte fluorescência azul com rendimentos quânticos ( $\Phi_f$ ) satisfatórios entre 26 e 56% em relação ao sulfato de quinina. Alguns dos compostos da presente série apresentaram mesomorfismo. Os resultados preliminares, sugerem um padrão geral de que o aumento do comprimento da parte rígida da molécula aumenta a tendência de apresentar uma mesofase. Outro fato que se pode observado a partir destes resultados, é de que um aumento

no comprimento molecular também aumenta a estabilidade térmica das mesofases devido a uma maior rigidez, o que facilita uma melhor orientação e ordenamento molecular nas mesofases.

**Palavras-chave:** Luminescência, Cristais líquidos, Acoplamento cruzado de Sonogashira, 2,1,3-Benzoxadiazol, 2,1,3-Benzotiadiazol, Tiofeno.

## LIST OF FIGURES

<b>Figure 1.</b> Different electronic states in a molecule. ....	21
<b>Figure 2.</b> Perrin–Jablonski diagram illustrating various phenomena during the photons absorption and emission and relative energy positions of the absorption, fluorescence and phosphorescence. ....	22
<b>Figure 3.</b> Diagrammatic definition of the Stokes shift. ....	25
<b>Figure 4.</b> The influence of molecular flexibility and rigidity on the fluorescence quantum yields. ....	26
<b>Figure 5.</b> Possible de-excitation pathways of the photo-excited molecules. <sup>21</sup> ....	27
<b>Figure 6.</b> Energy transfer by collisional quenching. ....	28
<b>Figure 7.</b> Energy transfer by coulombic interactions. ....	28
<b>Figure 8.</b> The molecular structure of cholesteryl benzoate. ....	31
<b>Figure 9.</b> Different states of matter and the molecular ordering present in them. ....	32
<b>Figure 10.</b> Preferential molecular alignments in liquid crystals. ....	33
<b>Figure 11.</b> Cross sections of normal and reverse micelles formed by surfactants. ....	35
<b>Figure 12.</b> General template of calamitic LCs where molecular length (l) >> breadth (b). ....	37
<b>Figure 13.</b> Representation of molecular arrangements in (a) nematics phase (b) helical macrostructure of chiral nematic or cholesteric phase. ....	38
<b>Figure 14.</b> Structural representation of (a) SmA (b) SmC (c) SmB viewed from side (left) from top (right). ....	40
<b>Figure 15.</b> General template of the DLCs molecular architecture. ....	40
<b>Figure 16.</b> Aromatic cores commonly used in discotic mesogens, triphenylene (6), hexaazatriphenylene (7), trisiazolotriazine (8), porphyrine (9). ....	41
<b>Figure 17.</b> Stacking of discotics into different kinds of columnar assemblies: (a) ordered column, (b) and (c) disordered columns, (d) helical column, and (e) tilted column. <sup>80</sup> ....	41
<b>Figure 18.</b> Structural representations of the well defined columnar phases (a) columnar hexagonal Colh, (b) columnar rectangular Colr and (c) columnar oblique Colob. ....	42
<b>Figure 19.</b> Schematic representation of various discotic nematic phases <sup>11</sup> (a) discotic nematic ND (b) chiral discotic nematic ND* (c) columnar nematic NCol (d) lateral nematic phase (NL). <sup>80</sup> ....	43

<b>Figure 20.</b> Structural representation of (a) main chain and (b) branched chain or comb shaped polymeric liquid crystals.....	44
<b>Figure 21.</b> Packing of main chain polymer mesogenic groups in (a) nematic and (b) smectic A phases. <sup>93</sup> .....	44
<b>Figure 22.</b> Molecular shapes of some non conventional LCs distorted away from rod and disc shapes.....	46
<b>Figure 23.</b> Illustration of cis-trans photoisomerization and consequent mesophase change.....	47
<b>Figure 24.</b> Self assembly of non-mesogenic components into supramolecular liquid-crystal. <sup>107</sup> .....	48
<b>Figure 25.</b> Schematic representation of light induced alignment changes in LCs doped with photochromic compound and potential applications of the doped system.....	48
<b>Figure 26.</b> Molecular structures of the 2,1,3-benzothiadiazole (10), 2,1,3-benzoxadiazole (11) and thiophene (12).....	50
<b>Figure 27.</b> Representative structures of the planned luminescent compounds.....	59
<b>Figure 28.</b> Retrosynthetic analysis of the target luminescent compounds.....	60
<b>Figure 29.</b> Retrosynthetic analysis of the central heterocycles.....	64
<b>Figure 30.</b> <sup>1</sup> H-NMR spectra of compounds 34 and 13 (CDCl <sub>3</sub> , 400 MHz) as representative of the spectral changes accompanying the bromination step.....	67
<b>Figure 31.</b> Proposed mechanism of the alkyne deprotection step.....	69
<b>Figure 32.</b> <sup>1</sup> H-NMR spectra of compounds 37 and 17 (CDCl <sub>3</sub> , 400-MHz) to show the spectral changes that occurred during the deprotection step.....	70
<b>Figure 33.</b> The IR spectrum of 1,2-bis(dodecyloxy)-4-ethynylbenzene 17 (in KBr disc) with characteristic bands.....	71
<b>Figure 34.</b> <sup>1</sup> H NMR spectrum (CDCl <sub>3</sub> , 400-MHz) showing formation of the homocoupled side product 38 as the major product.....	74
<b>Figure 35.</b> <sup>1</sup> H NMR spectrum of the homocoupled side product 38 (CDCl <sub>3</sub> , 400 MHz) after purification.....	75
<b>Figure 36.</b> <sup>1</sup> H NMR spectrum of compound 20 (CDCl <sub>3</sub> , 400 MHz) with peaks assignments.....	76
<b>Figure 37.</b> <sup>13</sup> C NMR spectrum of the compound 20 (CDCl <sub>3</sub> , 100 MHz) showing the important peaks in non-aliphatic region.....	77
<b>Figure 38.</b> FT-IR spectrum (in KBr disc) of compound 23 as representative model for the final compounds 18-23.....	78

<b>Figure 39.</b> UV-vis absorption spectra of the fluorescent compounds <b>18-23</b> taken in $5 \times 10^{-6}$ molar solutions in $\text{CHCl}_3$ .	80
<b>Figure 40.</b> (a) Emission spectra of the compounds 18-23 obtained by excitation at their respective $\lambda_{\text{max}}$ and (b) Photographs showing the fluorescence in chloroform solution under UV lamp ( $\lambda = 360\text{nm}$ ).	81
<b>Figure 41.</b> Cyclic voltammograms of the final compounds <b>18-23</b> obtained in their solutions in dichloromethane at the scan rate of $50 \text{ mV.s}^{-1}$ .	83
<b>Figure 42.</b> Determining the onset potentials in cyclic voltammogram for small current changes and wavy peaks.	83
<b>Figure 43.</b> Resonance in the final compounds.	88
<b>Figure 44.</b> Representative structures of the designed luminescent liquid crystals.	90
<b>Figure 45.</b> General retrosynthetic analysis of the bent shaped luminescent compounds.	91
<b>Figure 46.</b> Molecular structures of the terminal alkynes <b>39</b> and <b>40</b> .	92
<b>Figure 47.</b> $^1\text{H-NMR}$ (400 MHz, $\text{CDCl}_3$ ) spectra of compounds <b>41</b> , <b>42</b> (aromatic region) and <b>40</b> (aromatic region) showing gradual emergence of the second order pattern during the course of $-\text{C}\equiv\text{C}-$ insertion.	94
<b>Figure 48.</b> $^1\text{H NMR}$ spectra of the mono-coupled intermediate <b>49</b> (400 MHz, $\text{CDCl}_3$ ) showing two distinct doublets around 7.16 and 6.94 ppm for the thiophenic hydrogens.	97
<b>Figure 49.</b> UV-vis absorption spectra of compounds <b>45 - 51</b> taken in $1 \times 10^{-5}$ molar solutions in $\text{CHCl}_3$ .	99
<b>Figure 50.</b> Photograph showing the fluorescence in chloroform solution under UV lamp ( $\lambda = 360\text{nm}$ ).	99
<b>Figure 51.</b> POM photographs of compound <b>47</b> on cooling (I $\rightarrow$ N) at $3^\circ\text{C}/\text{minute}$ : (a) Appearance of spherical droplets at $166.6^\circ\text{C}$ (magnification $10 \times 10$ ); (b) Schlieren texture of a nematic phase at $135.8^\circ\text{C}$ (magnification $10 \times 10$ ).	103
<b>Figure 52.</b> Differential scanning thermogram of compound <b>47</b> as a function of temperature for the second heating and cooling cycles (at scan rate $10^\circ\text{C min}^{-1}$ ).	104
<b>Figure 53.</b> POM photographs of compound <b>51</b> on second cooling (I $\rightarrow$ SmC) at $3^\circ\text{C}/\text{minute}$ : (a) batonnet texture at $92^\circ\text{C}$ (magnification $10 \times 10$ ); (b) fan shaped texture of SmC phase at $86.5^\circ\text{C}$ (magnification $10 \times 10$ ); (c) Appearance of a Schlieren texture of the SmC phase after rubbing the glass lamina at $80^\circ\text{C}$ (magnification $10 \times 10$ ).	105
<b>Figure 54.</b> Differential scanning thermogram of compound <b>51</b> as a function of temperature for the second heating and cooling cycles (at scan rate $10^\circ\text{C min}^{-1}$ ).	106

<b>Figure 55.</b> Illustration of the absorption edge for determination of the optical bandgap. ....	112
<b>Figure 56.</b> Schematic diagram of a three electrode electrochemical cell. ....	141
<b>Figure 57.</b> Schematic diagram representing the HOMO, LUMO levels and their relationship with the vacuum level (VL). ....	145
<b>Figure 58.</b> A DSC thermogram of a liquid crystalline compound showing the thermal transitions. <sup>182</sup> .....	147
<b>Figure 59.</b> Bragg diffraction by crystal plane. ....	148
<b>Figure 60.</b> Characteristic relationship between low angle diffraction patterns of more structured <b>(a)</b> 1-D layer (smectic) phases, <b>(b)</b> 2-D hexagonal phases, <b>(c)</b> 3-D cubic phases, and <b>(d)</b> of the un-aligned nematic phases. ....	150
<b>Figure 61.</b> General template for banana mesogen. ....	151
<b>Figure 62.</b> Schematic representation of <b>(a)</b> bent core molecule from different angles <b>(b)</b> Formation of polar ferroelectric, antiferroelectric and chiral phases due to directional packing of the bent core molecules in layers. <sup>194</sup> .....	151
<b>Figure 63.</b> Different ways to release macroscopic polarization of the polarized layers. ....	152

## LIST OF TABLES

<b>Table 1.</b> Photophysical data of the final compounds <b>18-23</b> .....	79
<b>Table 2.</b> Electrochemical data and molecular orbital energies of the final compounds.....	85
<b>Table 3.</b> Values of the ionization potentials, electron affinities and energy band gaps estimated form cyclic voltammetric and optical absorption methods. ....	87
<b>Table 4.</b> Photophysical data of the final compounds. ....	100
<b>Table 5.</b> Thermal behaviour of the symmetrical and asymmetrical final compounds.....	102

## LIST OF SCHEMES

<b>Scheme 1.</b> Molecular structures of the target luminescent compounds; X = S, O. ....	55
<b>Scheme 2.</b> Molecular structures of the target luminescent liquid crystals; R = C <sub>12</sub> H <sub>25</sub> . ....	56
<b>Scheme 3.</b> Route A for the synthesis of the target compounds. Reactions conditions: Pd(PPh <sub>3</sub> ) <sub>2</sub> Cl <sub>2</sub> , PPh <sub>3</sub> , CuI, Et <sub>3</sub> N, 80-85 °C, 12-14h. ....	62
<b>Scheme 4.</b> Route B for the synthesis of the target compounds. Reactions conditions: Pd(PPh <sub>3</sub> ) <sub>2</sub> Cl <sub>2</sub> , PPh <sub>3</sub> , CuI, Et <sub>3</sub> N, 80-85 °C, 12-14h. ....	63
<b>Scheme 5.</b> Detailed synthetic route to the central cores 13-15.....	65
<b>Scheme 6.</b> Synthetic route to the terminal alkyne 16. ....	68
<b>Scheme 7.</b> Synthetic route to 3,4-didodecyloxyphenylacetylene <b>17</b> . ...	69
<b>Scheme 8.</b> Mechanistic depiction of the alkyne homocoupling during catalyst activation. ....	72
<b>Scheme 9.</b> Summary of the final Sonogashira coupling reactions leading to the target compounds.....	73
<b>Scheme 10.</b> Synthesis of the 2,5-diiodothiophene. ....	94
<b>Scheme 11.</b> Syntheses of the bent shaped symmetrical compounds. Conditions: Pd(PPh <sub>3</sub> ) <sub>2</sub> Cl <sub>2</sub> , PPh <sub>3</sub> , CuI, Et <sub>3</sub> N, 80-85 °C, 12-14h.....	95
<b>Scheme 12.</b> Syntheses of the bent shaped asymmetrical compounds. Conditions: Pd(PPh <sub>3</sub> ) <sub>2</sub> Cl <sub>2</sub> , PPh <sub>3</sub> , CuI, Et <sub>3</sub> N, 80-85 °C, 12-14h.....	96

## LIST OF ABBREVIATIONS

CMC	Critical micelle concentration
Col <sub>hd</sub>	Columnar hexagonal disordered
Col <sub>ho</sub>	Columnar hexagonal ordered
Col <sub>ob</sub>	Columnar oblique
Col <sub>r</sub>	Columnar rectangular
Cr	Crystalline phase
CRTs	Cathode ray tubes
CV	Cyclic voltammetry
DLCs	Discotic liquid crystals
DMF	Dimethylformamide
DSC	Differential scanning calorimetry
EA	Electron affinity
E <sub>g</sub>	Bandgap energy
Et <sub>4</sub> NClO <sub>4</sub>	Tetraethylammonium perchlorate
Fc	Ferrocene
FONs	Fluorescent organic nanoparticles
HOMO	Highest occupied molecular orbital
IC	Internal conversion
IL	Isotropic liquid
IP	Ionization potential
ISC	Intersystem crossing
LCDs	Liquid crystals displays
LCs	Liquid crystals
LLCs	Lyotropic liquid crystals
LUMO	Lowest unoccupied molecular orbital
MS	Mass spectrometry
N	Nematic mesophase
N*	Chiral nematic (Cholesteric) mesophase
NBS	<i>N</i> -Bromosuccinimide
<i>n</i>	Director
N <sub>Col</sub>	Columnar nematic mesophase
N <sub>D</sub>	Discotic nematic mesophase
N <sub>D</sub> *	Chiral nematic discotic mesophase
OLEDs	Organic light emitting diodes
POM	Polarizing optical microscopy
PTC	Phase transfer catalyst
SCE	saturated calomel electrode
SHE	Standard hydrogen electrode

Sm	Smectic mesophase
SmA	Smectic A mesophase
SmC	Smectic C mesophase
TBAF <sub>4</sub>	Tetrabutylammonium tetrafluoroborate
TBAPF <sub>6</sub>	Tetra-n-butylammonium hexafluorophosphate
TCLCs	Thermotropic calamitic liquid crystals
TDLCs	Thermotropic discotic liquid crystals
TGA	Thermogravimetric analysis
TLCs	Thermotropic liquid crystals
TPLCs	Thermotropic polymeric liquid crystals
UV	Ultraviolet
VL	Vacuum level
VR	Vibrational relaxation
XRD	X-Ray diffraction
$\Phi_f$	Fluorescence quantum yield

## TABLE OF CONTENTS

<b>1. INTRODUCTION .....</b>	<b>19</b>
1.1. LUMINESCENCE .....	20
1.2. GENERAL TERMS IN LUMINESCENCE .....	20
1.3. MECHANISM OF LUMINESCENCE .....	21
1.4. THE STOKES SHIFT .....	24
1.5. QUANTUM YIELD .....	25
1.5.1. Factors that Affect Quantum Yield .....	26
1.6. LIQUID CRYSTALS .....	29
1.7. HISTORY OF LIQUID CRYSTALS .....	30
1.8. DESCRIPTION OF THE LIQUID CRYSTALLINE STATE .....	31
1.9. CLASSES OF THE LIQUID CRYSTALS .....	33
1.9.1. Thermotropic Liquid Crystals .....	33
1.9.2. Lyotropic Liquid Crystals .....	34
1.9.3. Amphotropic or Amphitropic Liquid Crystals .....	36
1.10. MOLECULAR STRUCTURES AND MESOPHASES OF THERMOTROPIC LIQUID CRYSTALS .....	36
1.10.1. Thermotropic Calamitic Liquid Crystals .....	37
1.10.1.1. Nematic Mesophase .....	37
1.10.1.2. Cholesteric Mesophase .....	38
1.10.1.3. Smectic Mesophases .....	39
1.10.2. Thermotropic Discotic Liquid Crystals .....	40
1.10.2.1. Columnar Mesophases of Discotic Liquid Crystals .....	42
1.10.2.2. Nematic Mesophases Of Discotic Liquid Crystals .....	43
1.10.3. Thermotropic Polymeric Liquid Crystals .....	43
1.10.4. Non Conventional Liquid Crystals .....	45
1.11. FUNCTIONALIZATION OF THE LIQUID CRYSTALS .....	46
1.12. A BRIEF REVIEW OF THE 2,1,3-BENZOTHIADIAZOLE .....	49
1.13. A BRIEF REVIEW OF THE 2,1,3-BENZOXADIAZOLE .....	49
1.14. A BRIEF LITERATURE REVIEW OF THE THIOPHENE .....	50
<b>2. OBJECTIVES .....</b>	<b>53</b>
<b>3. RESULTS AND DISCUSSION.....</b>	<b>57</b>
3.1. SYNTHESSES AND CHARACTERIZATION OF LUMINESCENT COMPOUNDS CONTAINING 2,1,3-BENZOXADIAZOLE AND 2,1,3 BENZOTHIADIAZOLE AND THEIR OPTICAL AND ELECTROCHEMICAL PROPERTIES .....	58
3.2. MOLECULAR DESIGN .....	59
3.3. RETROSYNTHETIC ANALYSIS .....	59
3.4. SYNTHETIC PLAN .....	60
3.4.1. Syntheses and Characterizations of The Central Cores .....	64
3.4.2. Synthesis of The Terminal Acetylenes .....	67
3.4.3. Synthesis of The Final Compounds .....	71

3.5. OPTICAL PROPERTIES .....	78
3.6. ELECTROCHEMICAL PROPERTIES .....	82
3.7. THE $E_g$ , IP AND EA FROM OPTICAL ABSORPTIONS .....	85
3.8. SYNTHESSES AND CHARACTERIZATION OF THIOPHENE BASED LUMINESCENT LIQUID CRYSTALS.....	89
3.9. MOLECULAR DESIGN OF THE TARGET COMPOUNDS .....	90
3.10. SYNTHETIC PLAN.....	91
3.10.1. Synthesis of The Terminal Alkynes .....	92
3.10.2. Synthesis and Characterization of The Final Compounds .....	94
3.11. OPTICAL PROPERTIES .....	98
3.12. MESOMORPHIC AND THERMAL PROPERTIES .....	100
<b>4. CONCLUSIONS .....</b>	<b>107</b>
<b>5. EXPERIMENTAL DETAILS .....</b>	<b>109</b>
5.1. GENERAL MATERIALS .....	110
5.2. INSTRUMENTATION AND METHODS.....	110
5.2.1. Structural Characterizations .....	110
5.2.2. Optical Analyses.....	110
5.2.3. Determination of The Optical Bandgaps .....	111
5.2.4. Cyclic Voltammetric Analysis.....	112
5.2.5. Thermal Analysis.....	113
5.3. EXPERIMENTAL PROCEDURES AND SPECTRAL DATA OF THE SYNTHESIZED COMPOUNDS.....	113
<b>6. APPENDIX.....</b>	<b>139</b>
<b>7. BIBLIOGRAPHY .....</b>	<b>153</b>
<b>8. PUBLISHED PAPER .....</b>	<b>173</b>

## **1. INTRODUCTION**

## 1.1. LUMINESCENCE

Luminescence is the radiative emission of ultraviolet, visible or infrared photons from an electronically excited species to return to its ground state. In the ground state, the bonding electrons occupy the highest occupied molecular orbital (HOMO). When sufficient energy is provided to a molecule, its electrons can overcome the energy barrier required to move from their ground state (HOMO) to a higher energy level (LUMO). The excited molecule may be organic, inorganic or organometallic in nature. These excited molecules can partially lose the energy radiatively (emit light radiations) when electrons go from the excited state back to the ground state and this phenomenon of light emission is called luminescence.

Molecules that exhibit luminescence are very important in modern day technology and find important uses in diverse fields like organic light-emitting diodes (OLEDs) for electroluminescent devices and flat panel display technology,<sup>1,2</sup> fluorescent organic nanoparticles (FONs),<sup>3</sup> as solid state light sources for sign boards and light appliances, fluorescent probes in medical science for locating tumor cells,<sup>4</sup> photoconductors for solar cells<sup>5</sup> and chemical sensors.<sup>6</sup>

## 1.2. GENERAL TERMS IN LUMINESCENCE

Although there are various methods of inducing excitation and subsequent emission, e.g. thermoluminescence, excitation by thermal heating, chemiluminescence, based on the production of electromagnetic radiation observed when a chemical reaction yields an electronically excited product, bioluminescence (by biochemical process),<sup>7</sup> sonoluminescence, (by ultrasounds), electroluminescence, (by electric field), solvoluminescence,<sup>8</sup> and mechanoluminescence<sup>9</sup> etc, the present discussion is related to photoluminescence in which a species is excited by absorption of photon and subsequently the excited species loses part of the absorbed energy radiatively resulting in luminescence. The photoluminescence is further classified into *fluorescence* or *phosphorescence* depending on whether the excited species responsible for emission is in the singlet or triplet state (**Fig. 1**).

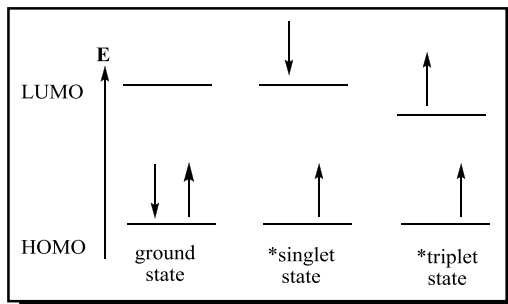


**Figure 1.** Different electronic states in a molecule.

Organic molecules contain an even number of electrons and have a singlet ground state with a net spin of zero. The ground singlet state is usually labeled as  $S_0$  and the first, second and higher electronic excited singlet states are represented by  $S_1$ ,  $S_2$  and  $S_n$  respectively, with  $n = 3, 4, 5$  and so on. A molecule exhibits a singlet state when there is no net electronic spin associated with the state i.e. all of the spins are paired. The spin multiplicity formula ( $M = 2S + 1$ ) gives the number of the states *which* can arise, where the 'S' is the total spin quantum number. In the case when all the electrons of a molecule are spin-paired,  $S = 0$ , the spin multiplicity is 1, which represents the singlet state. In contrast, the excited states in which the two electron spins are parallel have an overall spin momentum ( $S = 1$ ) and the spin multiplicity = 3. Having unpaired electrons, they exhibit magnetic properties and, in a magnetic field, split into three sub-states of slightly different energies. These states are therefore referred as "triplet" states" and are labelled as  $T_1$ ,  $T_2$ , and so on, where 'T' indicates that there are three possibilities of spin orientation of the two unpaired electrons.<sup>10</sup>

### 1.3. MECHANISM OF LUMINESCENCE

The various excitation and relaxation processes involved in photoluminescence are illustrated in the Jablonski diagram presented in **fig. 2**. Diagrams of this type were introduced by A. Jablonski (1935) on the mechanism of phosphorescence. The straight arrows represent various possible radiative transitions, whereas the wavy arrows show the non-radiative transitions between electronic or vibrational states. When the molecule is excited, one of the paired electrons moves up to an

orbital of higher energy. Its spin may still be paired with that of the electron left behind and so a whole series of excited states exists in which the total electron spin is still zero. Energy of the absorbed photons determine which excited state the electrons reach and transitions such as  $S_0 \rightarrow S_1$ ,  $S_0 \rightarrow S_2$ ,  $S_0 \rightarrow S_3$ , etc can be achieved by the absorption of photons of specific energies. Within each energy level, there are several closely spaced vibrational states and excited electrons will undergo vibrational relaxation (VR) to the lowest vibrational level within the same electronic state. If the molecule is excited to the singlet excited state higher than  $S_1$ , ( $S_0 \rightarrow S_2, S_3$  etc), it rapidly relaxes to the lower level  $S_1$  via internal conversion (IC) – a rapid non-radiative transition between two electronic states of the same spin multiplicity. In most organic molecules, internal conversion from the higher excited states to the lowest or first excited singlet state ( $S_n \rightarrow S_1$ ) occurs much more rapidly ( $10^{-12}$  s or less)<sup>11</sup> than the decay from the lowest excited state to the ground state ( $S_1 \rightarrow S_0$ ). The measured fluorescence thus occurs mainly from the lowest excited state ( $S_1 \rightarrow S_0$ ) with typical lifetime of  $10^{-10}$  to  $10^{-7}$  s, even if the molecule is initially excited to a higher state. This generalization is often called Kasha's rule after Michael Kasha, who first formalized it.<sup>12</sup>

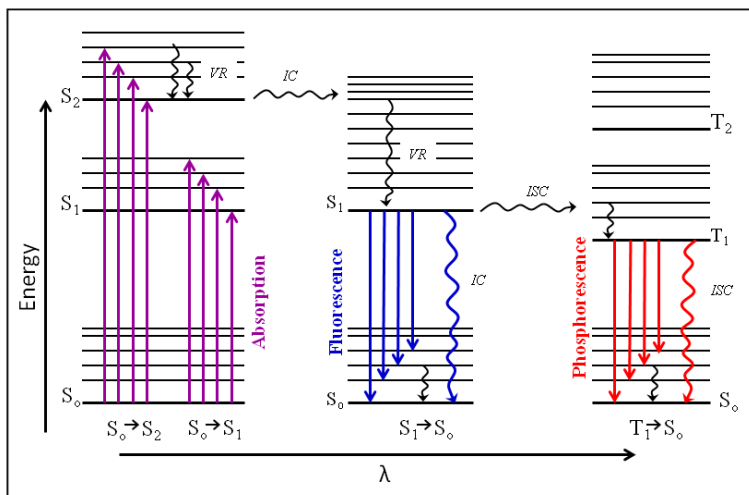


**Figure 2.** Perrin–Jablonski diagram illustrating various phenomena during the photons absorption and emission and relative energy positions of the absorption, fluorescence and phosphorescence.

Direct transitions from the ground singlet state to the excited triplet states ( $S_0 \rightarrow T_1$ ,  $S_0 \rightarrow T_2$  etc) cannot occur because they violate one of the laws of quantum mechanics: the "selection rule" which states that the spin of the electron cannot be changed during the transitions associated with the absorption or emission of radiation. In the excited state, however, the two electrons occupying separate orbitals are no longer restricted by the Pauli principle, and consequently, molecules can adopt the triplet states (the *Hund's rule*) by intersystem crossing or in some cases by other processes such as chemical reactions. Intersystem crossing (ISC) is a non-radiative transition between two isoenergetic vibrational levels belonging to electronic states of different multiplicities. Crossing between states of different multiplicity is in principle forbidden, but coupling between the orbital magnetic moment and the spin magnetic moment (i.e. spin-orbit coupling)<sup>13</sup> can be large enough to make it possible. Intersystem crossing often occurs with a rate constant on the order of  $10^6 - 10^8 \text{ s}^{-1}$  and its probability depends on the singlet and triplet states involved. If the transition  $S_0 \rightarrow S_1$  is of  $n \rightarrow p$  type for instance, intersystem crossing ( $S_1 \rightarrow T_1$ ) is often efficient. Also the presence of heavy atoms (i.e. whose atomic number is large, for example Br, I, Pb) increases spin-orbit coupling and thus favors intersystem crossing. Typical lifetimes of excited triplet states range from  $10^{-6}$  s to more than 1 s.<sup>14</sup>

After ISC, the molecule at the higher vibrational energy levels of  $T_1$  state can release the excess energy via vibrational relaxation (VR) to the lowest vibrational energy level of  $T_1$  state. Subsequently, the triplet can then emit light (phosphorescence) as it decays back to the singlet ground state. In principle, electronic transition from the triplet states to the ground singlet state ( $T_1 \rightarrow S_0$ ) is "forbidden". In practice, the selection rule is not so rigorous and there is a small probability that such a forbidden transition can still occur. Thus, after an intersystem crossing from  $S_1$  to  $T_1$ , the latter, if not deactivated by some other processes, can eventually return to the singlet ground state  $S_0$  with the emission of a photon. It is this principle that accounts for the long lifetime of the triplet state and the associated phosphorescence emission. The rate constants for phosphorescence are several orders of magnitude smaller ( $10^6 - 10^0 \text{ s}^{-1}$ ) than those for fluorescence due to the fact that the transition from  $T_1$  to  $S_0$  is spin-forbidden.<sup>11</sup> The lifetime for phosphorescence is above  $10^{-4}$  second and the emission length varies greatly,<sup>15</sup> e.g. for aromatic hydrocarbons, the radiative lifetime for

phosphorescence is typically on the order of 30 s. In contrast, the fluorescence emission occurs very quickly ( $10^{-8}$  s) after it reaches its excited state,<sup>16</sup> because it does not involve any spin change and goes back to the ground state immediately after its excitation.

Due to its forbidden nature, phosphorescence is quite rare in organic materials. Nevertheless, it is commonly observed in metal complexes due to spin-orbit coupling.<sup>17</sup> Phosphorescence is, however, not the only fate of a molecule in the triplet state. In the presence of quenchers such as  $O_2$  or  $Br_2$ , intersystem crossing (ISC) from the triplet state to the ground state ( $T_1 \rightarrow S_0$ ) may compete with the phosphorescence. Also, reverse intersystem crossing  $T_1 \rightarrow S_1$  can occur when the energy difference between  $S_1$  and  $T_1$  is small and when the life time of  $T_1$  is long enough. This results in delayed fluorescence with the same spectral distribution as normal fluorescence but with a much longer decay time because the molecules stay in the triplet state before emitting from  $S_1$ . Delayed fluorescence is thermally activated and consequently, its efficiency increases with increasing temperature. Delayed fluorescence is very efficient in fullerenes.<sup>18</sup>

#### 1.4. THE STOKES SHIFT

Since the luminescence occurs from the lowest excited states ( $S_1$  and  $T_1$ ) and the excited molecule loses some energy through the processes of vibrational relaxation (VR) and internal conversion (IC) etc, the re-emitted light has lower energy than that absorbed, hence the emission wavelength is always longer than the excitation wavelength as shown in **fig. 3**. This red shift of the emission relative to the absorption i.e. difference between the positions of the band maxima in absorption and emission spectra, is called the Stokes shift after George Stokes, a British mathematician and physicist who, in 1852, discovered that the mineral fluor spar emits visible light when it is illuminated with UV light. Stokes also described the red shift of the fluorescence of quinine, coined the term “fluorescence,” and was the first to observe that a solution of hemoglobin changes from blue to red when the protein binds  $O_2$ .<sup>14</sup> As  $T_1$  is often lower in energy than  $S_1$ , phosphorescence generally occurs at lower frequency relative to fluorescence resulting in Stokes shift greater than in the case of fluorescence.<sup>11</sup>

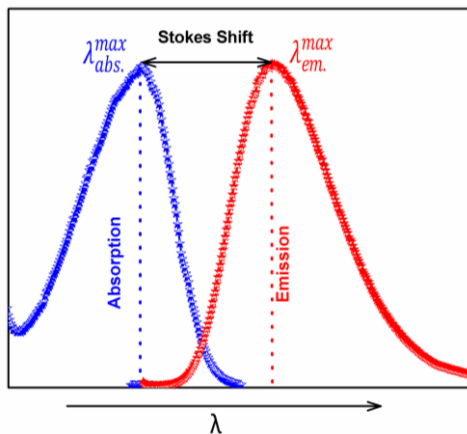


**Figure 3.** Diagrammatic definition of the Stokes shift.

### 1.5. QUANTUM YIELD

The efficiency of a fluorescence emission process is measured as the quantum yield ( $\Phi_f$ ), which is defined as the ratio of the number of photons emitted to the number of photons absorbed. In other words, the quantum yield gives the probability of the excited state being deactivated by fluorescence rather than by another, non-radiative mechanism. Ideally, a perfectly efficient molecule will emit all the absorbed photons and have a quantum yield of 1. However, besides the radiative relaxation, the excited molecules do lose part of the absorbed energy through the non-radiative decay processes such as VR, IC and conformational changes. Typically, the non-radiative processes depend on several factors such as the nature of the molecular structure in particular its molecular flexibility and rigidity, and the energy gap ( $\Delta E$ ) between the excited ( $S_1$  or  $T_1$ ) and the ground state  $S_0$ . In general, molecules with high degree of flexibility tend to have decreased fluorescence due to greater conformational and collisional probability. In other words, the more rigid a molecule, the greater is the quantum yield. For example,  $\Phi_f$  of the trans- (compound 1) and cis (compound 3) stilbenes are 0.05 and 0.00 respectively. However,  $\Phi_f$  of the structurally more rigid derivatives (compounds 2 and 4) are almost 1.00 (**Fig. 4**).<sup>19</sup>

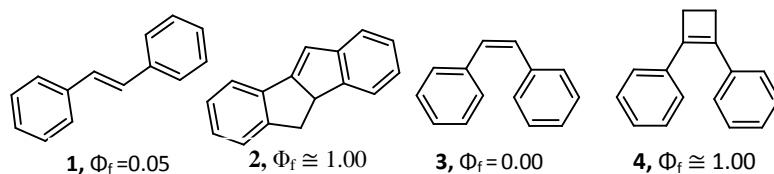


**Figure 4.** The influence of molecular flexibility and rigidity on the fluorescence quantum yields.

In principle, the non-radiative overlap (IC, ISC) between two spin states is inversely proportional to the  $\Delta E$  between the two states; the smaller the  $\Delta E$ , the greater the overlap, consequently, the faster the transitions (i.e. non-radiative decay) between the two states. For organic molecule, if  $\Delta E$  is less than 209 kJ/mol, the non-radiative process becomes the dominant process leading to a lower fluorescence quantum yield ( $\Phi_f$ ).<sup>19</sup> This is also the reason that the triplet states in aromatic hydrocarbons decay very efficiently because the  $T_1$  state is often lower in energy than the  $S_1$  state.<sup>20</sup>

### 1.5.1. Factors that Affect Quantum Yield

Besides the intramolecular processes, interaction of the excited species with other molecules such as electron transfer, proton transfer, excimer or exciplex formation etc, may compete with radiative de-excitation. Some of these processes are shown in **figure 5**. Subsequently, the efficiency of fluorescence and phosphorescence is reduced.

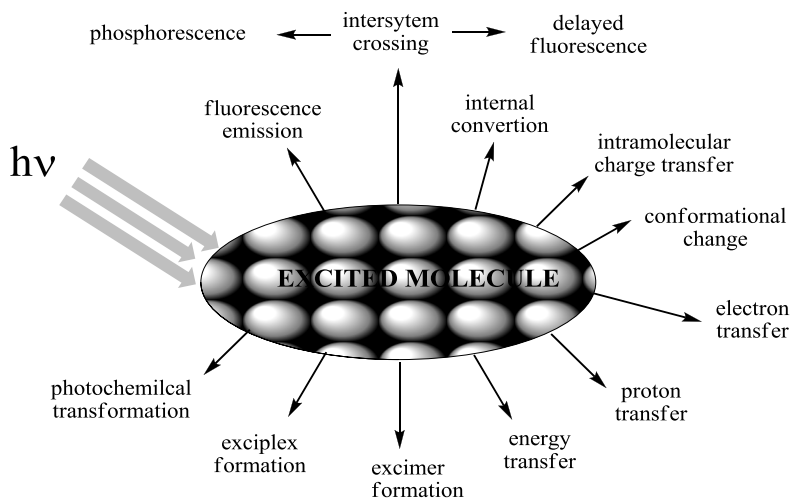
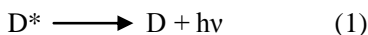


**Figure 5.** Possible de-excitation pathways of the photo-excited molecules.<sup>21</sup>

In the presence of external quenchers (e.g. oxygen and halides), the excitation energy in a molecule can be lost through energy transfer and electron transfer processes. There are many mechanisms to describe the quenching processes, but in general, they can be categorised into three mechanisms, (i) ‘trivial’, (ii) collisional quenching, and (iii) Coulombic interaction. ‘Trivial’ is when the donor (D) emits fluorescence and the acceptor (A) absorbs the fluorescence (**Schemes 1 and 2**).<sup>22</sup> The A does not influence the emission ability of D, but it reduces the amount of observed photons emitted from D, as a result the recorded  $\Phi_f$  will be less than the real one.



In the second quenching mechanism, the collisional quenching, the excitation energy of  $D^*$  is lost when it comes into physical contact with A in solution. This mechanism is shown in **scheme 3** and **figure 6**.<sup>19</sup> In this mechanism, the electron in the lowest unoccupied molecular orbital (LUMO) of  $D^*$  ‘jumps’ to the LUMO of the ground state A, and at the same time, an electron in the highest occupied molecular orbital

(HOMO) in A ‘jumps’ to the HOMO of D\*. As a result, the excited state of D is quenched.

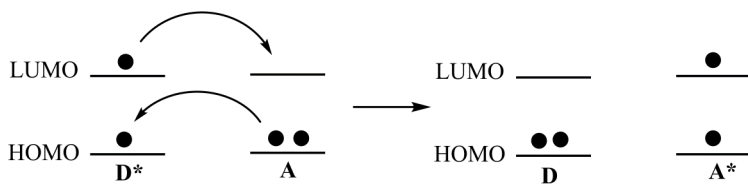
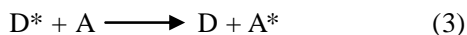


**Figure 6.** Energy transfer by collisional quenching.

The third quenching mechanism is Coulombic interaction or dipole-dipole interaction between D and A. The principle of this quenching is depicted in **Figure 7**.<sup>19</sup> The major distinction between the collisional quenching and the coulombic interaction is that in the latter, physical contact is not necessary. Förster proposed<sup>23</sup> that the magnitude of the coulombic interaction is dependent on the magnitude of the dipoles ( $D \mu$  and  $A \mu$ ) and the distance between them. According to him, a significant interaction can be caused by the large dipole moments of D and A ( $D \mu$ ,  $A \mu$ ) and the small separation between them. Interaction between an excited molecule and a solvent molecule in a polar solvent is a typical quenching example via coulombic interaction. Due to the strong dipole moment interactions, the excitation energy can be lost from the excited molecules to solvent molecules thereby reducing the  $\Phi_f$  in polar solvents compared to non-polar solvents.

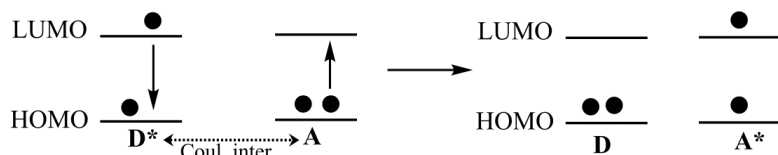


**Figure 7.** Energy transfer by coulombic interactions.

The quantum yield is one of the most difficult quantities to be determined accurately.<sup>21,24</sup> This is because its value measured for a solution varies depending on the experimental conditions including the kind of solvent, the concentrations of the sample, dissolved oxygen in the solution, temperature and the excitation wavelength.

## 1.6. LIQUID CRYSTALS

Liquid crystals (LCs) represent phases of matter with the molecular order intermediate between a fully ordered crystalline solid and an isotropic liquid. This phase has the property to flow like liquids and retains varying degrees of arrangement of molecules like crystals. They occupy a key position in our modern world and have many technological, scientific, artistic and medical applications. This is because they can be functionalized in a variety of ways and they consume a barely perceptible amount of energy when they change their state under external influences such as temperature, electric field, mechanical stress or whatever. The most familiar and prominent commercial application of LCs is their use in display technology.<sup>25</sup> We see them in our digital watches, computer displays, laptops, TV screens, telephones and calculators, polarized light emitting displays, car dashboards, photo-cameras, etc. Liquid crystals displays (LCDs) are superior over the cathode ray tubes (CRTs) used in the recent past and they have dominated the displays market especially in portable instruments due to a combination of physical properties e.g. low power consumption, low operating voltage, light-weight, slim shape and reduced size for the same screen dimensions.<sup>26</sup> Apart from their applications in the area of displays which depend on their electro-optical properties, their thermo-optical properties (thermochromic effect) are exploited in a number of temperature sensors. These include liquid crystal thermometer for medical use to read body temperature by placing against the forehead, mood rings, hot warning indicators, monitoring devices for the packaging of chilled food and colour changing jewellery. In scientific laboratories, they are used in chromatography where they create an anisotropic medium that promotes the separation of close-boiling isomers which are very difficult or impossible to separate on classical stationary phases.<sup>27</sup> Being anisotropic fluids, LCs can be used as organized reaction media.<sup>28</sup> Because of the orientation of the reactants dissolved in the liquid crystal, the

regioselectivity and chemoselectivity of organic reactions in liquid crystalline solvents differ from those observed in conventional organic solvents.<sup>29,30</sup> They are used as anisotropic solvents for certain spectroscopic applications. For example, anisotropic chemical shifts<sup>31</sup> and enantiomeric excess<sup>32</sup> can be measured from NMR spectra taken in liquid crystals as solvents. Other applications of liquid crystals include their use in light modulators and gates for photonics, liquid crystal lasers, skin-care cosmetic products, soaps and detergents, as charge transport materials,<sup>33</sup> as intelligent lubricants,<sup>34</sup> artificial muscle, chemical sensors,<sup>35</sup> optical data storage<sup>36</sup> and drug delivery systems etc.

### 1.7. History of liquid crystals

In 1888, an Austrian botanical physiologist Friedrich Reinitzer observed that cholesteryl benzoate and some other cholesterol derivatives show a strange thermal behaviour, i.e. possessing double melting points. He observed that the solid cholesteryl benzoate (**5**) changed into a turbid viscous fluid on first melting at 145.5°C, which on second melting at 178.5°C, turned in to a clear and transparent liquid. Moreover, he also observed the appearance of a blue glow just before the turbid liquid transformed into the clear form. Surprised and curious by these observations, he sent these samples to Otto Lehmann, a polarizing microscopy expert who had developed a polarization microscope with a heating stage. Investigating the samples of Reinitzer under his microscope and passing polarized light through the strange cloudy fluid, Lehmann noticed birefringence, a phenomenon associated with crystals. He also observed the same phenomenon in other substances that pass through such intermediate cloudy liquids and understood that he was dealing with a new state of matter, which at first, he gave the name *fliessende Kristalle* (flowing crystals).<sup>37</sup> Later he thought that the term *flüssige Kristalle* (liquid crystals) corresponds better to the essence of mesophases and used it as a title of the very first book on liquid crystals.<sup>38</sup>

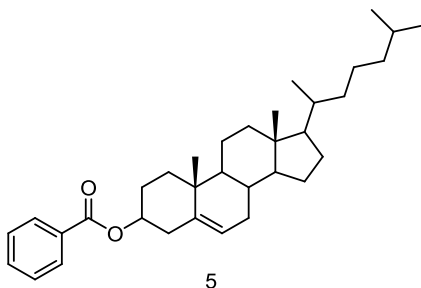


**Figure 8.** The molecular structure of cholesteryl benzoate.

Lehmann's idea of considering the birefringent fluid, which he called liquid crystals, as a novel state of matter was not accepted by majority of the scientists<sup>39</sup> who considered it to be colloidal suspension<sup>40</sup> or mixture of tautomers.<sup>41</sup> However, the systematic work of George Friedel continued to steadily provide a growing body of evidence supporting the view that liquid crystals do represent a true state of matter. In 1922, the famous publication<sup>42</sup> by George Friedel proved to be a real seal of universal acceptance of liquid crystals as a distinct phase of matter. Friedel studied the orientations of liquid crystals in the presence of electric field and introduced a classification scheme for liquid crystals on the basis of differences in molecular ordering.

Today liquid crystals are known to represent the fourth state of matter, structurally (molecular arrangement) and thermodynamically located between the highly ordered crystalline solid and the disordered liquid states. Being at the mesophase, liquid crystals partially exhibit properties of both the crystalline solids e.g. optical anisotropy, as well as the liquids e.g. fluidity. In other words, liquid crystals are anisotropic liquids with a certain long-range order in their molecular arrangement and represent a partially ordered and delicate phase of the matter.<sup>43</sup>

## 1.8. DESCRIPTION OF THE LIQUID CRYSTALLINE STATE

In crystalline solids, the molecules (in molecular crystals) are highly organized occupying fixed positions and having defined relative orientations, i.e. the molecules possess both positional and orientational order. The intermolecular forces responsible for holding the molecules into their fixed positions in a crystal need not be the same in all directions especially if the molecules are geometrically anisotropic as in

the cases of mesogenic compounds i.e. compounds structurally suitable to give mesophases.<sup>44</sup> In such cases, the transition from crystalline phase to the isotropic liquid and vice versa is not direct and single stepped but occurs via one or more intermediate steps. Upon heating a mesogenic compound, the molecules vibrate and overcome the weaker organizing forces first but they still remain bound by the stronger forces and lose some or all of their positional order while still maintaining some orientational order. This non crystalline and anisotropic liquid phase of the matter with partial long range orientational order qualifies to what is called the liquid crystal phase or the mesophase (**Fig. 9**).

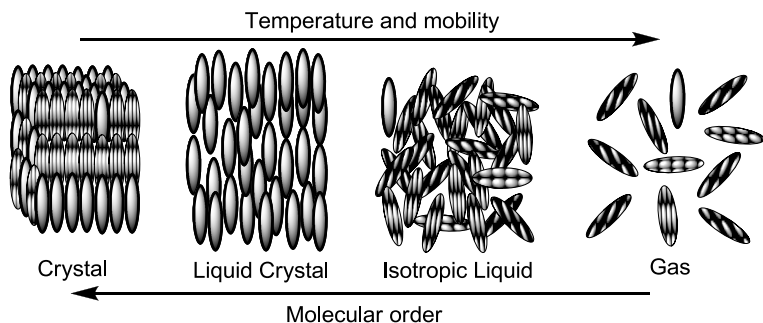


**Figure 9.** Different states of matter and the molecular ordering present in them.

Shapes of the individual molecules and incompatibility of the molecular segments are the two key factors that drive organization in the liquid crystal phases. Molecular axes of the individual molecules in liquid crystals remain relatively aligned and parallel to each other leading to a preferred direction in space known as *director* denoted by  $n$ . In some cases, the molecules tend to further associate in layers. The physical properties of the bulk system vary with the average alignment of the director (**Fig. 10**). Large alignment tends towards anisotropic materials while small alignment means loss of the orientational orders and tends towards the isotropic materials.

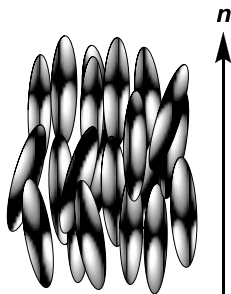


**Figure 10.** Preferential molecular alignments in liquid crystals.

## 1.9. CLASSES OF THE LIQUID CRYSTALS

In liquid crystals, transitions to the mesophases may be brought about by purely thermal processes or by the influence of the solvents. Based on the physical parameters that control the entrance of mesogenic compounds into mesophase, there are three distinct classes of liquid crystals i.e. thermotropic LCs, lyotropic LCs and amphotropic or amphitropic LCs.<sup>45</sup>

### 1.9.1. Thermotropic Liquid Crystals

In thermotropic liquid crystals (TLCs) or “thermotropics”, transitions to the liquid crystalline states are induced by thermal triggering of the mesogenic compound. The mesophase can be obtained by either cooling an isotropic liquid below the clearing point or by heating the solid mesogenic compound above its melting point, i.e. one can arrive at the liquid crystalline state by raising the temperature of a solid and/or lowering the temperature of a liquid. At much higher temperature, the thermal motions destroy ordering of the mesophase and transform the material into a conventional isotropic liquid phase. At lower temperatures, most liquid crystal materials form a conventional crystal.

The thermotropic liquid crystal may be monotropic, where a particular mesophase can be achieved only from one direction (irreversible process) in the thermal cycle usually upon cooling,<sup>46</sup> or enantiotropic, where a certain mesophase can be achieved either by heating or cooling (reversible cycles) of the mesogen. Depending on the

kind of bonding interactions, the mesogenic compound may be ionic,<sup>47,48</sup> metallomesogenic<sup>49-51</sup> or supramolecular<sup>52,53</sup> in nature. Many thermotropic liquid crystals are polymorphic (shows polymorphism) and exhibit a variety of different mesophases as a function of temperature. In these cases a mesophase is obtained by heating or cooling from a different adjacent mesophase.<sup>54</sup>

### 1.9.2. Lyotropic Liquid Crystals

Lyotropic liquid crystals (LLCs) are formed as a result of solvent-induced aggregation of the constituent mesogens into micellar structures. Contrary to the thermotropic liquid crystals which are pure compounds, lyotropic liquid crystals are always mixtures of at least two components and are obtained when an appropriate amount of a suitable material is dissolved in some non mesogenic solvent, usually water. The aqueous media can be replaced by other solvents, such as organic solvents,<sup>55,56</sup> inorganic salts<sup>57</sup> or ionic liquids,<sup>47,58</sup> however, the best known solvent to date in the assembly process is water. The other component of such a system is usually an amphiphilic compound. The amphiphilic compounds, e.g. soaps, detergents and lipids, possess a polar or ionic hydrophilic part (the head group) that interacts strongly with water and a non polar hydrophobic part (the tail) that is water insoluble. When these partially water miscible surfactants are dissolved in very low concentration, the molecules are distributed randomly throughout the water without any order. However, upon increasing the concentration above a well defined limit known as the *critical micelle concentration* (CMC), they form aggregates termed as *micelles*. The micelle formed may be normal or inverse. The normal micelle refers to “oil in water” morphology with hydrophobic part (the tail) inside the micelle core and hydrophilic part (head group) exposed to the aqueous medium. Inverse micelles are formed in non polar solvents and refer to “water in oil” morphology having its head groups at the centre and the tails extending out towards the solvent (**Fig. 11**).

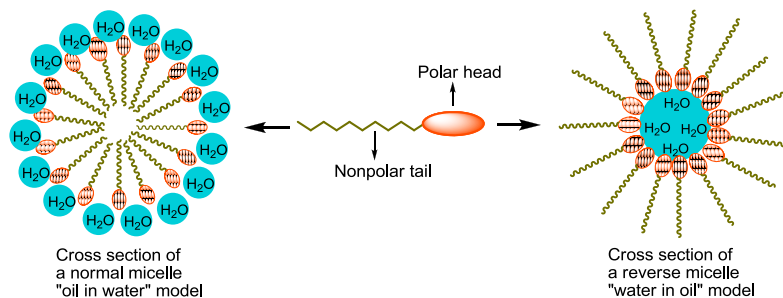


**Figure 11.** Cross sections of normal and reverse micelles formed by surfactants.

Although the micelles are formed in different sizes and shapes, three types of them are important from perspective of liquid crystals, i.e. disc shaped, rod like and spherical micelles.<sup>59</sup> The shape and size of a micelle is a function of the size and geometry of the surfactant molecules,<sup>60</sup> and solution conditions such as surfactant concentration, temperature, pH, and ionic strength. These *micelles* are the building blocks of the liquid crystalline phases. As the concentration increases beyond the CMC, the micelles increase in size and eventually coalesce to separate the newly formed liquid crystalline state from the solvent. In these phases, the solvent molecules fill the space around (and/or in) the structures to provide fluidity to the system. The driving force for the formation of liquid crystalline phases of these amphiphilic molecules is the micro-segregation of hydrophilic and hydrophobic molecular parts into different regions.

Because lyotropics are comprised of at least two chemical constituents, concentration is a much more important parameter compared to temperature. However being in the form of solution, the mesophase transitions in lyotropic liquid crystals are also sensitive to other factors that affect the solution conditions e.g. temperature, pH, ionic strength, counter ion polarizability and charge etc.<sup>61</sup> Like thermotropics, the lyotropic liquid crystals also exhibit polymorphism and different phases can be observed as the concentration of the solution is changed.<sup>62</sup>

### 1.9.3. Amphotropic or Amphitropic Liquid Crystals

Another class of liquid crystal which has received special attention is termed amphotropic or amphitropic.<sup>63,64</sup> Such particular compounds termed as *amphotrops*, show mesomorphism in their pure state on heating as well as form lyotropic mesophases on the addition of an inorganic or organic solvent in certain amounts. However, the mesophases observed in these two regimes are often quite different.<sup>65</sup> Examples of such amphotropic molecules are amphiphilic polyhydroxy compounds and carbohydrate derivatives.

## 1.10. MOLECULAR STRUCTURES AND MESOPHASES OF THERMOTROPIC LIQUID CRYSTALS

The recipe for a compound to be mesogenic is geometrical anisotropy at molecular level because compounds with pronounced shape anisotropy are able to form mesophases with temperature changes. The molecules need to possess some rigid as well as some flexible groups. The presence of a central rigid core, usually aromatic and conjugated systems, renders it the required rigidity which helps the molecules in self assembling or self alignment. The flexible groups (usually hydrocarbon chains) on the other hand, render some fluidity to the system by promoting dispersive interactions between the neighboring molecules due to their highly dynamic motions. A delicate balance of molecular rigidity and flexibility is required to partially acquire both the molecular alignment (orientational order) and fluidity at certain temperature i.e. to give the mesophase. To ensure geometrical anisotropy, molecular shape must be such that at least one axis is very different from the other two. Mostly they have rod or disc shaped molecules and classically thermotropic liquid crystals were classified as calamitic and discotic liquid crystals. However molecules with shapes other than rods or discs, e.g. lath-like, bent core, bowls etc, are also able to form liquid crystals and recently novel classes are being added to thermotropic liquid crystals. Now conventional thermotropic liquid crystals are classified into calamitic, discotic, bent core and polymeric LCs. Each of these classes have their own typical mesophases (i.e. amount of order in the material) such as nematic, smectic, columnar, cholesteric etc. Each mesophase possesses distinct opto-electronic properties which results in their characteristic optical texture.<sup>66</sup>

### 1.10.1. Thermotropic Calamitic Liquid Crystals

Calamitics are the most common type of LCs and they have cigar or rod like elongated molecules in which one molecular axis is much longer than the other two (**Fig. 12**). The rigid centre, which comprises the molecular long axis, often consists of one or more aromatic rings and usually long *n*-alkyl or alkoxy chain as the terminal end groups. The aromatic rings may be connected to each other directly or through linking groups like  $-\text{CH}_2\text{CH}_2-$ ,  $-\text{CH}=\text{N}-$ ,  $-\text{C}\equiv\text{C}-$ ,  $-\text{CH}_2\text{O}-$ ,  $-\text{COO}-$  etc. Sometimes small substituents (e.g.  $-\text{Cl}$ ,  $-\text{Br}$ ,  $-\text{NO}_2$ ,  $-\text{CH}_3$ ,  $-\text{OCH}_3$ ,  $-\text{CN}$ , etc) may also be present as lateral substituents. The nature of the central core, the linking groups, and the lateral substituents impart significant effect on the physical properties and mesophase morphology of the calamitic LCs.<sup>67</sup>

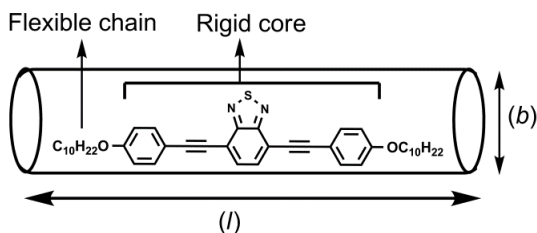


**Figure 12.** General template of calamitic LCs where molecular length ( $l$ )  $\gg$  breadth ( $b$ ).

The rod like polarizable core together with the flexible end chains orient themselves such that their long axes are, on average, parallel to each other (along the director,  $\mathbf{n}$ ) and facilitate liquid crystal formation. The most common types of mesophases exhibited by calamitic LCs are nematic, cholesteric and smectic phases.

#### 1.10.1.1. Nematic Mesophase

The term nematic is derived from the Greek word *nematos* for thread and relates to the thread-like texture of this mesophase observed under polarizing optical microscope. Nematic mesophase (N) is closest to the isotropic liquid (the least ordered) and the most frequently used

mesophase in display devices. This phase possesses long-range orientational order but no long-range positional order (**Fig. 13a**).

#### 1.10.1.2. Cholesteric Mesophase

The chiral version of nematic phase ( $N^*$ ) is comprised of the chiral molecules and is more specifically called as cholesteric mesophase because the first materials exhibiting this phase were cholesterol derivatives. The cholesteric mesophase can also be achieved by inducing chirality through the addition of a chiral dopant (not necessarily mesogenic) in small amount to a nematic material.<sup>68</sup> In such cases, the chiral dopant creates a chiral environment for the achiral nematic molecules causing a slight and gradual rotation of the director and, as result, a chiral helical macrostructure with a specific temperature dependent pitch is generated. Literally the cholesteric phase consists of local nematic “layers”, which are continuously twisted with respect to each other<sup>66</sup> (**Fig. 13b**). As apparent from **Fig. 13b**, the pitch refers to the distance along the helix over which the director rotates by  $360^\circ$ . The helical structure selectively reflects the light of wavelength equal to its pitch. The pitch length, and hence the reflected colors, are temperature dependant and this correlation has been successfully utilized in thermochromic thermometers and other devices that change color with temperature.

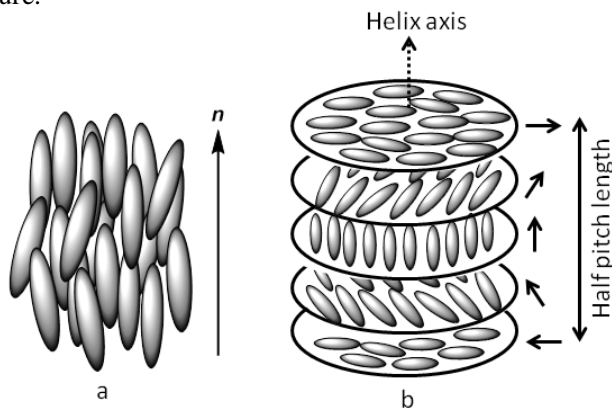


**Figure 13.** Representation of molecular arrangements in (a) nematics phase (b) helical macrostructure of chiral nematic or cholesteric phase.

### 1.10.1.3. Smectic Mesophases

The smectic mesophases (Sm) are formed at temperatures below the nematic phase and represent relatively more ordered phase structures. They have lamellar or layered structures characterized by arrangement of the molecules in the form of layers. In between the layers, they have a well-defined interlayer spacing<sup>69</sup> which can be measured by X-ray diffraction. Within a layer, the molecules may possess positional order (as in smectic B phase) so in addition to the orientational order, the smectic phases also possess short range positional order.<sup>70</sup> The interlayer attractions are weaker compared to the lateral forces between the molecules within a layer making the layers able to slide over one another relatively easily. This ease of sliding of the layers renders fluid property to the more viscous smectic systems.

There are several types of smectic mesophases characterized by molecular arrangements within and between the layers. They are classified on the basis of angle between the director ( $n$ ) and the layer normal into orthogonal (no tilt, angle of  $90^\circ$ ) and tilted (angle  $< 90^\circ$ ) smectic phases. Both the orthogonal and the tilted phases may have ordered (structured layers) or random molecular arrangement (unstructured layers) within the layers.<sup>45</sup> Of the various well defined smectic phases, SmA and SmC are the most commonly encountered. Molecules in Sm A possess the least order amongst all smectic phases. It is an orthogonal phase with director perpendicular to the layer planes and with unstructured layers (**Fig. 14a**). The molecules possess very short range positional order within the layer and there is no positional correlation between the layers. The SmC phase has the same layer structure as that of SmA but the molecules are tilted with respect to the layer normal (**Fig. 14b**). In this phase too, there is no positional order within and between the layers, i.e. both SmA and SmC possess unstructured layers. The less common SmB, SmF, and SmI phases are more ordered and the molecules in SmB possess hexagonal order within the layers (**Fig. 14c**).

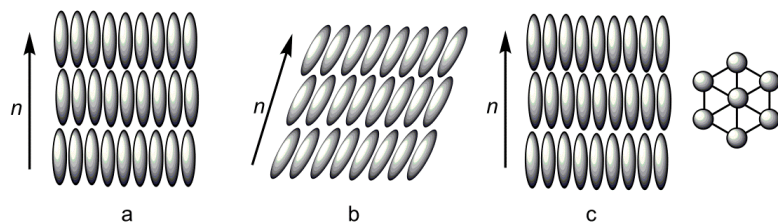


**Figure 14.** Structural representation of (a) SmA (b) SmC (c) SmB viewed from side (left) from top (right).

### 1.10.2. Thermotropic Discotic Liquid Crystals

Discotic liquid crystals (DLCs) are referred to the liquid crystals formed by the disc shaped molecules and were first reported by Chandrasekhar<sup>71</sup> seventy years after the discovery of the calamitics. Before this report, molecular linearity was considered to be an essential requirement to exhibit mesomorphism.<sup>72</sup> A typical discotic mesogen generally consist a central aromatic core functionalized with peripheral flexible chains (**Fig. 15**).

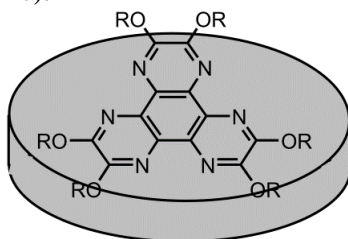


**Figure 15.** General template of the DLCs molecular architecture.

In beginning, small sized aromatic rings e.g. benzene, pyridine, triazine were used as the central core.<sup>73</sup> However later on, with the discoveries that the individual molecules group up as columns via  $\pi$ - $\pi$  stacking and that the larger polyaromatic cores are more efficiently stacked, the use of larger aromatic cores became more common. Today, in addition to the small sized aromatic rings, the typically used discotic cores consist of polyaromatic systems like triphenylenes<sup>74</sup> (6), hexaazatriphenylenes<sup>75</sup> (7), tristriazolotriazines<sup>76</sup> (8) and porphyrines<sup>77</sup> (9) to name few of the many known systems<sup>78</sup> (**Fig. 16**). Moreover, macromolecules with much larger dimensions like polyaromatic

hydrocarbons and macrodiscotic material with extended planar structures<sup>79</sup> have also been exploited as discotic cores.

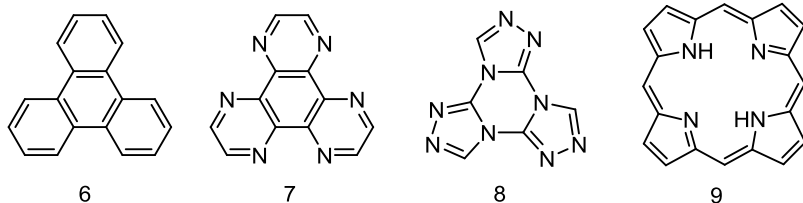


**Figure 16.** Aromatic cores commonly used in discotic mesogens, triphenylene (6), hexaazatriphenylene (7), trisiazolotriazine (8), porphyrine (9).

A characteristic feature of the discotic liquid crystals is stacking of the individual molecules to form columns which act as the basic units of their most typical columnar mesophases. Depending on the details of the intra-columnar interactions, different types of stackings are observed like “disordered columns” with an irregular stacking of the disks, “ordered columns” in which the central cores are stacked in a regularly ordered (equidistant) fashion while the flexible tails are still disordered, and “tilted columns” where the cores of the disks are tilted with respect to the column axis (**Fig. 17**).

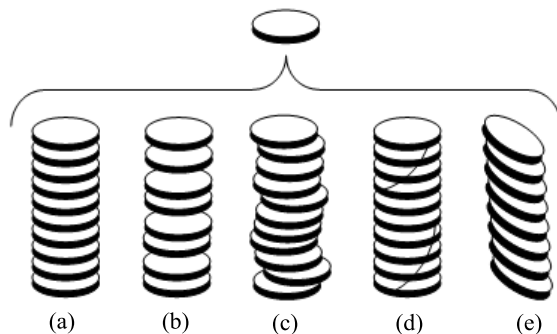


**Figure 17.** Stacking of discotics into different kinds of columnar assemblies: (a) ordered column, (b) and (c) disordered columns, (d) helical column, and (e) tilted column.<sup>80</sup>

These columns can self organize and serve as the structural units of the different types of columnar mesophases, typical of the discotic liquid crystals. Four types of mesophases are formed by the individual discs or columns, i.e. columnar, nematic, smectic and cubic.<sup>80</sup> Of them,

columnar and nematic phases are the most common and well defined, whereas the smectic and cubic phases are rarely observed.<sup>81</sup> In the smectic phase, also known as discotic lamellar phase ( $D_L$ ), the discs are arranged in a layered fashion separated by sub-layers of peripheral chains and are formed when there is a reduced number or an uneven distribution of peripheral chains.<sup>82</sup> Most of the discotics exhibit only one type of mesophase and fewer examples of DLCs showing polymorphism are known.<sup>83</sup>

### 1.10.2.1. Columnar Mesophases of Discotic Liquid Crystals

Columnar phases are the most common mesophases of DLCs. In these phases, the columns (ordered, disordered or tilted) formed by piling up of the discotic molecules self organize themselves parallel to each other in various fashions like hexagonal, tetragonal, oblique etc.<sup>84</sup> Seven types of columnar mesophases are found<sup>80</sup> depending on the degree of order in the molecular stacking and inter-columns orientations, out of them the structural arrangements of columnar hexagonal, columnar rectangular and columnar oblique mesophases are well defined. *Columnar hexagonal* phase ( $Col_h$ ) is characterized by a hexagonal packing (**Fig. 18a**) of the stacked columns. In the columnar rectangular mesophase ( $Col_r$ ), the columns are packed in a rectangular fashion (**Fig. 18b**) surrounded by the disordered aliphatic chains. In the columnar oblique mesophase ( $Col_{ob}$ ), tilted columns are involved that are arranged with an oblique unit cell (**Fig. 18c**).

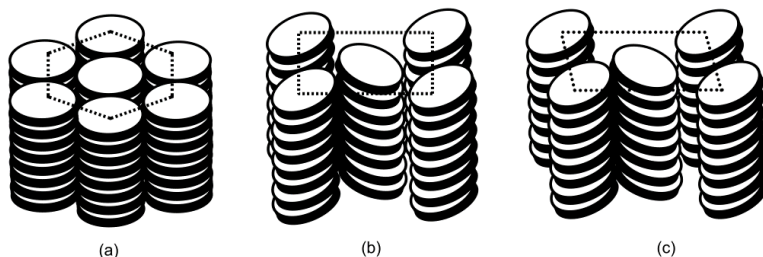


**Figure 18.** Structural representations of the well defined columnar phases (a) columnar hexagonal  $Col_h$ , (b) columnar rectangular  $Col_r$  and (c) columnar oblique  $Col_{ob}$ .

### 1.10.2.2. Nematic Mesophases Of Discotic Liquid Crystals

Four types of nematic phases are formed by the disc shaped mesogens i.e. discotic nematic phase ( $N_D$ ), chiral discotic nematic ( $N_D^*$ ), columnar nematic ( $N_{Col}$ ) and the less familiar nematic lateral ( $N_L$ ).<sup>80</sup> In discotic nematic ( $N_D$ ) phase, the individual (non-stacked) disc shaped molecules are arranged such that they possess only long range orientational order.<sup>85</sup>  $N_D$  has the same symmetry (**Fig. 19a**) as that of calamitic nematic phase but both are not miscible with one another owing to fundamental molecular structural differences. The chiral discotic nematic phase ( $N_D^*$ ) is the discotic version of cholesteric phase and possesses a helical structure (**Fig. 19b**) like the cholesteric phase. It is formed by either the pure chiral discotics<sup>86</sup> or when a chiral dopant (mesomorphic or non-mesomorphic) is added to an achiral discotic compound. Columnar nematic mesophase ( $N_{Col}$ ) consists of long columns that result by  $\pi$ - $\pi$  stacking of many disc shaped molecules.<sup>87</sup> The columns behave as supramolecular rods and are the building blocks of  $N_{Col}$  instead of individual molecules (**Fig. 19c**). In the recently reported<sup>88</sup> and less familiar nematic lateral phase ( $N_L$ ), the discotic molecules simply aggregate laterally into large superstructures (**Fig. 19d**) rather than stacking in the form of columns. These aggregates act as the building blocks of LC phase and show a nematic arrangement.<sup>89</sup>

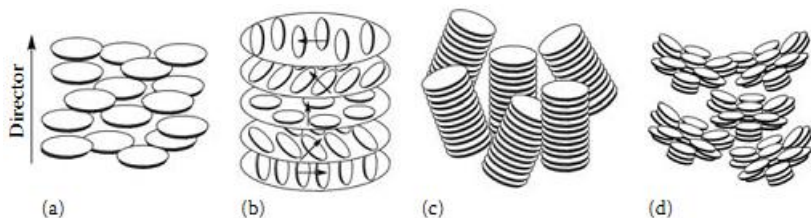


**Figure 19.** Schematic representation of various discotic nematic phases (a) discotic nematic  $N_D$  (b) chiral discotic nematic  $N_D^*$  (c) columnar nematic  $N_{Col}$  (d) lateral nematic phase ( $N_L$ ).<sup>80</sup>

### 1.10.3. Thermotropic Polymeric Liquid Crystals

Polymeric liquid crystals are basically the polymer versions of the aforementioned monomers. There are two types of polymeric arrangements which form thermotropic liquid crystals, the side chain

and the main-chain polymers (**Fig. 20**). In side-chain polymers,<sup>90</sup> the mesogenic units are attached to the polymer backbone by more or less flexible chains. In main-chain polymers, the mesogenic units are incorporated into the polymer backbone and separated from each other by flexible spacer chains.<sup>91</sup>

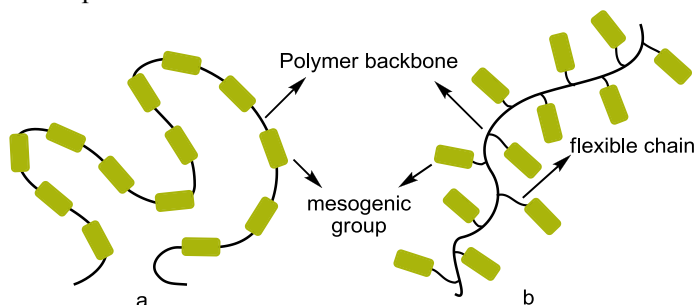


**Figure 20.** Structural representation of (a) main chain and (b) branched chain or comb shaped polymeric liquid crystals.

The flexibility in chains (spacers) is necessary to provide a certain freedom to mesogenic moieties to form an ordered structure.<sup>92</sup> Formation of nematic or smectic phase is quite natural for side chain polymeric mesogens because mesogenic units can easily be arranged parallel to each other. The main chain polymers require long enough flexible spacers between the mesogenic groups to form nematic and even smectic phases (**Fig. 21**).<sup>93</sup>

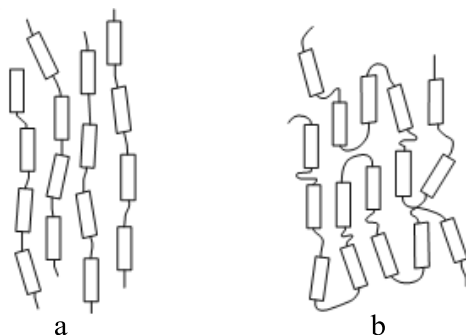


**Figure 21.** Packing of main chain polymer mesogenic groups in (a) nematic and (b) smectic A phases.<sup>93</sup>

#### 1.10.4. Non Conventional Liquid Crystals

In classical approach of thermotropic liquid crystals, only cigar or disc shaped structures can produce liquid crystalline phases. However, the fundamental requirement for mesogeneity is molecular anisotropy and many compounds with non conventional molecular shapes (other than rod or disc) are known to show mesomorphism.<sup>94</sup> Liquid crystals formed by compounds with molecules that are neither rod nor disc shaped are collectively termed as non conventional liquid crystals.

Theoretically, the non conventional LCs may present mesophases other than those of the conventional calamitics and discotics because the type of mesophase is determined by the molecular shape to a large extent.<sup>95</sup> Changing the shape of the rigid segments from classical rod or disc to other geometries leads to quite unusual mesophase morphologies<sup>96</sup> distinct from the conventional smectic and columnar mesophases of the classical rod and disc-like molecules.<sup>97</sup> For example some achiral bent shaped compounds that are neither perfectly linear nor discotic can form mesophases with chiral properties. A brief note about such liquid crystals is given in the index section. Examples of liquid crystals with non-conventional molecular topology include multiarm star-shaped,<sup>98,99</sup> board-like molecules with molecular structures at borderline between calamitic and discotic,<sup>100</sup> polycatenars,<sup>101,102</sup> shuttlecock shaped,<sup>103,104</sup> cone shaped,<sup>105</sup> ring shaped mesogens forming tubular liquid crystals<sup>106</sup> and other molecules that combine features of both the rods and discs. **Figure 22** shows some representative examples of the non conventional liquid crystals.

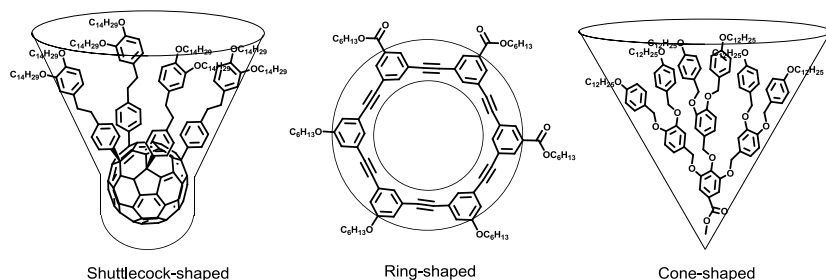


**Figure 22.** Molecular shapes of some non conventional LCs distorted away from rod and disc shapes.

### 1.11. FUNCTIONALIZATION OF THE LIQUID CRYSTALS

Future technological developments require multifunctional materials where several physical properties are met in a single material. Liquid crystals are multifunctional material because in addition to their unique property of being both dynamic (soft) as well as ordered, they can be functionalized by different ways.<sup>107</sup> Functionalization means rendering a stimulus-responsive desirable property (e.g. electric, optical, magnetic, luminescence etc) to the material for practical applications. Due to the anisotropic nature of LCs, these additional properties are directional and such systems can be used in ordered functional material. For example, the presence of electroactive moieties in mesomorphic molecules result in compounds with anisotropic (directional) electrical and electrochemical properties<sup>108</sup> that can be used in developing new electroactive materials.<sup>109</sup> Similarly ionic liquid crystals, due to the presence of charges, combine the properties of liquid crystals (anisotropy) and ionic liquids i.e. low vapor pressure, high solubilizing power and ion conductivity. Combination of anisotropic and ionic properties makes ionic liquid crystals very promising candidates to design ion-conductive materials.<sup>47</sup>

An intelligent and useful approach to LC functionalization is the insertion of a photo-isomerizable group to control molecular alignment by means of photoirradiation. For example, the azo group (-N=N-) undergoes reversible cis-trans photoisomerization and its insertion in a liquid crystal have shown to help control the molecular alignment through photo-irradiation. When the molecule is in the thermodynamically stable trans configuration, the high discotic

anisotropy promotes a columnar hexagonal mesophase. After photoisomerization to the *cis*- configuration, the material becomes an isotropic liquid (**Fig. 23**). This controlling mechanism of the molecular alignment makes them promising candidates as optical switch for controlling the conductivity in electro-optical devices.<sup>110</sup>

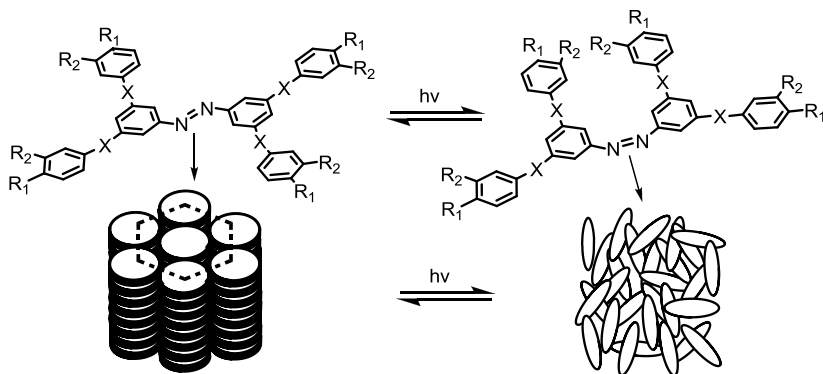


**Figure 23.** Illustration of *cis-trans* photoisomerization and consequent mesophase change.

Another common approach for LC functionalization is through the self-assembly of the rationally designed liquid crystals via non covalent interactions (especially hydrogen bonding)<sup>111</sup> into supramolecular liquid crystals with more complex but well-defined structures and new functions<sup>107</sup> (**Fig. 24**). One of the specific features of supramolecular liquid crystals is their dynamic structures due to involvement of weaker non covalent interactions.<sup>112</sup> The molecular order in these states can be switched on/off by external stimuli such as thermal treatment, light irradiation, electric fields etc. Moreover, these supramolecular LC assemblies show reversible mesomorphic–isotropic phase transitions as a result of reversible formation and breaking of the hydrogen bonds. Such systems can be used to prepare stimuli-responsive<sup>113</sup> dynamic material.

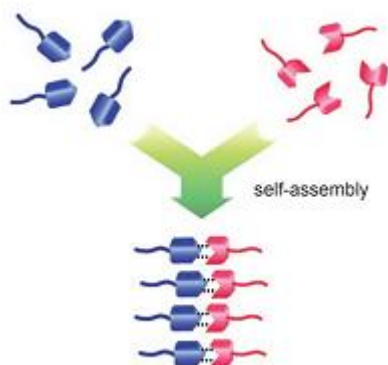


**Figure 24.** Self assembly of non-mesogenic components into supramolecular liquid-crystal.<sup>107</sup>

Another useful approach to LC functionalization is to control LC alignments and properties by doping with stimuli (thermal, electric, optical etc.) responsive dopants. For example, the properties of LCs can be reversibly photo-regulated by doping LCs with photochromic compounds. Photochromic dopants e.g. spiroxazine,<sup>114</sup> diarylethene,<sup>115</sup> fulgide,<sup>116</sup> thioindigo,<sup>117</sup> azobenzene etc, undergo reversible changes of their molecular structures through photo-radiations. Due to the dopant-LC molecular interactions, structural changes of the dopants induce changes in the LC alignments (**Fig. 25**). This provides a mechanism to reversibly regulate the various LC properties and functionalizing for various optical applications.<sup>118</sup>

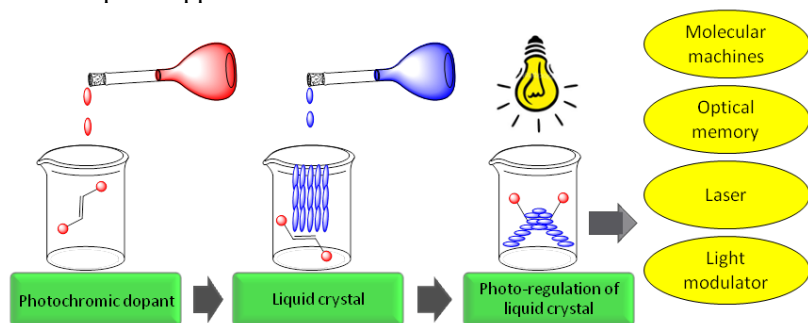


**Figure 25.** Schematic representation of light induced alignment changes in LCs doped with photochromic compound and potential applications of the doped system.

### 1.12. A BRIEF REVIEW OF THE 2,1,3-BENZOTHIADIAZOLE

The 2,1,3-benzothiadiazole (**10**) is an aromatic heterocycle with a planar molecular structure. The non-bonding electron pair of the sulfur atom makes part of the aromatic system making it electron deficient. It is an efficient luminescence precursor and its derivatives with extended conjugation are intensely fluorescent, usually with high quantum yields.<sup>119</sup> Depending on the type of substituents and conjugation length, the 2,1,3-benzothiadiazole based materials emit a variety of different colors including green,<sup>120</sup> red<sup>121</sup> and blue,<sup>122</sup> the three fundamental colors for full-color displays. Due to its rigid planar structure, ability to form well-ordered crystals and its significant polarizability leading to intermolecular interactions such as heteroatom-heteroatom contact and  $\pi$ - $\pi$  interactions, we have successfully used this system as the central core for luminescent liquid crystals.<sup>123-125</sup>

Linking an electron deficient aromatic system to electron rich systems in alternative fashion leads to a donor-acceptor-donor combination with enhanced intramolecular charge transfer. Due to its electron-deficient nature, the 2,1,3-benzothiadiazole have been used extensively as an acceptor unit in many  $\pi$  conjugated systems especially in donor-acceptor conjugated copolymers.<sup>126</sup> This enhanced charge transfer from electron-rich units to electron deficient 2,1,3-benzothiadiazole moieties in donor-acceptor conjugated copolymers,<sup>127</sup> lowers the band gap (HOMO-LUMO) significantly resulting in small band gap or even ultrasmall band gap<sup>128</sup> material. Such low band gap systems are very responsive to external optical and/or electrical stimuli and are highly desirable for use in solar cells,<sup>129</sup> light emitting diodes,<sup>130</sup> field-effect transistors<sup>131</sup> etc.

### 1.13. A BRIEF REVIEW OF THE 2,1,3-BENZOXADIAZOLE

The 2,1,3-benzoxadiazole heterocycle more specifically known as benzofurazan (**11**) is the oxygen containing analogue of 2,1,3-benzothiadiazole (**10**). It also possesses a planar and conjugated bicyclic molecular structure (**Fig. 26**) and its derivatives with extended conjugation are highly fluorescent. Due to the presence of oxygen in the heterocycle, the benzofurazan is more electronegative (more electron deficient) compared to 2,1,3-benzothiadiazole.

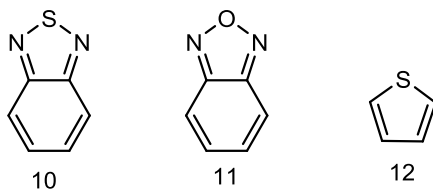


**Figure 26.** Molecular structures of the 2,1,3-benzothiadiazole (10), 2,1,3-benzoxadiazole (11) and thiophene (12).

The major application of benzofurazan heterocycle is in the design of various fluorescent derivatization reagents possessing benzofurazan structure<sup>132</sup> that are used as fluorogenic pre-column labeling reagents for amino acids and peptides analysis,<sup>133</sup> HPLC separation of enantiomers by converting to diastereomers<sup>134</sup> and heavy metals detection.<sup>135</sup> Recently the benzoxadiazole system has been used as an acceptor (electron deficient) unit in a  $\pi$ -conjugated donor-acceptor copolymer for potential application in organic solar cells<sup>136</sup> and in small molecular low band gap linear<sup>137</sup> and star-shaped<sup>138</sup> D- $\pi$ -A- $\pi$ -D structured organic dyes for solution-processable organic photovoltaic cells. However contrary to its sulfur containing analog, i.e. 2,1,3-benzothiadiazole, the benzofurazan derivatives are rarely reported for such kind of applications.<sup>127</sup>

#### 1.14. A BRIEF LITERATURE REVIEW OF THE THIOPHENE

Thiophene is a well known heteroaromatic compound with a five-membered flat ring. Being electron rich (six electrons delocalized over five atoms), it undergoes a range of electrophilic substitutions with preference for the 2- and 5-positions, i.e. adjacent to the heteroatom. Halogenations give initially 2-halo derivatives followed by 2,5-dihalothiophenes. Conjugated polymers are important materials for the development of new technologies in electronics and optoelectronics. Due to their chemical stability and synthetic versatility, thiophenes are ideal building blocks in transition metal-catalyzed cross-coupling reactions for the synthesis of most thiophene-based materials, in particular oligo- and polythiophenes.<sup>139</sup> Polythiophenes display the most unique combination of efficient electronic conjugation, chemical stability, high environmental stability of both its doped and undoped

states and solution processability.<sup>140</sup> The high polarizability of the sulfur atom in thiophene rings leads to stabilization of the conjugated chain and excellent charge transport properties<sup>141</sup> important for their applications such as thin-film transistors, conductors and organic semiconductors. Besides their extensive applications in the field of conducting polymers, the thiophene unit has also been used in the field of liquid crystals.<sup>142-144</sup>



## 2. OBJECTIVES

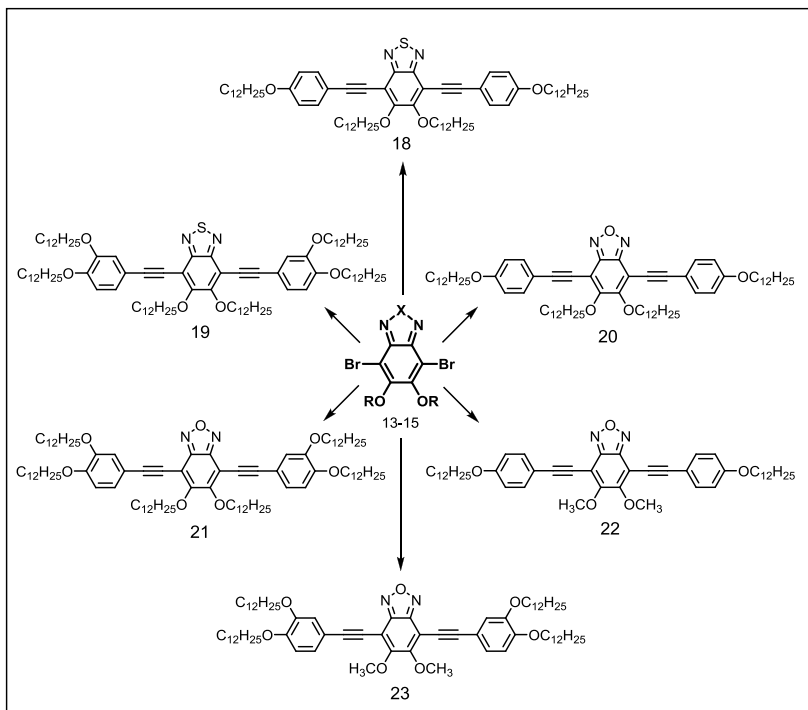
*"Management by objectives works if you  
first think through your objectives"*

*Peter F. Drucker*

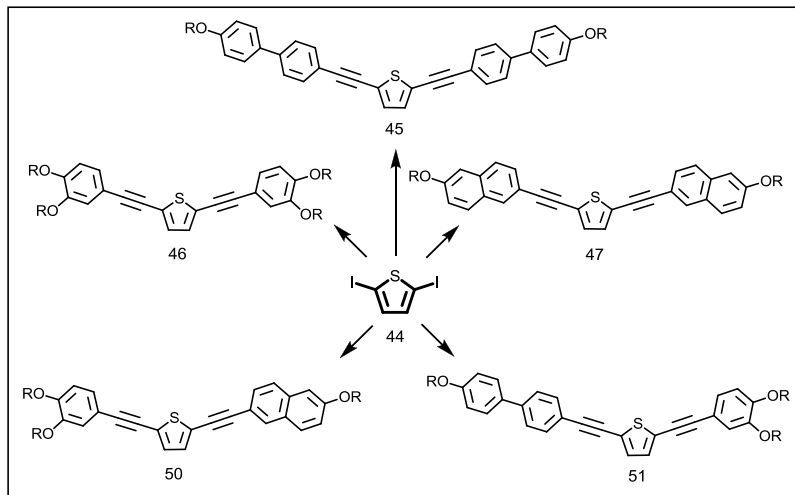
As discussed previously, compounds that present mesomorphism and luminescence possess great technological applications. This have greatly boosted up the design and synthesis of new organic compounds with suitable structures for potential applications in developing a variety of functional materials. In this context, the objective of this thesis work is the synthesis and characterization of some new luminescent and mesomorphic compounds. These compounds are derived from the 2,1,3-benzothiadiazole, 2,1,3-benzoxadiazole and thiophene heterocycles as the central units because these heterocycles have already shown their potential for generating luminescent and/or mesomorphic properties.

The specific objectives of this work include:

- Syntheses of new luminescent compounds derived from the 2,1,3-benzoxadiazole and 2,1,3-benzothiadiazole heterocycles with molecular structures shown in **scheme 1**.
- Syntheses of new bent shaped liquid crystals based on the 2,5-disubstituted thiophene with molecular structures shown in **scheme 2**.
- Structural characterization of the intermediate and final compounds through melting point, infrared spectroscopy (IR), hydrogen and carbon nuclear magnetic resonance spectroscopies ( $^1\text{H}$ NMR,  $^{13}\text{C}$ NMR) and mass spectrometry (MS).
- Studies of the thermal and mesomorphic properties (if presented) of the final compounds through DSC, TGA and POM.
- Investigation of the photophysical properties of the final compounds by using UV-Vis absorption and emission techniques and calculation of their molar absorptivity coefficients, stokes shifts, relative quantum yields and optical bandgaps.
- Studies of the electrochemical behaviour and calculation of the redox potentials, energies of the frontier orbitals ( $E_{\text{Homo}}$ ,  $E_{\text{Lumo}}$ ) and electrical bandgap of the final compounds by using cyclic voltammetry.



**Scheme 1.** Molecular structures of the target luminescent compounds; X = S, O.



**Scheme 2.** Molecular structures of the target luminescent liquid crystals; R =  $C_{12}H_{25}$ .

### 3. RESULTS AND DISCUSSION

To present and discuss the results in a precise way, this section is divided in two parts. **Part A** presents the syntheses and structural characterization of luminescent compounds containing 2,1,3-benzoxadiazole and 2,1,3 benzothiadiazole as the central units along with discussion of the results obtained from their optical and electrochemical analysis. In **part B**, the syntheses and characterizations of thiophene based luminescent liquid crystals and their mesomorphic and optical properties are presented and discussed.

## **Part A**

### 3.1. Syntheses and Characterization of Luminescent Compounds Containing 2,1,3-Benzoxadiazole and 2,1,3 Benzothiadiazole and Their Optical and Electrochemical Properties

### 3.2. MOLECULAR DESIGN

**Figure 27** shows structures of the designed compounds in a generalized form. These molecules were rationally designed to ensure observation of the desired properties. As already mentioned, conjugated derivatives of both the heterocycles are efficient fluorophores. We planned to extend the conjugation by connecting the central heterocycles to benzene rings using  $-C\equiv C-$  bond as the connecting group. These aromatic systems were connected through the connecting groups (and not directly) to avoid steric strain and the resulting torsion of the rings with respect to each other. This ensures to maintain all the rings in the same plane to facilitate delocalization. These molecules were designed such that besides the presence of rigid centers, they also possess varying number of flexible alkoxy chains. Due to the presence of rigid centre as well as flexible chains, these compounds can potentially present mesomorphism.

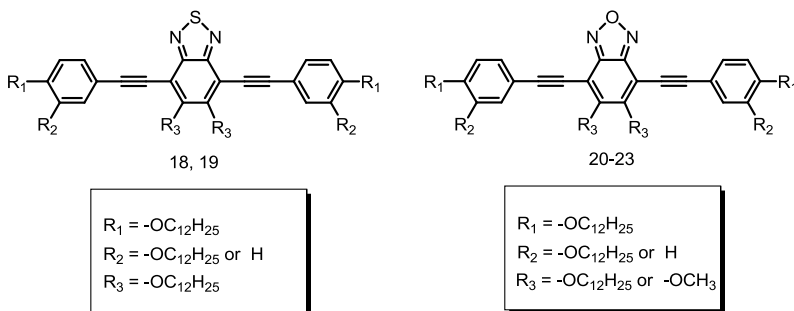


**Figure 27.** Representative structures of the planned luminescent compounds.

### 3.3. RETROSYNTHETIC ANALYSIS

As an essential part of the synthetic plan, retrosynthetic analysis of the target compounds was performed in the first step and is shown in **figure 28**. The target molecular architectures were planned to be achieved by connecting the terminal carbocyclic rings to the central heterocycles (through a  $-C\equiv C-$  linker) utilizing Sonogashira cross-coupling reaction for the C–C bond formation. This coupling requires a terminal alkyne and organic halide or triflate. Retrosynthetic analysis of the central heterocyclic units is shown in **figure 29**. The preliminary formation of either of the terminal alkynes A or B' will also utilize a C-

C bond formation for incorporation of the  $-C\equiv C-$  moiety. The alkoxide chains can be incorporated through the base catalyzed C–O bond formation between phenols and haloalkanes through Williamson etherification.

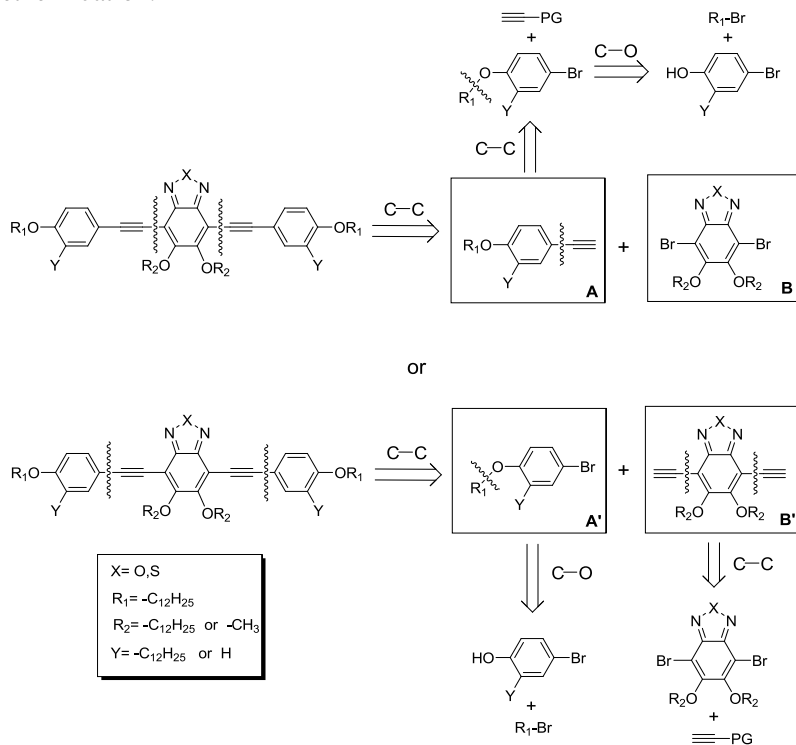


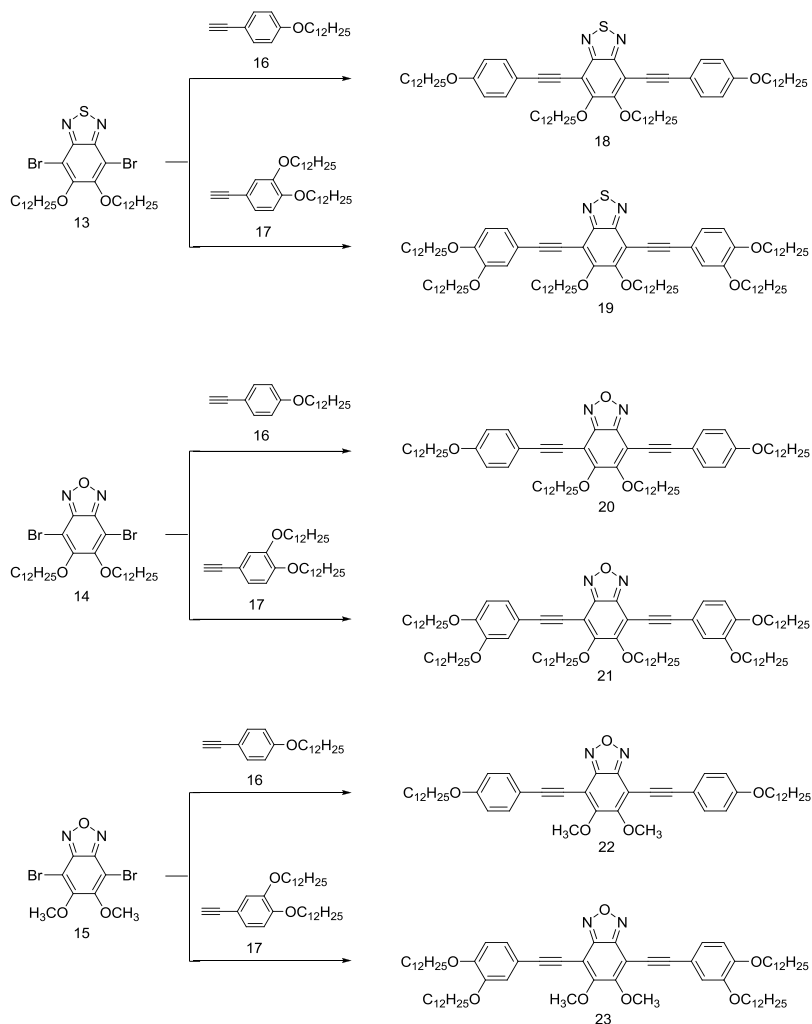
**Figure 28.** Retrosynthetic analysis of the target luminescent compounds.

### 3.4. SYNTHETIC PLAN

As also shown in the retrosynthetic analysis, the target fluorescent derivatives of the 2,1,3-benzothiadiazole and 2,1,3-benzoxadiazole (**18** - **23**) can be accessed by two routes. Both these routes utilize the Sonogashira C–C coupling reaction as the key synthetic step to incorporate the acetylene moiety as the spacer unit between the central heterocycle and the terminal aromatic rings. Both the possible synthetic routes are shown in detailed synthetic **schemes 3** and **4**. In route A, the acetylene functionality comes from the carbocyclic intermediates (**16**, **17**) and they couple with the bromine

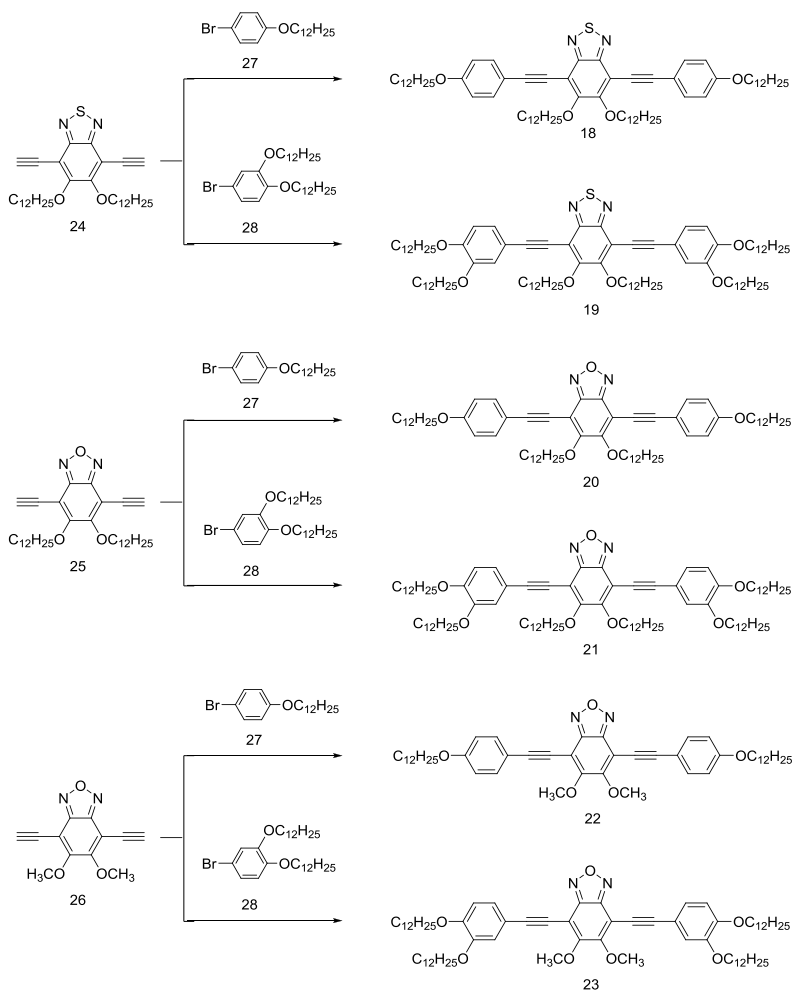
functionalized heterocycles (**13 - 15**) to furnish the target compounds. In route B, the functionalization and reaction sequence is reversed, i.e. the products are formed by coupling between the acetylene functionalized heterocycles (**24 - 26**) with the bromine functionalized carbocycles **27** and **28**. Route A was followed in this work as it is more preferable than route B in two ways. First, the route A involves fewer steps than the route B to make the substrates for the final step. The second and more important reason is the probable instability of the heterocyclic diynes **24 - 26**, since a closer analogue is reported to be only temporarily stable and darkens in the air in few minutes.<sup>119,145</sup>

## ROUTE A



**Scheme 3.** Route A for the synthesis of the target compounds. Reaction conditions:  $\text{Pd}(\text{PPh}_3)_2\text{Cl}_2$ ,  $\text{PPh}_3$ ,  $\text{CuI}$ ,  $\text{Et}_3\text{N}$ , 80-85 °C, 12-14h.

## ROUTE B



**Scheme 4.** Route B for the synthesis of the target compounds. Reaction conditions: Pd(PPh<sub>3</sub>)<sub>2</sub>Cl<sub>2</sub>, PPh<sub>3</sub>, CuI, Et<sub>3</sub>N, 80-85 °C, 12-14h.

## 3.4.1. Syntheses and Characterizations of The Central Cores

Retrosynthetic analysis of the heterocycles is shown in **figure 29**. The synthesis utilize commercial catechol as the starting material and the synthetic steps include formation of the ether linkage via the Williamson etherification, nitration of the aromatic ring, nitro group reduction and subsequent cyclization. The final step is bromine functionalization of the heterocycle for the final Sonogashira coupling.

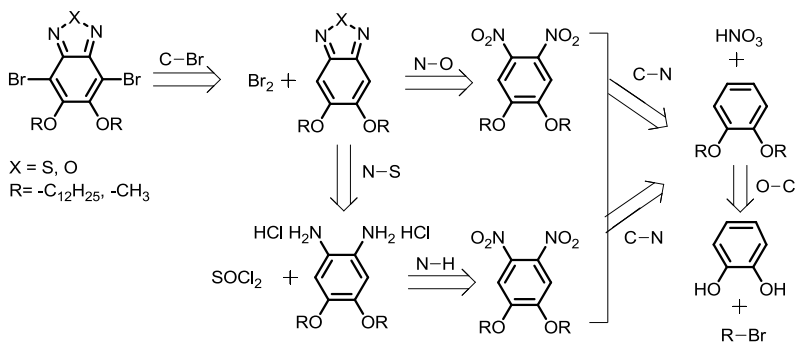
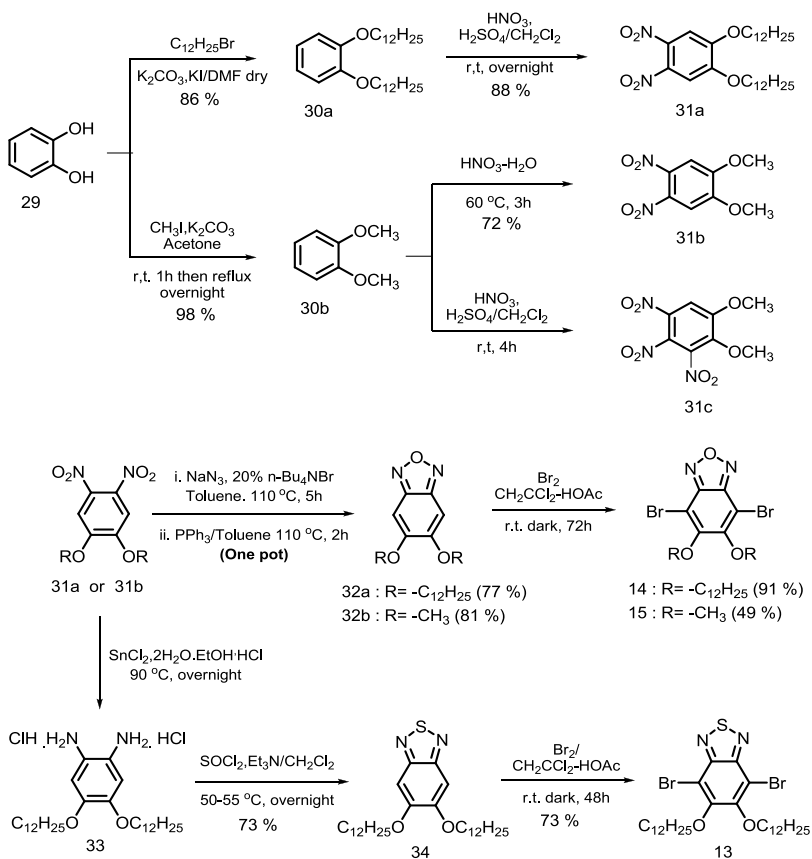


**Figure 29.** Retrosynthetic analysis of the central heterocycles.

A detailed route to the synthesis of the heterocycles is shown in **scheme 5**. Catechol **29** was alkylated to 1,2-bis(dodecyloxy)benzene **30a** with improved yield by a slight experimental and work-up modification of the procedure described in the literature.<sup>146</sup> The compound **30a** was nitrated to 1,2-bis(dodecyloxy)-4,5-dinitrobenzene **31a** at room temperature by stirring it with  $HNO_3-H_2SO_4$  as the nitrating mixture, a procedure already described for an analogous transformation.<sup>147</sup> Veratrol (**30b**) was formed by the methylation of catechol using iodomethane as the methylating agent in the presence of base. When the same nitration protocol of using  $HNO_3-H_2SO_4$  as the nitrating mixture was attempted to transform veratrol to 4,5-dinitroveratrol (**31b**), trinitration occurred and 3,4,5-trinitroveratrol (**31c**) was formed. This is probably due to the fact that unlike in **30a**, the *ortho* positions in **30b** are sterically less hindered due to small size of the methoxy groups. The desired transformation to **31b** was then achieved under milder conditions using 70% aqueous nitric acid as nitration mixture.<sup>148</sup>



**Scheme 5.** Detailed synthetic route to the central cores 13-15.

Stirring the intermediates **31a** or **31b** with sodium azide and tetra-*n*-butylammonium bromide as phase transfer catalyst (PTC) under reflux for 5 hours followed by stirring with triphenylphosphine furnished the bicyclic intermediates **32a** or **32b** respectively in a *one-pot* reaction.<sup>127</sup> In attempts to prepare the benzothiadiazole ring, first the 1,2-bis(dodecyloxy)-4,5-dinitrobenzene (**31a**) was reduced to the respective free ortho-diamine by hydrogenation in the presence of palladium on charcoal as catalyst. The free ortho-diamine intermediate is unstable in air so after the hydrogenation reaction, the catalyst was

filtered off and the diamine was directly reacted with thionyl chloride under argon to give the cyclized product (**34**). This route resulted in low yield and the product was purified through column chromatography. Alternative route in which the nitro groups of **31a** were reduced with tin chloride to the diammonium salt (**33**) and subsequently cyclized with thionyl chloride was found to work well in this case. This route furnished the same target compound (**34**) with improved yield and the product was more easily purified through recrystallization from ethyl alcohol. The sulfur containing analogue of compound **15** could not be synthesized because attempts to cyclize **31b** using both the  $\text{SnCl}_2$  reduction-cyclization and hydrogenation-cyclization routes led to a solid residue that was insoluble in all common organic solvents as well as in water and was not characterized. Finally, the cyclized products (**34**, **32a** and **32b**) were functionalized for the final cross-coupling step by their bromination with bromine in the dark.

Structures of the heterocyclic intermediates were characterized mainly by the  $^1\text{H-NMR}$  spectroscopy. **Figure 30** shows a comparison of the  $^1\text{H-NMR}$  spectra of **34** and **13** as representative of the spectral changes accompanying the bromination step. The  $^1\text{H-NMR}$  spectra of non-halogenated intermediates (**34**, **32a** and **32b**) contain aromatic singlets which disappear after bromination. The spectra of the halogenated intermediates (**13-15**) contain only peaks of the ethereal groups with a characteristic peak around 4 ppm corresponding to the  $\alpha$  hydrogens of the ethereal chains.

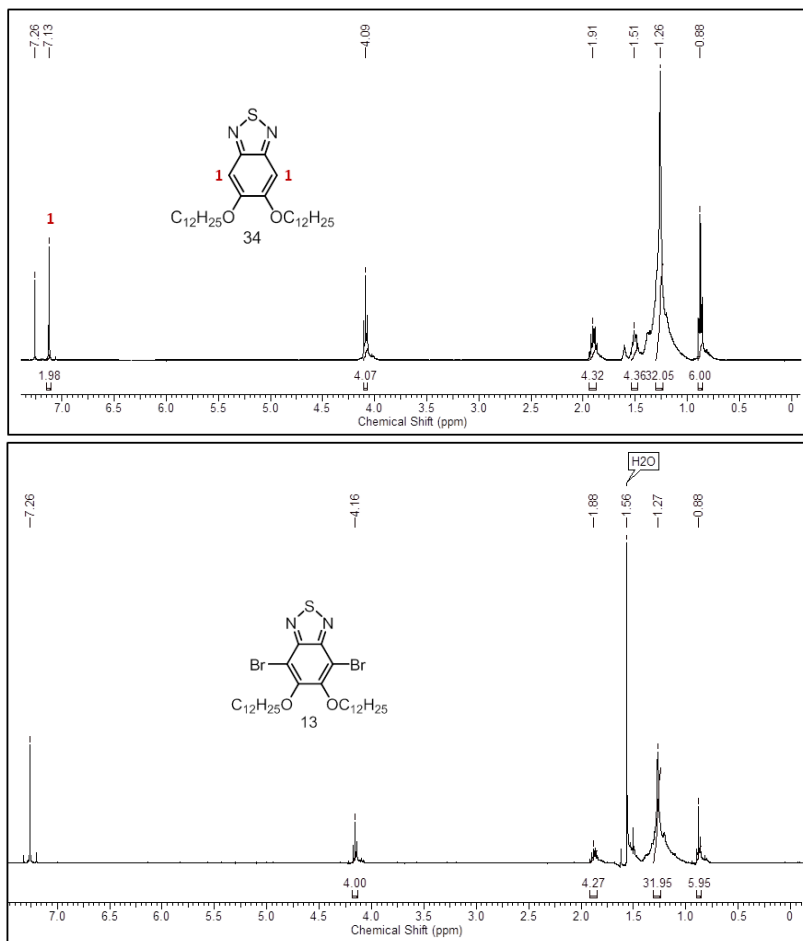
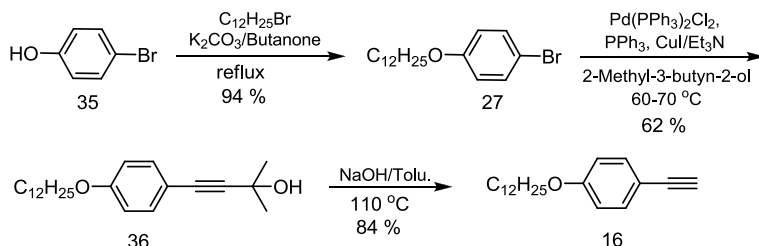


**Figure 30.**  $^1\text{H-NMR}$  spectra of compounds **34** and **13** ( $\text{CDCl}_3$ , 400 MHz) as representative of the spectral changes accompanying the bromination step.

### 3.4.2. Synthesis of The Terminal Acetylenes

The terminal acetylenic intermediate **16** with one alkoxy chain was prepared from 1-bromo-4-(dodecyloxy)benzene **35** in three steps as shown in **Scheme 6**. In first step, the flexible chain was incorporated through Williamson etherification reaction with 1-bromododecane in the presence of  $\text{K}_2\text{CO}_3$  as the base. Next, the acetylenic spacer unit was

inserted via Sonogashira cross coupling using 2-methyl-3-butyn-2-ol as the alkyne precursor. The 2-methyl-3-butyn-2-ol is much cheaper than trimethylsilyl-acetylene although relatively harsh conditions are required for release of the protecting group.<sup>149-51</sup> Subsequently, the terminal acetylenic moiety was liberated to furnish the intermediate **16**.



**Scheme 6.** Synthetic route to the terminal alkyne **16**.

Trofimov protocol,<sup>152</sup> which involves base catalyzed elimination of the protecting group in the form of acetone, was followed for all the deprotection steps leading to un-substituted terminal alkynes. In our case, the use of NaOH pellets dispersed in toluene as catalyst gave better yields than KOH in isopropanol. A microdistillation system was connected to the reaction flask and the acetone formed during reaction was distilled off, as acetone-toluene azeotrope, to drive the reaction in forward direction. The reaction is thought to be initiated by the base, abstracting the hydroxylic proton to form acetylide species **16a** which is partially stabilized by the counter ion from the base. In the next step, besides the added base, this acetylide may also abstracts proton from another substrate molecule **36** to give the free terminal alkyne **16** along with elimination of the acetylene (**Fig. 31**).

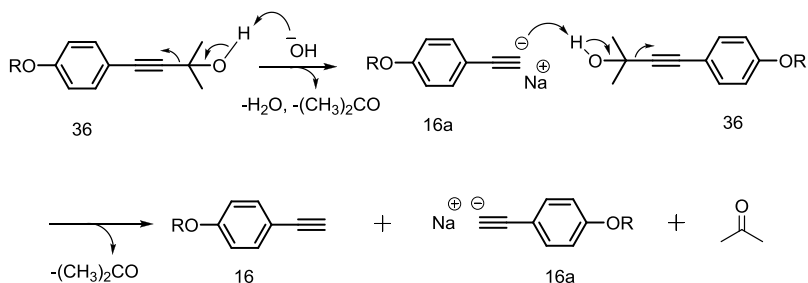
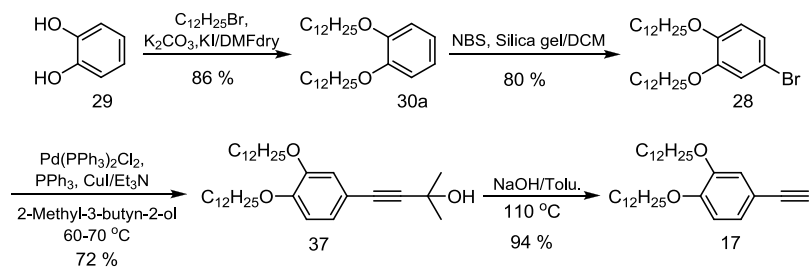


**Figure 31.** Proposed mechanism of the alkyne deprotection step.

The intermediate **17** possessing two flexible chains was synthesized from commercial catechol i.e. 1,2-dihydroxybenzene (**29**) according to **scheme 7**. In first step, the two chains were incorporated by alkylation of both the hydroxy groups through the Williamson etherification in dry dimethyl sulfoxide (DMF) at inert atmosphere. The **30a** was next mono-brominated by reacting with *N*-bromosuccinimide (NBS), a mild brominating agent to avoid multiple bromination. The common silica gel was used as the acid catalyst in this step. Next, the acetylene moiety insertion and subsequent deprotection, by the same procedures used in the case of compound **16** preparation, led to the target compound 1,2-bis(dodecyloxy)-4-ethynylbenzene **17**.



**Scheme 7.** Synthetic route to 3,4-didodecyloxyphenylacetylene **17**.

The  $^1\text{H-NMR}$  spectra of all the products from the Sonogashira reactions show a characteristic six protons singlet around 1.6 ppm corresponding to the two methyl groups of the acetylene protecting group. After deprotection step, this singlet disappears and the  $^1\text{H-NMR}$  spectra of the liberated terminal alkynes **16** and **17** show a characteristic

one proton singlet around 3 ppm corresponding to the acetylenic hydrogen ( $C \equiv C-H$ ) at the  $sp$  hybridized carbon. **Figure 32** shows a comparison of the  $^1H$ -NMR spectra as representative case of the spectral changes that accompany deprotection step of the terminal acetylene.

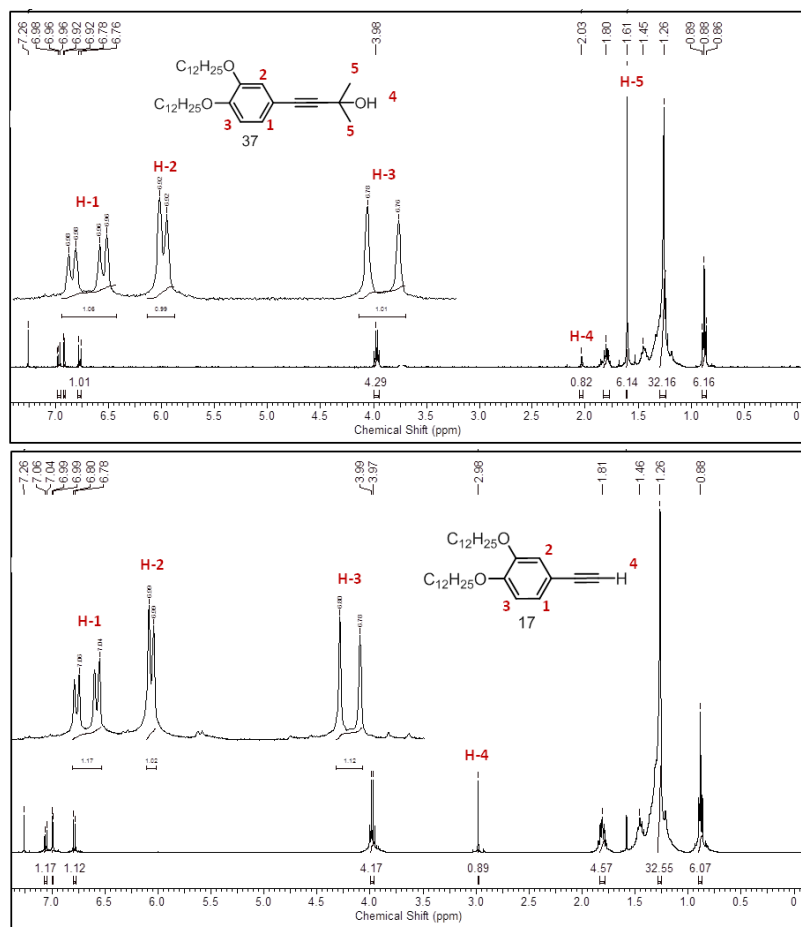


**Figure 32.**  $^1H$ -NMR spectra of compounds 37 and 17 ( $CDCl_3$ , 400-MHz) to show the spectral changes that occurred during the deprotection step.

Structures of the terminal alkynes **16** and **17** were also characterized by the IR spectroscopy. Their IR spectra showed a typical sharp band near  $3310\text{ cm}^{-1}$  characteristic of the alkyne C-H bond stretch ( $\nu\text{C}\equiv\text{C-H}$ ). The other prominent stretching bands include two closely located strong bands at  $2923\text{ cm}^{-1}$  and  $2853\text{ cm}^{-1}$  corresponding (respectively) to asymmetrical and symmetrical  $\text{sp}^3$  C-H stretching of the methylene groups and a weak and sharp band near to  $2108\text{ cm}^{-1}$  referring to C-C stretching ( $\nu\text{C}\equiv\text{C}$ ) of the triply bonded carbon atoms (**Fig. 33**).

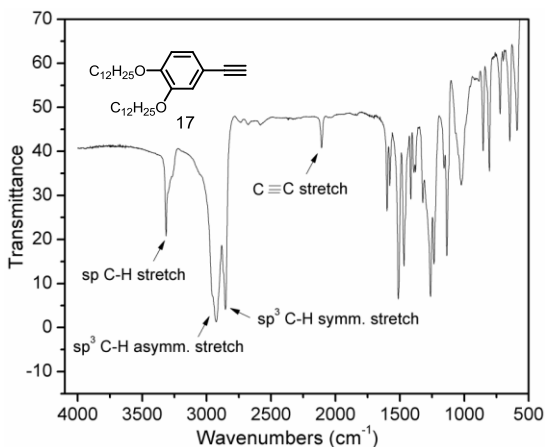
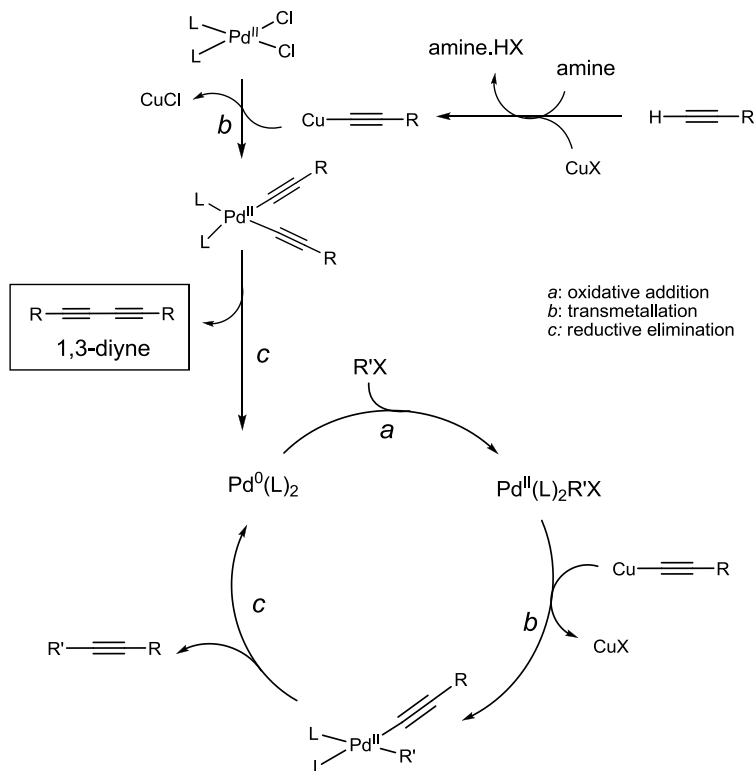


**Figure 33.** The IR spectrum of 1,2-bis(dodecyloxy)-4-ethynylbenzene **17** (in KBr disc) with characteristic bands.

### 3.4.3. Synthesis of The Final Compounds

As already mentioned, Sonogashira cross coupling of the acetylenes **16** and **17** with the halogen functionalized heterocycles **13-15** was used as the final and key step to furnish the target compounds. The Sonogashira reactions usually involve the  $\text{sp}^2$  -  $\text{sp}$  coupling reaction between aryl or alkenyl halides or triflates and terminal alkynes in the presence of Pd and copper (I) iodide and an amine as a base and as a solvent. The general reactivity order of the  $\text{sp}^2$  species is vinyl iodide > vinyl triflate > vinyl bromide > vinyl chloride > aryl iodide > aryl triflate > aryl bromide > aryl chloride. Although this reaction is widely used in the field of organic chemistry for the syntheses of a variety of molecular structures as natural products, pharmaceuticals and molecular

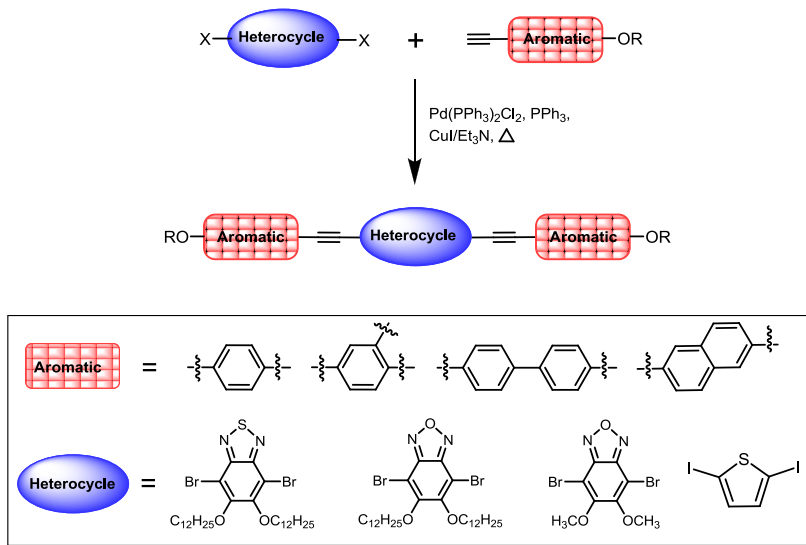
organic materials, the exact mechanistic details such as nature of the catalytically active species, role of the added CuI remain unknown.<sup>153,154</sup> This is mainly due to the difficulty to isolate and characterize the organometallic intermediates from the reaction mixtures to validate a mechanism beyond any doubt. The generally accepted mechanism is shown in **scheme 8**.



**Scheme 8.** Mechanistic depiction of the alkyne homocoupling during catalyst activation.

All the final steps leading to the target fluorescent and mesomorphic compounds are summarized in a generalized fashion in **scheme 9**. The final steps gave poor isolated yields (30-52 %). The poor isolated yields can be explained by considering several factors including difficulties in complete purification, the occurrence of incomplete

(mono-coupling) and competing (homocoupling) reactions and the structural features that affect efficiency of the Sonogashira coupling. The reactivity of aryl bromides is often rather low. Moreover, the presence of flexible chains at positions 5 and 6, i.e. next to the bromine, decreases the reactivity further due to their electron donating nature and may also sterically hinder the coupling.



**Scheme 9.** Summary of the final Sonogashira coupling reactions leading to the target compounds.

Due to low reactivity of the heterocyclic intermediates, mixture of products were formed including mono-coupled product due to incomplete reaction and the homocoupled 1,3-diynes formed by dimerization of the terminal alkynes (Glaser type reaction).<sup>155</sup> Attempts to improve the yield by using harsh conditions such as increasing reaction temperature, catalyst loadings and using the alkyne in large excess though slightly improved the yields, however, these conditions also favored the competing homocoupling reaction. The <sup>1</sup>H NMR spectrum shown in **figure 34** demonstrates the example of one such attempts in which the homocoupled product was formed as the major product. Both the target and side products possess very close R<sub>f</sub> values and they presented great difficulties in their purifications. Purifications were only achieved on chromatographic columns packed with flash

silica gel and eluted very slowly with 1-2 % ethyl acetate : hexane. In many cases, fractions collected from the column that appeared pure of the TLC plates still possessed traces of the homocoupled by-product that could only be seen in their  $^1\text{H}$  NMR spectra. In such cases, the fractions were needed to be chromatographed further to get the pure compound.

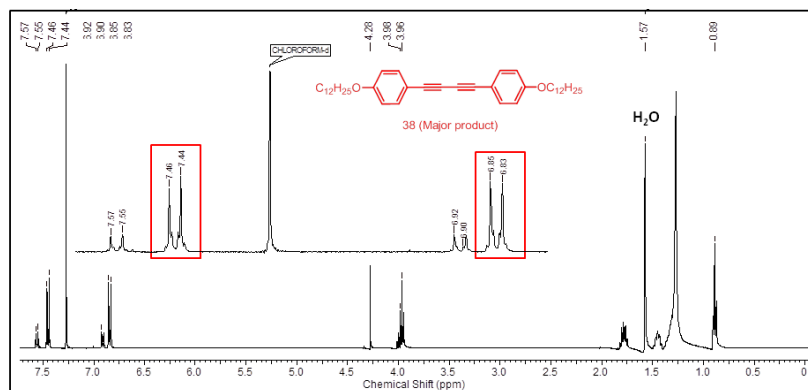


**Figure 34.**  $^1\text{H}$  NMR spectrum ( $\text{CDCl}_3$ , 400-MHz) showing formation of the homocoupled side product **38** as the major product.

The symmetrical 1,3-diyne formed by homocoupling of the alkyne is a common by-product that plagues Sonogashira reactions. This competing reaction is catalyzed by the copper salts<sup>156</sup> added as co-catalyst and it may be the major product if oxygen is not completely excluded from the reaction. Although the homocoupling reaction can be diminished by running the reaction under rigorous inert conditions and slow addition of the alkyne<sup>157</sup> to keep its concentration low in the reaction mixture, however, it cannot be eliminated completely.<sup>158</sup> In fact under the inert reaction conditions, the homo-coupled product is thought to be formed by initial reduction of the  $\text{Pd}^{\text{II}}(\text{L})_2(\text{Cl})_2$  precatalyst to generate the active catalytic complex  $\text{Pd}^0(\text{L})_2$ . The generally accepted active catalyst  $\text{Pd}^0(\text{L})_2$  is formed via transmetalation of an alkynyl copper, which is generated by the reaction of the amine base and  $\text{CuI}$ , followed by reductive elimination of the dialkynyl  $\text{Pd}^{\text{II}}$  species to give the active  $\text{Pd}^0(\text{L})_2$  and the alkyne dimer<sup>159</sup> (**Scheme 8**).

The homocoupled side product **38** was isolated and its  $^1\text{H}$  NMR spectrum along with molecular structure is given in **figure 35**. The spectrum possessed two doublets in the aromatic region like the

spectrum of its precursor terminal alkyne. Absence of the  $\text{C} \equiv \text{C}-\text{H}$  peak at 3.0 ppm showed the absence of free terminal alkyne moiety thus indicating formation of the homocoupled product. Furthermore, absence of the singlet around 4.3 ppm corresponding to hydrogens of the  $-\text{OCH}_3$  group and the peak integrations also indicated the product to be the homocoupled compound **38**.

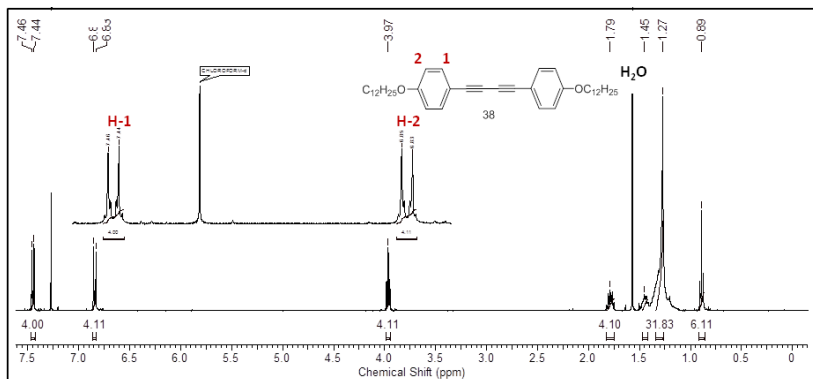


**Figure 35.**  $^1\text{H}$  NMR spectrum of the homocoupled side product **38** ( $\text{CDCl}_3$ , 400 MHz) after purification.

Pure fractions of the final compounds **18** - **23** obtained from the chromatographic columns were fully characterized by the  $^1\text{H}$  NMR,  $^{13}\text{C}$  NMR, FT-IR and CHNS analysis. The  $^1\text{H}$  NMR spectra of the target compounds are very similar to their precursor alkyne substrates in the aromatic regions. They differ, however, in the aliphatic region due to the presence of additional ethereal chains on the central heterocycles. On coupling to the electron deficient heterocyclic centers, the  $^1\text{H}$  NMR chemical shifts of the terminal aromatic rings (from alkyne intermediates) are shifted slightly downfield by 0.05 to 0.17 ppm and the  $-\text{OCH}_2$  peaks by 0.05 ppm. The  $^1\text{H}$  NMR peaks corresponding to the  $\alpha$  hydrogens of the ethereal chains on the heterocycles ( $-\text{OCH}_2$ ) are more influenced and shifted downfield by 0.25 to 0.3 ppm. In the final compounds **18** - **21**, the presence of two different types of aliphatic chains (i.e. the lateral chains on the central cores and the terminal chains on the benzene rings) were evidenced by the appearance of two distinct triplets around 4.4 and 4.0 ppm as shown in **figure 36**. Compounds **22** and **23** that possess a methoxy lateral group on the heterocycle,  $\alpha$

hydrogens of the lateral and terminal ethereal chains appeared as singlet and triplets respectively.

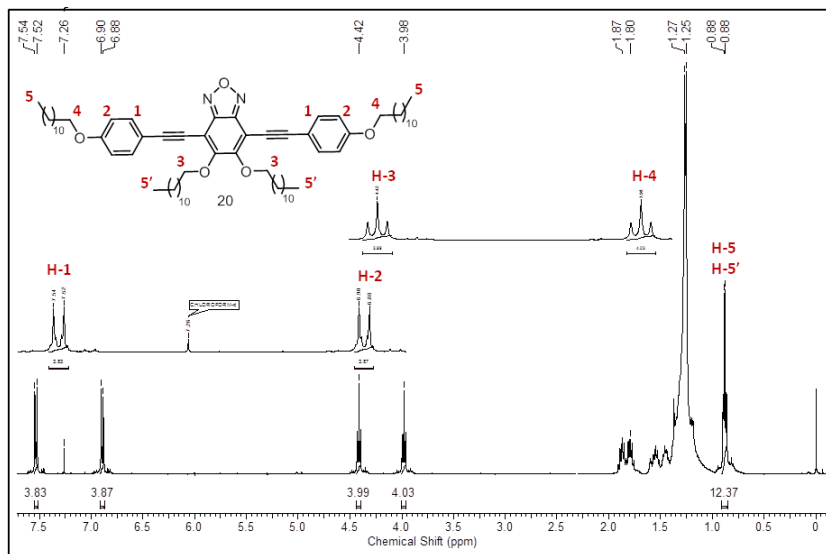


**Figure 36.**  $^1\text{H}$  NMR spectrum of compound **20** ( $\text{CDCl}_3$ , 400 MHz) with peaks assignments.

The presence of these two different aliphatic chains on the central heterocycles and on the terminal benzene rings was also confirmed in their  $^{13}\text{C}$  NMR spectra by the presence of two signals around 75 and 68-69 ppm referring to the  $-\text{OCH}_2$  carbons. In the final compounds, the  $^{13}\text{C}$  NMR peaks of the aromatic carbons are shifted slightly downfield by 1-2 ppm in comparison to their precursor intermediates. The  $^{13}\text{C}$  NMR peaks of the *sp* hybridized carbon atoms ( $\text{C} \equiv \text{C}$ ) that appeared around 84 and 76 ppm in the alkynes were also shifted downfield and appeared around 101 and 79-81 ppm. The  $^{13}\text{C}$  NMR spectrum of compound **20** is shown in **figure 37**. Only the non-aliphatic region is shown for better clarity. The  $^1\text{H}$  NMR and  $^{13}\text{C}$  NMR data of other compounds are presented in the experimental section.

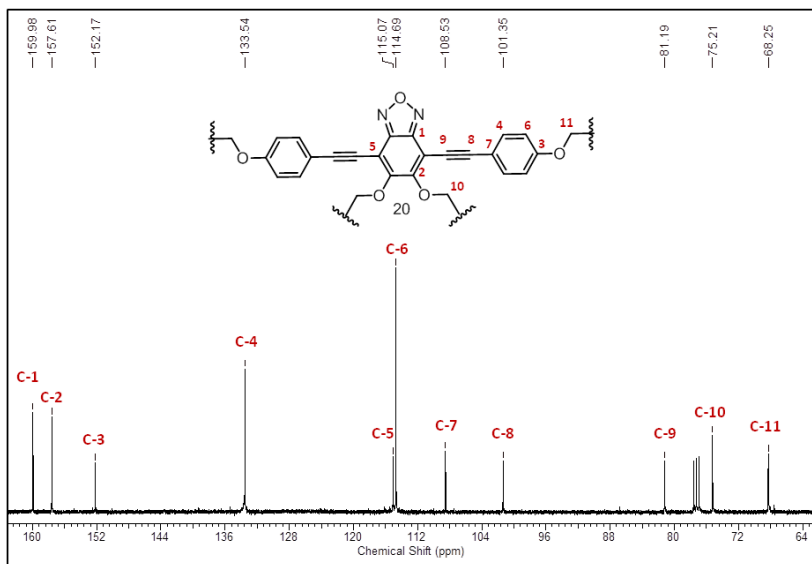


**Figure 37.**  $^{13}\text{C}$  NMR spectrum of the compound **20** ( $\text{CDCl}_3$ , 100 MHz) showing the important peaks in non-aliphatic region.

The FT-IR spectra of the final compounds **18-23** were found to be very similar. The IR spectrum of compound **23** is shown as representative model in **figure 38** while the IR data for other compounds are presented in the experimental section. The complete absence of sharp bands near the  $3310\text{ cm}^{-1}$  region, that were observed in the IR spectra of precursor alkynes for the  $\nu\text{C}\equiv\text{C-H}$  bond stretch, indicated the occurrence of the Sonogashira coupling. This was also indicated primarily by the appearance of intense luminescence in the reaction mixture. The bands in the  $2923$  to  $2853\text{ cm}^{-1}$  region for both the asymmetrical and symmetrical  $-\text{C-H}$  stretching of the methylene groups were almost un-affected. The sharp bands near to  $2108\text{ cm}^{-1}$ , referring to the  $-\text{C}\equiv\text{C}$ -stretching, were shifted to around  $2205\text{ cm}^{-1}$ .

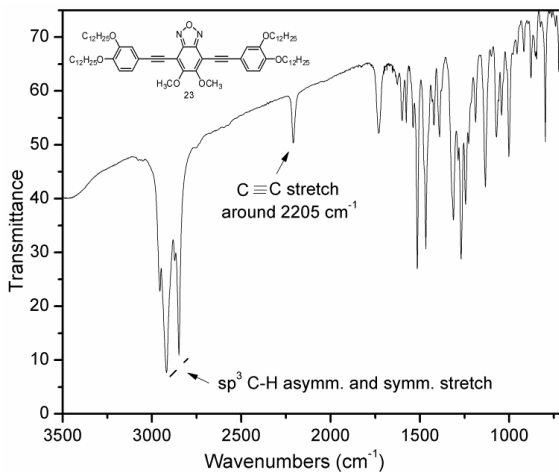


**Figure 38.** FT-IR spectrum (in KBr disc) of compound **23** as representative model for the final compounds **18-23**.

### 3.5. OPTICAL PROPERTIES

The whole series of compounds **18-23** was found to be intensely fluorescent and emit in the yellowish-green region of the visible spectrum under an UV light. To study influence of the molecular structure on their photophysical properties, their absorption and emission spectra were measured in dilute chloroform solutions using UV-absorption and fluorescence spectroscopic techniques. The measured wavelengths of their absorptions, excitations and emissions and their respective molar absorptivity coefficients ( $\epsilon$ ), Stokes shifts (nm) and fluorescence quantum yields ( $\Phi_f$ ) are presented in **table 1**.

**Table 1.** Photophysical data of the final compounds **18-23**.

Comp.	$\lambda_{abs}^{max}$ (nm) <sup>a</sup>	$\epsilon$ Lmol <sup>-1</sup> cm <sup>-1</sup>	$\lambda_{ex}^{max}$ (nm) <sup>b</sup>	$\lambda_{em}^{max}$ (nm) <sup>b</sup>	Stokes (nm) <sup>c</sup>	$\Phi_f^d$
<b>18</b>	429	19400	442	543	101	0.32
<b>19</b>	428	30200	440	535	95	0.32
<b>20</b>	429	26400	436	535	99	0.31
<b>21</b>	437	25200	449	552	103	0.28
<b>22</b>	426	18600	435	536	101	0.31
<b>23</b>	435	26000	448	555	107	0.27

<sup>a</sup> Absorption spectra were taken in solutions of  $5 \times 10^{-6}$  mol L<sup>-1</sup> in CHCl<sub>3</sub>.

<sup>b</sup> Irradiated with wavelengths corresponding to their respective low energy absorption bands.

<sup>c</sup> Stokes shifts =  $\lambda_{em}^{max} - \lambda_{ex}^{max}$

<sup>d</sup> Measured in CHCl<sub>3</sub>, using 4,7-bis(phenylethynyl)-2,1,3-benzothia-diazole ( $\Phi_f=0.37$ ) as the standard<sup>119</sup>

Due to similarities in their molecular structures, all the compounds showed very similar absorption patterns. As can be seen in **figure 39** which shows the UV-absorption spectra of the final compounds, all compounds showed bands with maximum absorptions ( $\lambda_{abs}^{max}$ ) between 426 and 437 nm. These bands possess high molar absorptivity coefficients ranging from 18600 to 30200 Lmol<sup>-1</sup>cm<sup>-1</sup> and appear due to the symmetry allowed  $\pi$ - $\pi^*$  transitions.

Length of the lateral flexible chains (on the heterocycles) showed negligible influence on the absorptions behaviour as can be seen by comparing the wavelengths of maximum absorptions of compounds **20** and **21** with those of compounds **22** and **23** respectively. Contrary to length of the lateral chain, the number of chains showed a greater effect on the absorption behaviour. The presence of additional -OC<sub>12</sub>H<sub>25</sub> chains on both the terminal aromatic rings in **21** and **23** caused a moderate red shift (8-9 nm) in the low energy absorption bands compared to compounds **20** and **22**. However, the same pattern was not observed in the case of their sulfur containing analogs **18** and **19**. Compared to the benzoxadiazole **21**, its sulfur-containing analogue **19** absorb at slightly shorter wavelength. This blue shift (of 9 nm) in the absorption may be attributed to a slightly diminished delocalization of the lone pair on sulfur atom towards nitrogen due to the difference in the sizes of the participating orbitals.

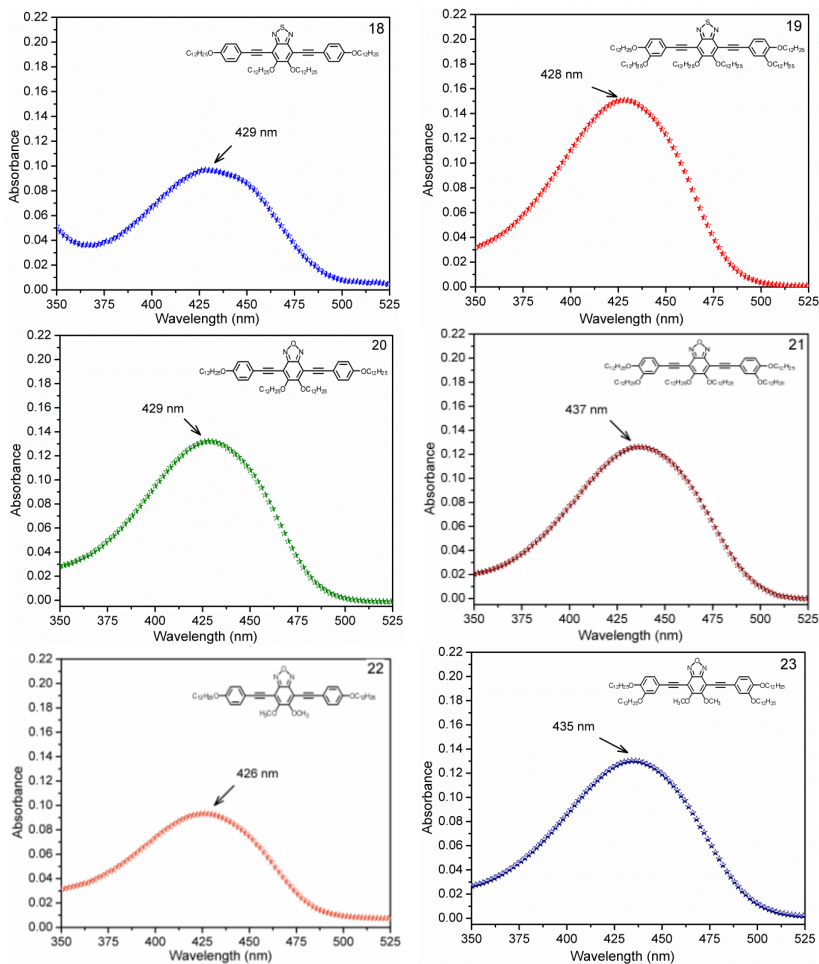


**Figure 39.** UV-vis absorption spectra of the fluorescent compounds **18-23** taken in  $5 \times 10^{-6}$  molar solutions in  $\text{CHCl}_3$ .

The chloroform solutions of all the final compounds of the series showed intense yellowish green (lime green) fluorescence. Their photoluminescence spectra showed wavelengths of the maximum emissions ( $\lambda_{em}^{max}$ ) between 535-555 nm. Their combined emission spectra and fluorescence image are shown in **figure 40**. They showed

reasonably high Stokes shifts in the range of 95-107 nm which results in only a small region of coincidence between energies of the absorption and emission. This finding suggests that re-absorption of the emitted light is almost negligible, which is very important in order to avoid undesired losses in the LED performance.

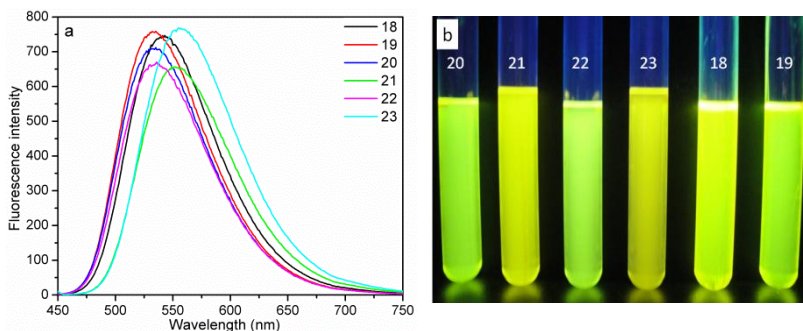


**Figure 40.** (a) Emission spectra of the compounds 18-23 obtained by excitation at their respective  $\lambda_{\text{max}}$  and (b) Photographs showing the fluorescence in chloroform solution under UV lamp ( $\lambda = 360\text{nm}$ ).

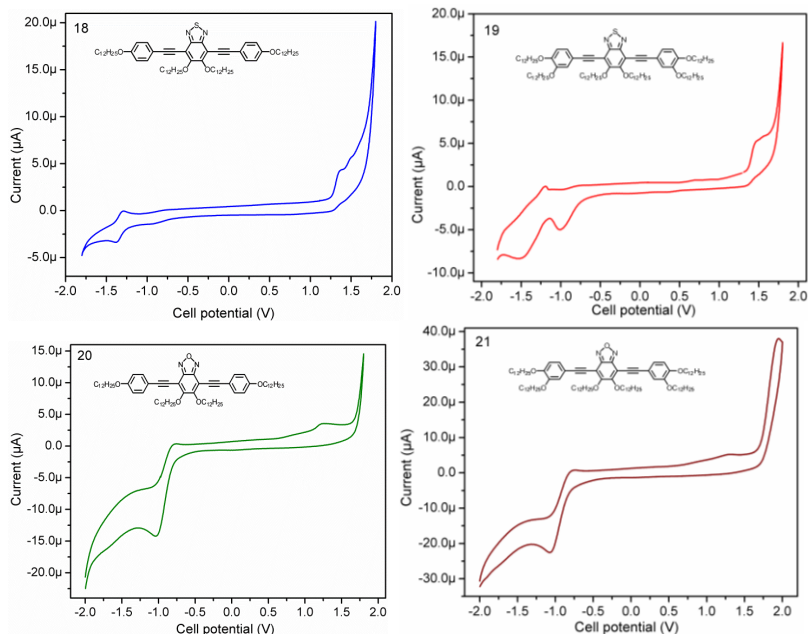
The fluorescence quantum yields were determined relative to the 4,7-bis(phenylethynyl)-2,1,3-benzothiadiazole ( $\Phi_f = 0.37$ ) in  $\text{CHCl}_3$  solutions according to the procedure described in the experimental section. A comparison of the calculated quantum yields showed the benzothiadiazole derivatives **18** and **19** to be slightly more efficient ( $\Phi_f = 0.32$ ) than the benzoxadiazoles ( $\Phi_f = 0.27 - 0.31$ ). However, this difference is negligible and within the range of experimental error. In the latter case, compounds **20** and **22** that possess two terminal chains showed slightly higher quantum yields than compounds **21** and **23** which possess four terminal chains. This finding can be rationalized by considering that in compounds **21** and **23**, relatively a greater fraction of the absorbed energy is lost non-radiatively due to more energy needed for conformational changes of the additional flexible chains.

Overall, the calculated fluorescence quantum yields are low-medium between 27% - 32%. These low to medium values can be rationalized by considering molecular structures of the compounds. Due to the presence of flexible alkoxy chains, the excited molecules require a considerable fraction of the absorbed energy for the conformational

changes of the chains and consequently the efficiency of fluorescence is decreased.

### 3.6. ELECTROCHEMICAL PROPERTIES

Electrochemical properties of the final compounds were studied using cyclic voltammetry. The experimental details are given in the experimental section. The cyclic voltammograms of all the six compounds are shown in **figure 41**. Due to their structural similarities, all the compounds showed very similar oxidation and reduction profiles within the available potential range of the dichloromethane solvent system.



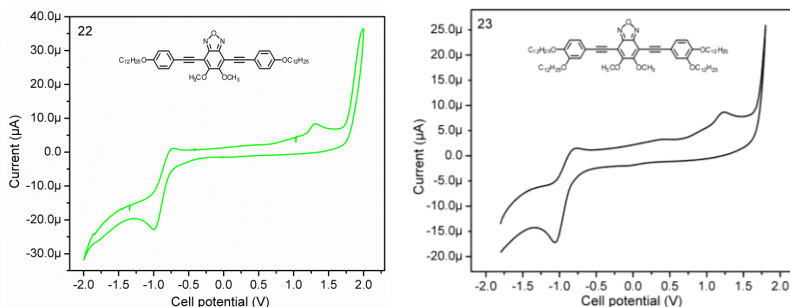


**Figure 41.** Cyclic voltammograms of the final compounds **18-23** obtained in their solutions in dichloromethane at the scan rate of 50 mV.s.<sup>-1</sup>

The onset potentials were determined from the intersection of two tangents drawn at the rising oxidation or reduction current and background current as shown in **figure 42**. To determine this point graphically, a straight line was extended from left to right along the linear portion of the initially flat curve, i.e. the cell current. Similarly, a line was drawn from the linear portion of the rising oxidation current. The onset potential was taken at the intersection of the extrapolated lines near the bottom of the steeply rising portion rather than the peak maximum.<sup>160,161</sup> For the reverse scan, the onset potential for the reverse process was taken at the intersection of the lines extrapolated in the reverse order compared to the forward scan.

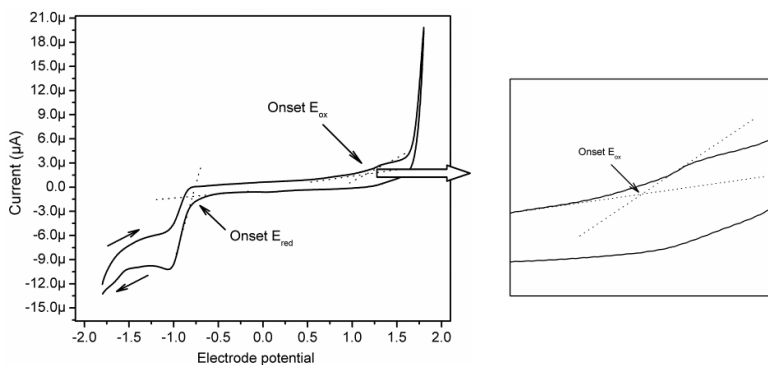


**Figure 42.** Determining the onset potentials in cyclic voltammogram for small current changes and wavy peaks.

As apparent from **figure 41**, the oxidative cycles exhibit single and irreversible waves rather than peaks between 1.07 to 1.36V vs. Ag/AgCl. The cathodic sweeps show single reduction peaks with reduction potentials between -0.78 and -1.29 V vs. Ag/AgCl. These results were used to assess the HOMO and LUMO energy levels and to calculate the electrochemical band gaps. For this purpose, initially both the oxidation and reduction potentials, measured originally relative to Ag<sup>+</sup>/AgCl reference electrode, were converted relative to the ferrocene–ferrocenium (FOC) redox couple (the internal reference) by considering the potential difference between FOC and Ag/AgCl in the same solutions.<sup>162</sup> Since the redox potentials ( $E_{ox}$ ,  $E_{red}$ ) were measured in solution and not in vacuum, the HOMO and LUMO energy levels (alternatively the IP and EA values respectively) were then estimated by relating the corrected anodic and cathodic potentials to the vacuum scale using the standard approximation that the Fc/Fc<sup>+</sup> HOMO level is - 4.8 eV.<sup>131,162</sup> with respect to the vacuum level (**Equ. 1, 2**). The band gap energy  $E_g$  was then calculated by taking the difference between ionization potential and electron affinity (equivalent to HOMO and LUMO energy levels respectively) according to **equation 3**. The estimated redox potentials, HOMO and LUMO positions together with the electrochemical bandgaps are summarized in **table 2**.

$$IP = E_{ox} + 4.8 \quad \text{or} \quad IP = -E_{ox} - 4.8 \quad (1)$$

$$EA = E_{red} + 4.8 \quad \text{or} \quad EA = -E_{red} - 4.8 \quad (2)$$

$$E_{gap} = EA - IP \quad (3)$$

**Table 2.** Electrochemical data and molecular orbital energies of the final compounds.

Compounds	$E_{\text{ox}}^a$	$E_{\text{red}}^a$	$E_{\text{HOMO}}^b$ (eV)	$E_{\text{LUMO}}^c$ (eV)	$E_{\text{gap}}^d$ (eV)
<b>18</b>	0.85	-1.72	-5.65	-3.08	2.57
<b>19</b>	0.93	-1.21	-5.73	-3.59	2.14
<b>20</b>	0.70	-1.24	-5.50	-3.56	1.94
<b>21</b>	0.80	-1.27	-5.60	-3.53	2.07
<b>22</b>	0.76	-1.22	-5.56	-3.58	1.98
<b>23</b>	0.64	-1.27	-5.44	-3.53	1.91

*a* All redox potentials are referenced to the Fc/Fc<sup>+</sup> redox couple.

*b*  $E_{\text{HOMO}} = (-4.8 - E_{\text{ox}})$ .

*c*  $E_{\text{LUMO}} = (-4.8 - E_{\text{red}})$ .

*d*  $E_{\text{gap}} = E_{\text{HOMO}} - E_{\text{LUMO}}$ .

### 3.7. THE $E_g$ , IP AND EA FROM OPTICAL ABSORPTIONS

The ionization potentials (IP) and electron affinities (EA) were also estimated from the optical bandgap energy ( $E_g^{\text{opt}}$ ) values which were, in turn, determined from the absorption spectra according to procedure described in the experimental section. Usually, the optical bandgap ( $E_g^{\text{opt}}$ ) of a compound is determined to help calculate the ionization potential or electron affinity in cases where these values cannot be obtained directly from the voltammetric data. For an analyte that undergoes only oxidation, the EA (and consequently the energy bandgap  $E_{\text{gap}}$ ) cannot be determined electrochemically. Similarly for analyte that undergoes only reduction, the IP and the  $E_{\text{gap}}$  cannot be determined directly. In the absence of direct measurement through CV, the EA is estimated<sup>163</sup> by subtraction of the optical gap energy  $E_g^{\text{opt}}$  from the IP (**Equ. 4**)<sup>161</sup> which is determined through the CV. Similarly, for the analyte that undergoes only reduction, the IP is calculated from the optical gap energy  $E_g^{\text{opt}}$  using **equation 5**. Equations 8 and 9,

however, give good estimates only when the electrochemical and optical band gaps are the same.

$$EA = IP - E_g^{opt} \quad (4)^{161}$$

$$IP = EA + E_g^{opt} \quad (5)^{160}$$

Values of the electron affinity, ionization potential and band gap determined from the electrochemical and optical absorption are presented in **table 3** for comparison purpose. Note that the negative of HOMO and LUMO energies (from table 2) are approximated as  $IP_{cv}$  and  $EA_{cv}$  respectively.<sup>164</sup> As apparent from the **table 3**, these values calculated from the optical and electrochemical methods are different from each other. The fact that the optical and electrochemical bandgaps can be different has already been reported in many cases<sup>165,166</sup> though in some cases they may be comparable.<sup>167,168</sup> This discrepancy in the estimated values is due to the difference in the energy processes contributing to the band gap estimations.<sup>169</sup> In the optical absorption method, usually energy at the longer wavelength region of the absorption band is revealed as the band gap. The position of this band is dictated by the molecular planarity and length of the conjugation. Cyclic voltammetry, on the other hand, provides band gap information based on the HOMO and LUMO energy levels on the sites of oxidation and reduction respectively. If the conjugation is extended over both the oxidation and reduction sites (i.e. the donor and acceptor segments are in complete conjugation), in redox process the electrons are extracted from or injected into the fully conjugated system. In such cases, the optical and electrochemical band gaps are comparable. On the other hand, structures in which the oxidation and reduction segments are discrete and the conjugation is not effectively extend over both these components, energies of the absorption and redox processes are different. Consequently, the HOMO–LUMO gap and the optical band gap values are not the same i.e. the optical and electrochemical band gap should not converge.<sup>170</sup>

**Table 3.** Values of the ionization potentials, electron affinities and energy band gaps estimated from cyclic voltammetric and optical absorption methods.

Compound	$E_g^{cv}$	$E_g^{opt}$	$IP_{cv}^a$	$IP_{opt}^b$	$EA_{cv}^c$	$EA_{opt}^d$
<b>18</b>	2.57	2.54	5.65	5.62	3.08	3.11
<b>19</b>	2.14	2.55	5.73	6.14	3.59	3.18
<b>20</b>	1.94	2.56	5.50	6.12	3.56	2.94
<b>21</b>	2.07	2.50	5.60	6.03	3.53	3.10
<b>22</b>	1.98	2.55	5.56	6.13	3.58	3.01
<b>23</b>	1.91	2.50	5.44	6.03	3.53	2.94

$$^a E_{HOMO} \cong IP^{[163,164]}$$

$$^b IP = EA + E_g^{opt[160]}$$

$$^c E_{LUMO} \cong EA^{[64]}$$

$$^d EA = IP - E_g^{opt[161]}$$

In case of compounds **18** - **23**, though various canonical forms may be drawn, none of them possess a complete conjugation of the whole unsaturated system. **Figure 43** shows the two most favorable canonical forms of the target compounds in a generalized fashion. Of them, the resonance form A is less stable due to more charge separation and presence of the cumulated unsaturated bonds and is the minor contributor. The two equivalent canonical forms B and B' are, however, more stable due to aromaticity of the central heterocycle, less charge separation and are the major contributors to the real structure. Since there is no complete conjugation between all the molecular segments, the IPs, EAs, and energy band gaps determined by the voltammetric and optical methods are different.

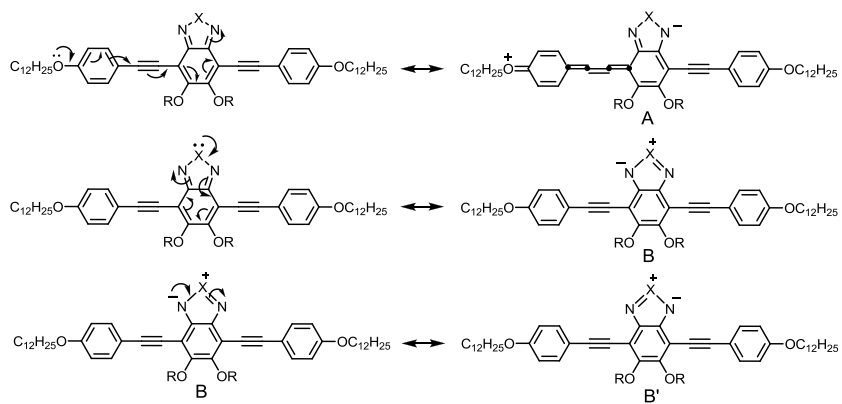


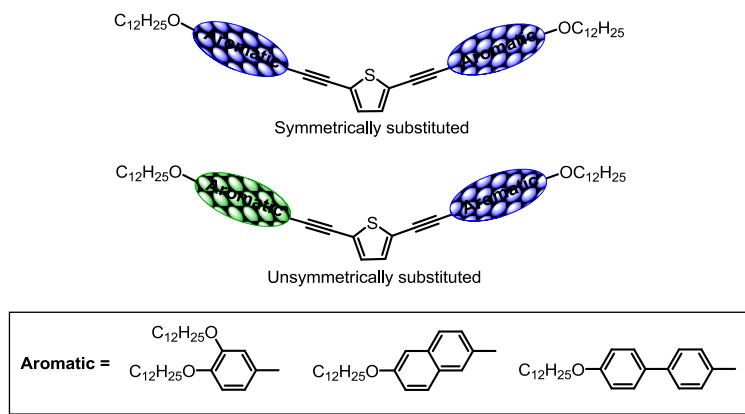
**Figure 43.** Resonance in the final compounds.

**Part B:**

3.8. Syntheses and Characterization of Thiophene Based Luminescent Liquid Crystals.

## 3.9. MOLECULAR DESIGN OF THE TARGET COMPOUNDS

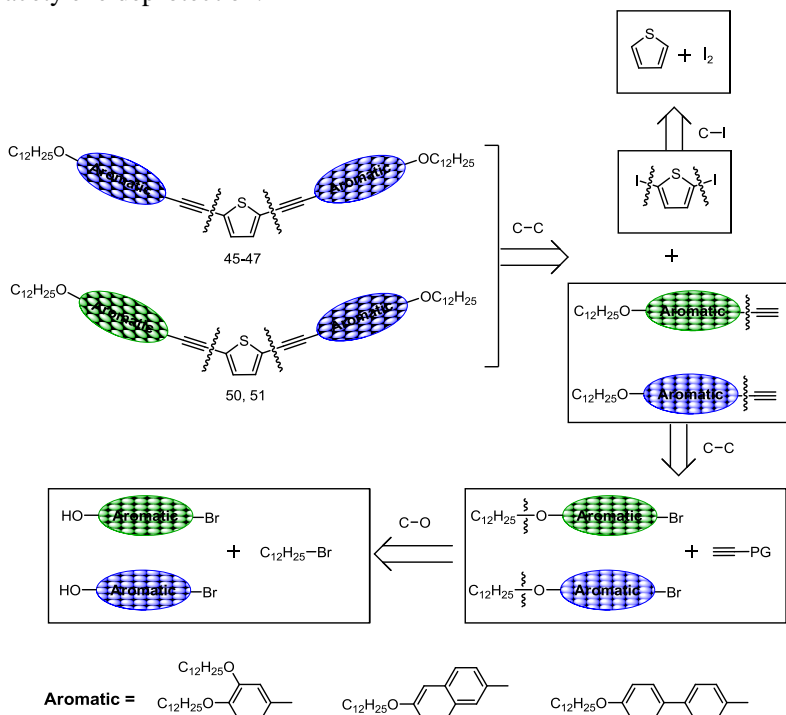
**Figure 44** shows representative structures of the designed molecules with potential as luminescent liquid crystals. These molecules were rationally designed by selecting a suitable core fragment, linking group and terminal groups to ensure observation of luminescence as well as mesomorphism. The compounds were designed with two arms (symmetrical or unsymmetrical) about the thiophene ring. In order to study the effect of structure on optical and mesomorphic properties, different aromatic moieties (benzene, naphthalene and biphenyl) were selected to lengthen the rigid center and the conjugation length. These aromatic moieties were linked to the thiophenic core through a  $-C\equiv C-$  bond to produce a conjugated structure. In addition to varying the length of the rigid core, the number of flexible alkoxy chains were also varied to find the influence on the observed properties.



**Figure 44.** Representative structures of the designed luminescent liquid crystals.

## 3.10. SYNTHETIC PLAN

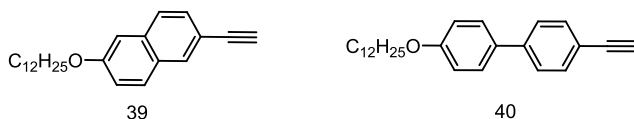
The preliminary retrosynthetic analysis of the target compounds is shown in **figure 45**. The target molecules can be achieved by connecting the terminal alkynes to the 2,5-diiodothiophene through C–C bond formation. The 2,5-diiodothiophene can be prepared by iodination at positions 2 and 5 that are more reactive (towards electrophilic aromatic substitution) than positions 3 and 4. The terminal aromatic alkynes can be prepared through a sequence of reactions including Williamson etherification, Sonogashira cross coupling and acetylene deprotection.



**Figure 45.** General retrosynthetic analysis of the bent shaped luminescent compounds.

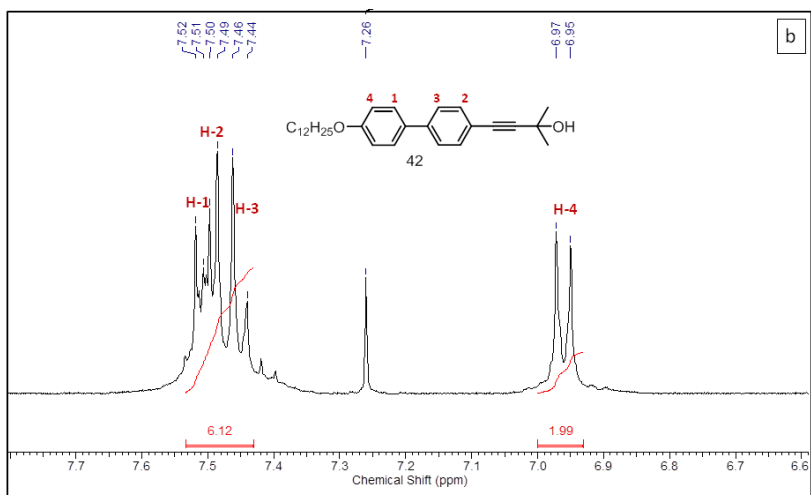
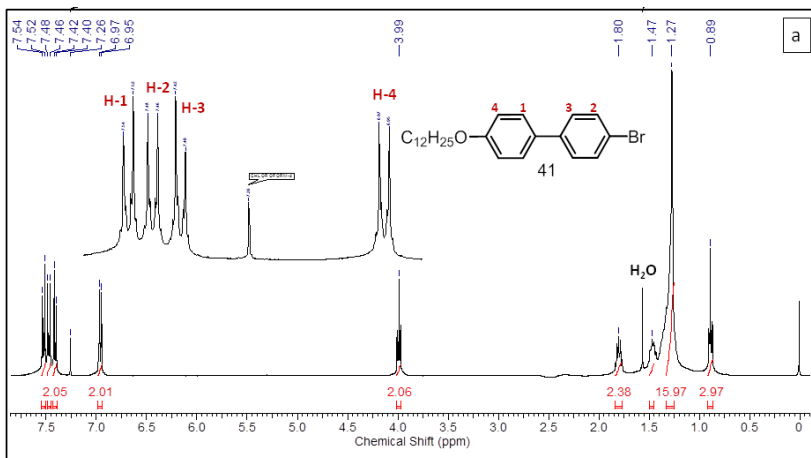
## 3.10.1. Synthesis of The Terminal Alkynes

The naphthalene and biphenyl based terminal alkynes **39**, **40** were prepared via the same synthetic steps through which the compounds **16** and **17** were prepared. The 4-bromo-4'-(dodecyloxy)biphenyl **41** was prepared in one pot from the available 4-bromo-[1,1'-biphenyl]-4-ol acetate. First the hydroxyl group was liberated by saponification of the ester group with NaOH then followed by etherification of the liberated hydroxyl in the same pot.



**Figure 46.** Molecular structures of the terminal alkynes **39** and **40**.

During the preparation of intermediate **40**, a gradual collapse of the <sup>1</sup>H NMR peaks was observed in the aromatic region. <sup>1</sup>H NMR spectrum of the precursor compound **41** (**Fig. 47a**) showed four well defined doublets in the aromatic region as expected for the biphenyl unit. Of them, three closely spaced doublets are located downfield to the chloroform and an isolated upfield doublet. After insertion of the acetylenic moiety, the compound **42** showed a second order <sup>1</sup>H NMR spectrum in the aromatic region with the three closely spaced doublets partially overlapped (**Fig. 47b**). Upon deprotection of the acetylenic group, this second order pattern was enhanced further and the aforementioned doublets appeared as a multiplet (6H integrals) due to greater overlap of the peaks (**Fig. 47c**).



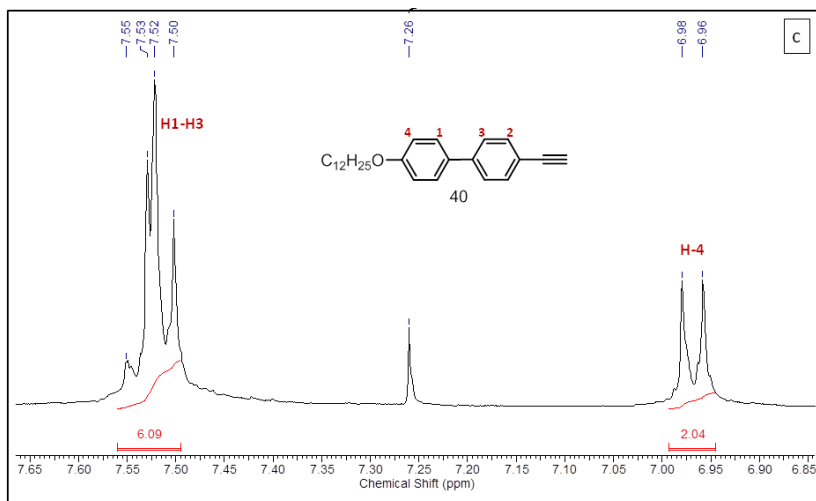
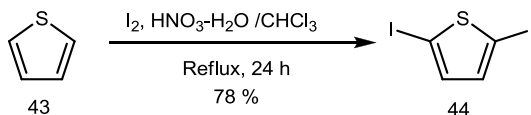


**Figure 47.**  $^1\text{H-NMR}$  (400 MHz,  $\text{CDCl}_3$ ) spectra of compounds **41**, **42** (aromatic region) and **40** (aromatic region) showing gradual emergence of the second order pattern during the course of  $-\text{C}\equiv\text{C}-$  insertion.

### 3.10.2. Synthesis and Characterization of The Final Compounds

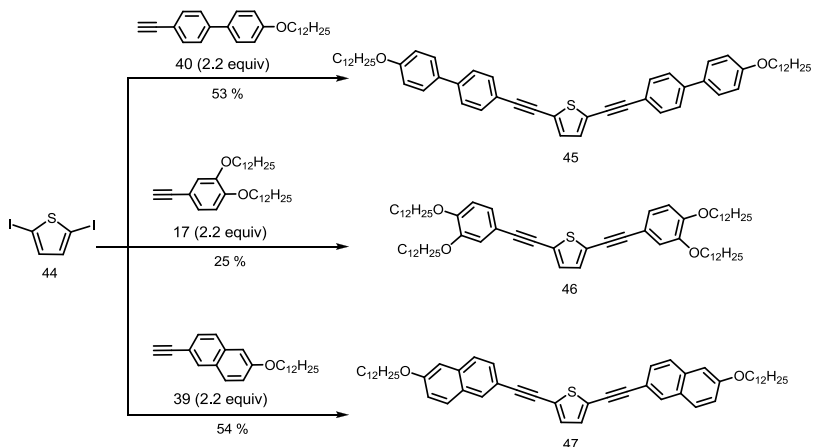
In the case of thiophene based compounds too, the same synthetic strategy of using Sonogashira cross-coupling of the separately prepared terminal acetylenes (**17**, **39**, **40**) with the 2,5-diiodothiophene as the final step was applied. The 2,5-diiodothiophene intermediate **44** was formed in a single step by iodination of the thiophene as shown in **scheme 10**.



**Scheme 10.** Synthesis of the 2,5-diiodothiophene.

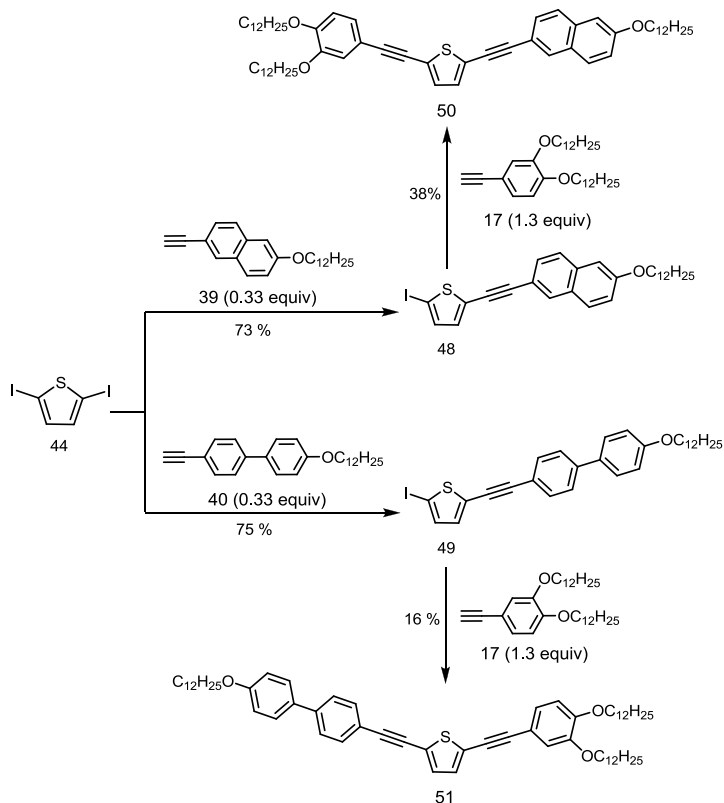
The symmetrical products (**45** - **47**) were obtained by using 2.2 equivalents of the terminal acetylenes (**Scheme 11**). Compounds **45** and **49** containing the biphenyl unit was sparingly soluble in a vast range of organic solvents such as  $\text{CDCl}_3$ ,  $\text{DMSO-d}_6$ ,  $\text{acetone-d}_6$ . The low

solubility makes their structural analysis difficult and they were characterized only by the  $^1\text{H NMR}$  spectra.



**Scheme 11.** Syntheses of the bent shaped symmetrical compounds. Conditions:  $\text{Pd}(\text{PPh}_3)_2\text{Cl}_2$ ,  $\text{PPh}_3$ ,  $\text{CuI}$ ,  $\text{Et}_3\text{N}$ ,  $80-85^\circ\text{C}$ , 12-14h.

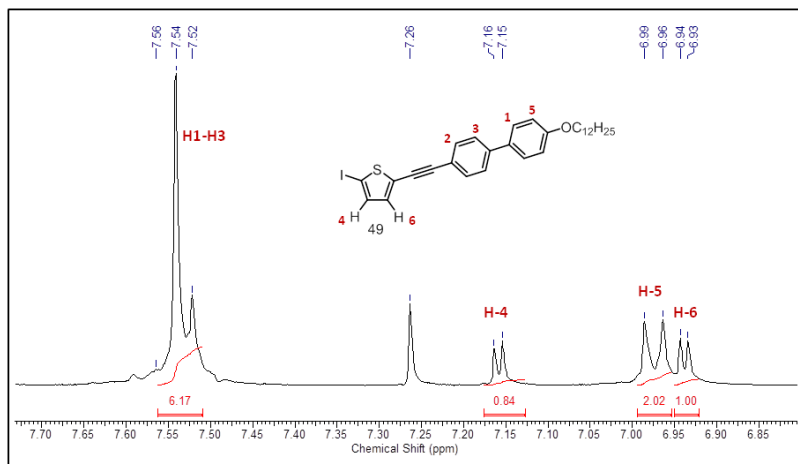
For the asymmetrical compounds, first the mono-coupling products (**48**, **49**) were formed by using the acetylenes as limiting reactants and 2,5-diiodothiophene in excess (**Scheme 12**). This stoichiometry lead to the mono-coupled compounds **48** and **49** as the major products and the excessive unreacted 2,5-diiodothiophene was easily separated on silica gel column.



**Scheme 12.** Syntheses of the bent shaped asymmetrical compounds. Conditions:  $\text{Pd}(\text{PPh}_3)_2\text{Cl}_2$ ,  $\text{PPh}_3$ ,  $\text{CuI}$ ,  $\text{Et}_3\text{N}$ ,  $80\text{--}85^\circ\text{C}$ , 12–14h.

Formation of the mono-coupled intermediates **48** and **49** was confirmed by their  $^1\text{H}$  NMR spectra which showed two distinct doublets around 7.16 and 6.94 ppm for each of the thiophene hydrogens. The aromatic region of the  $^1\text{H}$  NMR spectrum of compound **49** is shown in **figure 48**. This was also indicated by the quenching or complete absence of luminescence due to the presence of Iodine which is a well known fluorescence quencher. Next, the mono-coupled products were coupled with a different acetylenic intermediate to furnish the asymmetrical products (**50**, **51**). In these cases also, 1,3-diyne were formed as byproducts of the competing homocoupling reactions making purifications of the final compounds difficult. One of the homocoupled

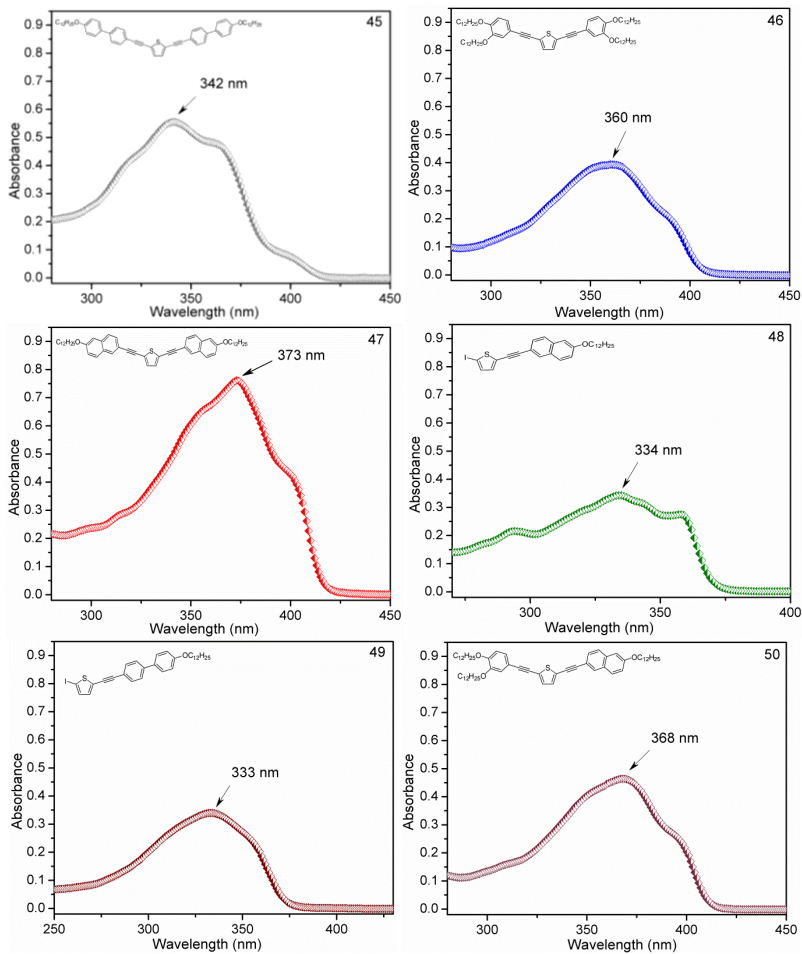
byproduct 1,4-bis(6-(dodecyloxy)naphthalen-2-yl)buta-1,3-diyne **52** was isolated and its  $^1\text{H}$  NMR spectrum along with molecular structure is given in the experimental section. The experimental details and spectral data of all the other intermediates and final compounds are given in the experimental section.



**Figure 48.**  $^1\text{H}$  NMR spectra of the mono-coupled intermediate **49** (400 MHz,  $\text{CDCl}_3$ ) showing two distinct doublets around 7.16 and 6.94 ppm for the thiophenic hydrogens.

## 3.11. OPTICAL PROPERTIES

The ultraviolet-visible absorption spectra of compounds **45** - **51** measured in their chloroform solutions is shown in **figure 49**. The corresponding results are listed in **table 4**.



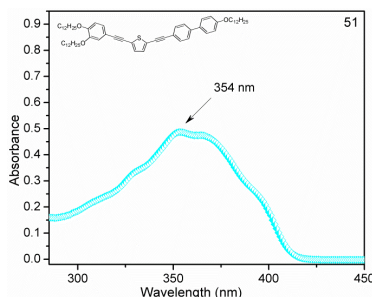


**Figure 49.** UV-vis absorption spectra of compounds **45** - **51** taken in  $1 \times 10^{-5}$  molar solutions in  $\text{CHCl}_3$ .

Compounds **47** and **50** containing the naphthalene group were shown to absorb at longer wavelengths. This is due to extended and efficient conjugation of the naphthalenic groups. Compared to the naphthalene unit, the presence of biphenyl unit caused a blue shift of the absorption wavelength. For example, compounds **45** and **51**, that differ from **47** and **50** (respectively) in the sense that the naphthalene is replaced by the biphenyl unit, absorbed at much shorter wavelengths. This indicates less efficient conjugation in **45** and **51**. The monocoupled products **48** and **49** absorb at much shorter wavelengths as expected.

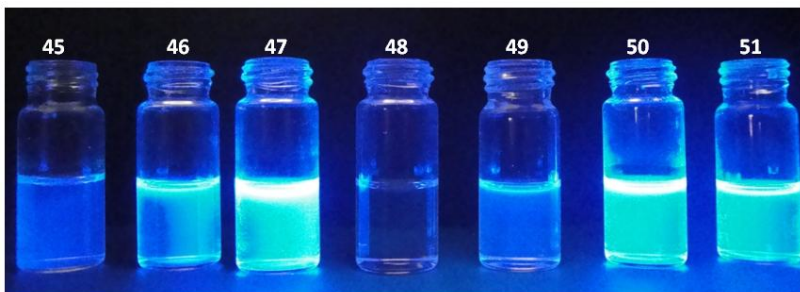


**Figure 50.** Photograph showing the fluorescence in chloroform solution under UV lamp ( $\lambda = 360\text{nm}$ ).

All the products were shown to emit in the blue region of visible spectrum when their solutions in chloroform were irradiated with ultraviolet radiations. **Figure 50** shows the fluorescence photograph of these compounds. Note that the monocoupled compounds **48** and **49** showed low fluorescence due to the presence of iodine, a well known

fluorescence quencher. The fluorescent quantum yields were determined relative to quinine sulfate used as the standard. **Table 4** summarize results of the absorption and emission studies and relative quantum yields of the final compounds.

**Table 4.** Photophysical data of the final compounds.

Comp.	$\lambda_{abs}^{max}$ (nm) <sup>a</sup>	$\epsilon$ Lmol <sup>-1</sup> cm <sup>-1</sup>	$\lambda_{ex}^{max}$ (nm) <sup>b</sup>	$\lambda_{em}^{max}$ (nm) <sup>b</sup>	Stokes (nm) <sup>c</sup>	$\Phi_f^d$
<b>45</b>	342	55500	345	404	59	0.48
<b>46</b>	360	39400	358	405	47	0.34
<b>47</b>	373	76200	370	409	39	0.56
<b>50</b>	368	46400	365	408	43	0.29
<b>51</b>	354	48700	361	411	50	0.26

<sup>a</sup> Absorption spectra were taken in solutions of  $1 \times 10^{-5}$  mol L<sup>-1</sup> in CHCl<sub>3</sub>.

<sup>b</sup> Irradiated with wavelengths of their respective low energy absorption bands.

<sup>c</sup> Stokes shifts =  $\lambda_{em}^{max} - \lambda_{ex}^{max}$

<sup>d</sup> Relative to quinine sulfate (in 1 N H<sub>2</sub>SO<sub>4</sub>,  $\Phi_f = 0.546$ ) as the standard.

### 3.12. MESOMORPHIC AND THERMAL PROPERTIES

The mesophases for these compounds were identified by polarized optical microscopy upon cooling from the isotropic phase and the phase transition temperatures were determined using differential scanning calorimetry. Furthermore, thermal stability of the compounds were investigated using thermogravimetric analysis. The results of DSC coupled with POM and TGA are summarized in **table 5**.

The TGA analysis reveals that under the protection of an inert atmosphere, the final compounds show good thermal stabilities with decomposition temperatures between 292 - 396 °C. As evident from the table, change in the length of the rigid core results in very interesting thermal properties. The general pattern showed that increasing the length of the rigid part of the molecule increased the tendency to form a liquid crystalline phase. For example, compound **46** that contains two terminal benzene rings have the smallest molecular length among the

final compounds and it did not show any mesomorphism. However, molecular length is not the only reason and the fact that **46** did not show any mesophase is also partially attributed to its greater flexibility, since an analogous compound with only two flexible dodecyloxy chains have been reported to present mesophase.<sup>171</sup> Although compound **50** possesses a slightly extended molecular length than compound **46** as one of the terminal benzenes is replaced by the naphthalene unit, it still did not possess an adequate balance between the molecular rigidity and flexibility and no mesophase formation was observed in POM and/or DSC.

**Table 5.** Thermal behaviour of the symmetrical and asymmetrical final compounds

Compound	Transitions	T ( $\Delta H$ ) <sup>a,b</sup> Heating	T ( $-\Delta H$ ) <sup>a,b</sup> Cooling	T <sub>dec</sub> <sup>c</sup>
<b>45</b>	<i>d</i>	-	-	396
<b>46</b>	-	-	-	305
<b>47</b>	Cr - N	130.2 (39.5)	-	388
	N - I	169.0 (1.7)	-	
	I - N	-	166.4 (2.4)	
	N - Cr	-	115.2 (40.8)	
<b>50</b>	-	-	-	297
<b>51</b>	Cr - Cr'	81.8 ( <i>e</i> )	-	292
	Cr' - SmC	85.4 (26.6)	-	
	SmC - I	125 <sup>f</sup>	-	
	I - SmC	-	123 <sup>f</sup>	
	SmC - Cr'	-	-60.1 (29.7)	
	Cr' - Cr	-	54.1 ( <i>e</i> )	

<sup>a</sup> Determined by the POM and DSC measurements<sup>b</sup>  $\Delta H$  Units: KJ mol<sup>-1</sup><sup>c</sup> Determined by TGA, the values are taken at the 5% decomposition in inert atmosphere<sup>d</sup> DSC indicate the presence of impurities<sup>e</sup> Overlapped with mesophase transition peak<sup>f</sup> Observed by POM but not detected in DSC measurements

It was envisioned that either an extension of the molecular rigidity or a diminution of the number or length of the flexible chains or a combination of both will possibly lead to the formation of mesophase. The molecular length was extended further in compound **47** by substituting both the active positions on thiophene (through  $-\text{C} \equiv \text{C}-$  linking group) with the naphthalenic units. Furthermore, compound **47** possesses only two chains and consequently, it presented mesophase.

The POM of compound **47** showed a nematic mesophase between 129 and 168 °C with a broad mesophase range of 39 °C. The mesophase was identified to be nematic as indicated by the appearance of spherical droplets on cooling from the isotropic melt (**Fig. 51a**), which on further cooling developed into a Schlieren texture as shown in **figure 51b**.

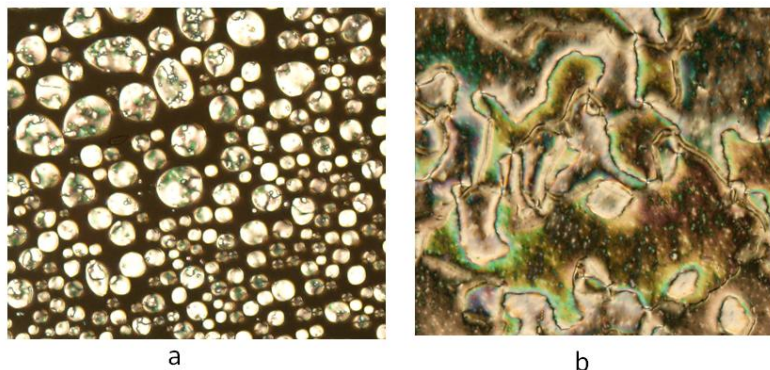


**Figure 51.** POM photographs of compound **47** on cooling (I → N) at 3 °C/minute: (a) Appearance of spherical droplets at 166.6 °C (magnification 10 x 10); (b) Schlieren texture of a nematic phase at 135.8 °C (magnification 10 x 10).

The confirmation for this phase was supported by a DSC peak in the heating and cooling cycles and enthalpy changes on the DSC thermogram. The DSC thermogram (**Fig. 52**) showed appearance of small peaks around 70 - 75 °C both on cooling and heating probably due to pre- and post-translational arrangements. The intense peak at 130.15 °C in the heating cycle corresponds entrance to the nematic mesophase. The transitions of nematic phase to the isotropic melt and vice versa were marked by very small peaks at 169.0 °C and 166.4 °C respectively. Unlike the POM observation which indicated a direct N-Cr transition, the cooling cycle in DSC showed that the transition is not direct and the crystallization is preceded by a closely located metastable (short lived) mesophase.

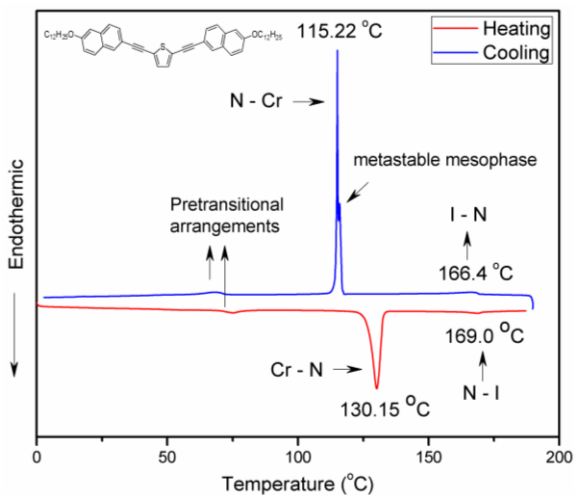


**Figure 52.** Differential scanning thermogram of compound **47** as a function of temperature for the second heating and cooling cycles (at scan rate  $10\text{ }^{\circ}\text{C min}^{-1}$ ).

Compound **51** which possesses a single biphenyl unit, and hence is longer than the compound **50**, have also shown mesomorphism. Cooling from the isotropic melt, the POM showed appearance of the bâtonnets (**Fig. 53a**) which indicate the formation of a Sm phase.<sup>66</sup> On further cooling, the Sm bâtonnets grew anisotropically until they nucleated to give a fan shaped texture of the Sm C phase and is shown in **figure 53b**. At this point, the sample slide was removed from the heating stage and the upper glass lamina was slightly displaced by rubbing quickly such that part of the sample remain uncovered from the top. Under the POM, this uncovered part presented Schlieren like texture (**Fig. 53c**) which affirm identity of the mesophase as the SmC phase.

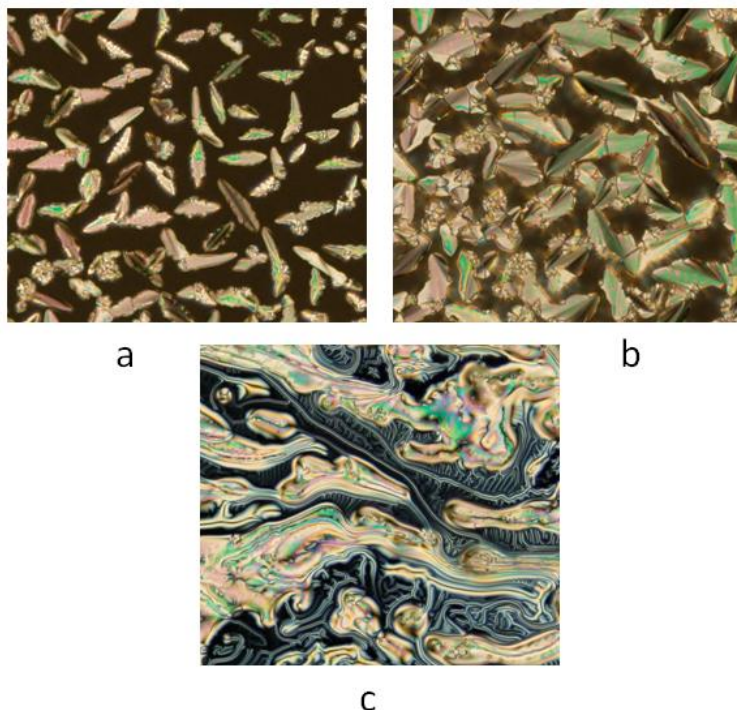


**Figure 53.** POM photographs of compound **51** on second cooling (I  $\rightarrow$  SmC) at 3 °C/minute : (a) batonnet texture at 92 °C (magnification 10 x 10); (b) fan shaped texture of SmC phase at 86.5 °C (magnification 10 x 10); (c) Appearance of a Schlieren texture of the SmC phase after rubbing the glass lamina at 80 °C (magnification 10 x 10).

The POM observations for compound **51** were supported by the DSC thermogram which is shown in **figure 54** below. The intense peak at 85.4 °C in the heating cycle corresponds entrance to the SmC mesophase. The appearance of a shoulder at 81.8 °C indicates that a Cr-Cr' transition peak is overlapped with Cr'-SmC transition. The same transitional pattern was observed in the cooling cycle. Transitions of smectic phase to the isotropic melt and vice versa were not observed in the DSC experiments even in experiments in which more sample was used and the temperature was changed at higher (20 °C min<sup>-1</sup>) and lower (5 °C min<sup>-1</sup>) change rates. The values shown for these transitions in **table 5** are the ones obtained from the POM.

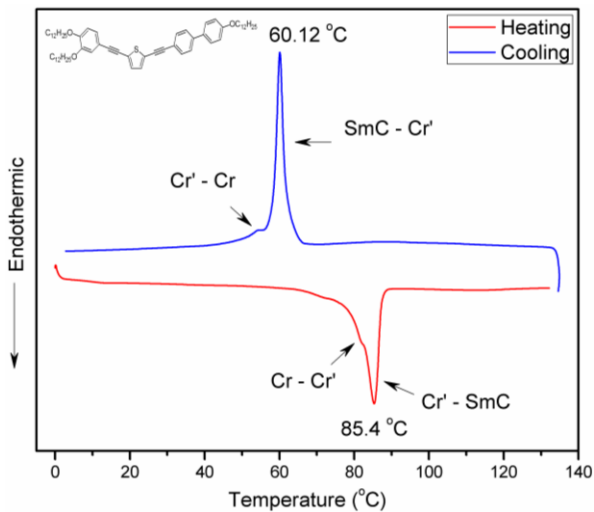


**Figure 54.** Differential scanning thermogram of compound **51** as a function of temperature for the second heating and cooling cycles (at scan rate 10 °C min<sup>-1</sup>).

#### 4. CONCLUSIONS

Two series of compounds were successfully synthesized using the Sonogashira cross-coupling as the key synthetic step. A common feature of all the compounds of both the series is the presence of a planar and highly conjugated rigid center and the presence of several flexible alkoxy chains. The first series consists of luminescent compounds containing 2,1,3-benzoxadiazole and 2,1,3 benzothiadiazole heterocycles as the central units to which benzene rings with varying number of flexible alkoxy chains were connected through  $-C \equiv C-$  bonds. Nature of the central heterocycle and length of the lateral alkoxy chains (directly attached to the heterocycle) did not show a significant influence on the absorption and emission behavior. However, the number of terminal alkoxy chains attached to the terminal benzenes showed a moderate effect on the absorption behaviour. Connecting the central heterocycle to the benzene rings through the  $-C \equiv C-$  linking group resulted in extension of the conjugation and consequently, these compounds showed yellowish-green fluorescence with fluorescence quantum yields ( $\Phi_f$ ) between 27 to 32 %. Theirs absorption and emission spectra showed only a small region of coincidence between them and high Stokes shifts of 95 - 107 nm. Although compounds of this series possess rigid as well as flexible groups making them eligible to be liquid crystals, none of them presented mesomorphism. Cyclic voltammograms of all compounds of this series possess single oxidation and reduction peaks. Calculations based on the voltammetric and optical measurements revealed the presence of small band gaps (1.91 to 2.57 eV) between their HOMO and LUMO energy levels making them attractive candidates for potential use in solar cells and OLEDs.

In the second series, aiming at the synthesis of fluorescent liquid crystals, compounds containing thiophene as the central core were successfully synthesized. As in the previous series, the Sonogashira cross-coupling was used as the key synthetic step in these synthetic routes as well. The molecular lengths and the degree of conjugation were varied through the use of benzene, naphthalene and biphenyl groups and their effects on the optical, thermal and mesomorphic properties were determined. All the final compounds showed good thermal stabilities with decomposition temperatures between 292 - 396 °C. Their photophysical parameters were measured in chloroform solutions. The optical absorptions were influenced by the length of the

conjugation as was expected. Their solutions in chloroform showed strong blue fluorescence with good quantum yields of 26 to 56 % relative to quinine sulfate. The Stokes shifts determined for these compounds were between 39 to 66 nm. The preliminary results showed a general pattern that increasing the length of the rigid part of the molecule increased the tendency to form a liquid crystalline phase. Another general conclusion that can be drawn from these results is that increase in the molecular length also enhanced the thermal stability of the mesophases. This is due to increased rigidity which facilitates a better orientational order and molecular packing in the mesophases.

## **5. EXPERIMENTAL DETAILS**

## 5.1. GENERAL MATERIALS

4-Bromophenol 97%, 1-bromododecane 98%, methyl iodide and thionyl chloride 97% were purchased from Sigma-Aldrich; catechol 99%, 2-methyl-3-butyn-2-ol 98% and tin (II) chloride dihydrate were purchased from Acros Organics and used as received. N-bromosuccinimide was recrystallized from water (10mL H<sub>2</sub>O per 1 g of NBS) prior to its use. Toluene and dimethylformamide were dried over activated molecular sieves. Triethylamine was dried by heating under reflux in the presence of KOH and subsequent distillation. The progress of the reactions was monitored using thin-layer chromatography. The intermediates were purified either by recrystallization in commercial grade solvents or via column chromatography on silica-gel 60-200 (mesh 60A). The final compounds were purified by column chromatography using flash silica gel. Preliminary purity tests were performed by developing thin layer chromatographs using silica-gel Si 60-F254 TLC plates purchased from Merck.

## 5.2. INSTRUMENTATION AND METHODS

### 5.2.1. Structural Characterizations

Melting points were determined with an Olympus BX50 microscope equipped with a Mettler Toledo FP-82 hot stage. <sup>1</sup>H and <sup>13</sup>C NMR spectra were recorded on a Varian Mercury Plus spectrometer operating at 400 and 100.6 MHz, respectively. The data for <sup>1</sup>H NMR spectra are reported as: chemical shift, multiplicity (s = singlet, d = doublet, dd = doublet of doublet, t = triplet, q = quintet, b = broad and m = multiplet), integration and coupling constant (Hz). Fourier transform infrared spectra were recorded with a Varian 3100 FT-IR Spectrometer in the spectral region of 600-4000 cm<sup>-1</sup>. The IR spectra are reported as neat in the cm<sup>-1</sup> units. Mass spectra were obtained using Bruker APCI/MS/MS Ion Trap mass spectrometer.

### 5.2.2. Optical Analyses

UV-Vis and fluorescence spectra were recorded in HPLC grade Chloroform. All of the UV-Vis absorption spectra and extinction

coefficients were measured on a Hewlett-Packard 8453 diode array spectrophotometer using standard 1 cm width quartz cells. Emission spectra were obtained on Cary Eclipse Varian s (Dr. Haidi Fiedler's laboratory) and Hitachi F-4500 (Dr. Edson Minatti's laboratory) spectrofluorimeters located in the Department of Chemistry, Federal University of Santa Catarina. For calculations of the Stokes shifts, first the emission spectra were taken by irradiating each compound at the wavelengths of their respective lowest-energy absorption bands. The emission wavelengths were then used for excitations. The quantum yields were determined relative to the 4,7-bis (phenylethynyl) -2,1,3-benzothiadiazol ( $\Phi_f = 0.37$  in chloroform) and quinine sulfate in 1 N  $\text{H}_2\text{SO}_4$  ( $\Phi_f = 0.546$ ) as the standard.

Since the inner filter effects reduce the fluorescence intensity at high concentrations of the fluorescent compound, the quantum yields were determined using dilute solutions. Initially, concentrations of both the sample and reference compounds were adjusted such that they exhibit the same absorbance at a particular wavelength. For accurate quantum yield measurements, the absorbance was kept around 0.044. Since such a low absorption cannot be measured without error, first the product was dissolved and the absorbance of the solution was adjusted to around 0.44 and then this solution was diluted by a factor of 10 to get a solution with absorbance of 0.044.<sup>172</sup> The area of each emission spectrum was integrated and the fluorescence quantum yields were calculated by using **equation 6**.

$$\Phi_f = \Phi_s \times \left( \frac{A_s}{A_x} \right) \left( \frac{F_x}{F_s} \right) \left( \frac{n_x^2}{n_s^2} \right) \quad (6)$$

where  $\Phi_f$  is quantum yield of the fluorescence process and the subscripts  $x$  and  $s$  denote the unknown and standard samples respectively.  $A$  is the absorbance at the excitation wavelength,  $F$  is the integrated emission intensity and  $n$  is the refractive index of the solvent used.

### 5.2.3. Determination of The Optical Bandgaps

The optical bandgap ( $E_g^{opt}$ ) energy values were calculated from the absorption band edge (absorption onsets) rather than the peak maxima. The absorption onsets were determined by the most widely

accepted procedure in which the line of maximum slope at the low energy absorption edge is extrapolated till it crosses the corrected baseline as shown in **figure 55**. The wavelength at the point of intersection was retrieved as the bandgap energy after converting the  $\lambda$  to energy units using **equation 7**.

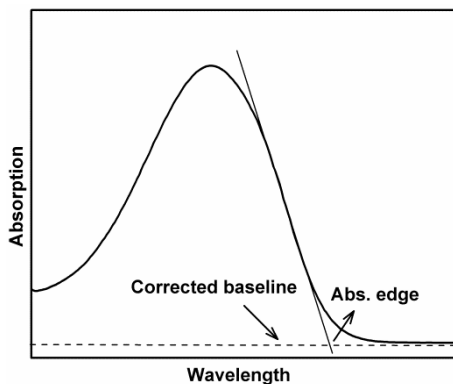


**Figure 55.** Illustration of the absorption edge for determination of the optical bandgap.

$$E_g^{opt} = h \cdot C/\lambda \quad (7)$$

where  $h$  is the planks constant ( $6.626 \times 10^{-34}$  J.s),  $C$  is the speed of light ( $3.0 \times 10^8$  ms<sup>-1</sup>) and  $\lambda$  is the absorption wavelength edge. This gives the optical bandgap in Joules unit which is converted to the eV unit using the conversion factor ( $1 \text{ eV} = 1.6 \times 10^{-19}$  J).

#### 5.2.4. Cyclic Voltammetric Analysis

Cyclic voltammetry was carried out on an Autolab PGSTAT128N potentiostat, connected to data processing software (GPES, version 4.9.007, Eco Chemie). The experiments were performed at a scan rate of 50 mV/s in solutions of 0.1 M tetra-n-butylammonium hexafluorophosphate (TBAPF<sub>6</sub>) in CH<sub>2</sub>Cl<sub>2</sub> as the supporting electrolyte and (Fc/Fc<sup>+</sup>) redox couple as the internal reference.<sup>173</sup> A three electrode cell was used, comprised of a glassy carbon electrode (GCE) as the working electrode, a platinum wire as the counter electrode and an

$\text{Ag}^+/\text{AgCl}$  electrode as the reference electrode. Prior to experiment, any dissolved oxygen was removed from the solution by bubbling argon through the solution. This is because oxygen is electroactive and is reduced quite easily. The solutions were allowed to become quiescent before the experiment, however, a blanketing layer of inert gas was maintained over the solution to ensure absence of the interfering oxygen during the experiment.

### 5.2.5. Thermal Analysis

The transition temperatures and latent heats were determined using a TA DSC Q2000 differential scanning calorimeter. Samples between 3 and 5 mg were weighted into aluminum pans covered by a hold-cap and heated in a static nitrogen atmosphere. Measurements were performed at the heating and cooling rates of  $10\text{ }^\circ\text{C min}^{-1}$ . For compound **51**, the DSC measurements were also performed at the heating and cooling rates of  $20\text{ }^\circ\text{C min}^{-1}$  and  $5\text{ }^\circ\text{C min}^{-1}$ . The first DSC scan was retained as a valid curve to obtain information on first and second-order thermodynamic transitions. TGA measurements were carried out using Shimadzu TGA-50 equipment with a TA-60 WS thermal analyzer at heating rate of  $10\text{ }^\circ\text{C min}^{-1}$  and nitrogen flow of  $50\text{ mL min}^{-1}$ . The mesophases were characterized by their textures using an Olympus BX53 polarizing optical microscope equipped with a Mettler Toledo FP-90 hot stage control unit.

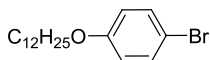
## 5.3. EXPERIMENTAL PROCEDURES AND SPECTRAL DATA OF THE SYNTHESIZED COMPOUNDS

### *Preparation of $\text{Pd}(\text{PPh}_3)_2\text{Cl}_2$*

The active  $\text{Pd}^0$  catalyst is air sensitive/unstable so it was generated in-situ by reduction of the  $\text{Pd}(\text{PPh}_3)_2\text{Cl}_2$  as pre-catalyst. The pre-catalyst was formed by following the general procedure of Heck.<sup>174</sup> First a mixture of Palladium (II) Chloride (0.5 g, 2.82 mmol) and Lithium Chloride (0.24 g, 5.64 mmol) in methanol (8 mL) was stirred at  $55\text{-}60\text{ }^\circ\text{C}$  till their complete dissolution. Then triphenylphosphine (1.6 g, 6.1 mmol) was added in portions. Upon  $\text{PPh}_3$  addition, the color changed from reddish brown solution to a bright yellow suspension. After complete addition of the  $\text{PPh}_3$ , the reaction mixture was heated till

80 °C and stirred for an hour to complete the formation of the catalyst as an insoluble yellow solid. The reaction mixture was cooled to ambient temperature and the yellow product (1.6 g, 81%) was collected by vacuum filtration, washed with methanol (20 mL) and dried overnight in a desiccator prior to use.

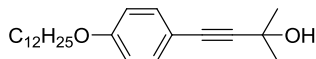
*1-Bromo-4-(dodecyloxy)benzene (27)*



In a 250 mL flask, a mixture of 4-bromophenol (2.67 g, 15.43 mmol),  $K_2CO_3$  (4.15 g, 30 mmol) and 1-bromododecane (4.57 g, 18 mmol) in butanone (30 mL) was stirred under reflux for 24 h. After reaction completion (indicated by TLC), the reaction mixture was cooled to room temperature, filtered off and washed with butanone (20 mL). The filtrate was concentrated under reduced pressure and the residue recrystallized from ethanol to give the 1-bromo-4-(dodecyloxy)benzene **27** as white crystals.

**Yield:** 4.8 g, 94 %; **m. p.** 32.0 - 33.2 °C;  **$^1H$  NMR (CDCl<sub>3</sub>):**  $\delta$  = 7.36 (d, 2H, J = 8.98 Hz), 6.77 (d, 2H, J = 8.98 Hz), 3.91 (t, 2H, J = 8.01 Hz), 1.76 (qui, 2H, J = 8.01 Hz), 1.44 (qui, 2H, J = 8.01 Hz), 1.26 (m, 16H), 0.88 (t, 3H, J = 7.03 Hz);  **$^{13}C$  NMR (CDCl<sub>3</sub>):**  $\delta$  = 158.37, 132.31, 116.41, 112.66, 68.39, 32.07, 29.80, 29.74, 29.50, 29.31, 26.14, 22.85, 14.28; **FT-IR (KBr, cm<sup>-1</sup>):** 2942, 2903, 2835, 2537, 2277, 2037, 1872, 1584, 1488, 1459, 1289, 1246, 1175, 1103, 1072, 1032, 1004, 821, 599, 506.

*4-(4-(Dodecyloxy)phenyl)-2-methylbut-3-yn-2-ol (36)*

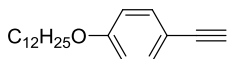


In a flame dried 3-necked flask (250 mL) under argon and fitted with a dropping funnel, a mixture of the 1-bromo-4-(dodecyloxy)benzene **27** (8.0 g, 23.44 mmol),  $Pd(PPh_3)_2Cl_2$  (0.75 g, 1.07 mmol),  $PPh_3$  (0.28 g, 1.07 mmol) and  $CuI$  (0.4 g, 2.13 mmol) in  $Et_3N$  (50 mL) was stirred at 75 °C for 30 minutes. A solution of 2-

methyl-3-butyn-2-ol (1.83 g, 21.31 mmol) in triethylamine (15 mL) was added drop-wise. After complete addition, the reaction mixture was stirred overnight at 90 °C. The reaction mixture was cooled to room temperature, filtered through a celite pad and washed with tetrahydrofuran. After vacuum evaporation of the solvent, the crude product was purified on silica gel column (3-7 % ethyl acetate : hexane) to furnish the 4-(4-(dodecyloxy)phenyl)-2-methylbut-3-yn-2-ol **36** as a pale yellow solid.

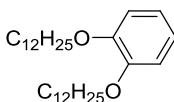
**Yield:** 4.52 g, 61.6 %; **m. p.** 46.2 - 48.5 °C;  $^1\text{H NMR}$  ( $\text{CDCl}_3$ ):  $\delta$  7.33 (d, 2H,  $J = 8.98$  Hz), 6.81 (d, 2H,  $J = 8.98$  Hz), 3.93 (t, 2H,  $J = 6.64$  Hz), 1.77 (qui, 2H,  $J = 8.01$  Hz), 1.61 (s, 6H), 1.44 (qui,  $J = 8.01$  Hz), 1.26 (m, 16H), 0.88 (t, 3H,  $J = 7.03$  Hz);  $^{13}\text{C NMR}$  ( $\text{CDCl}_3$ ):  $\delta$  159.36, 133.26, 114.60, 92.47, 82.33, 68.26, 65.89, 32.15, 31.81, 29.90, 29.87, 29.83, 29.80, 29.59, 29.41, 26.23, 22.93, 14.37; **FT-IR** ( $\text{KBr}$ ,  $\text{cm}^{-1}$ ): 3331, 2922, 2850, 1606, 1509, 1247, 1168, 834.

*1-(Dodecyloxy)-4-ethynylbenzene (16)*



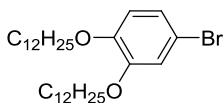
A mixture of NaOH (0.42 g, 10.5 mmol) and toluene (20 mL) in a 100 mL flask was heated to 80 °C and then the compound 4-(4-(dodecyloxy)phenyl)-2-methylbut-3-yn-2-ol **36** (1.0 g, 2.90 mmol) was added. A microdistillation apparatus was set and the reaction mixture was stirred under reflux (oil bath temperature 115 - 120 °C) for 4 h. After cooling to room temperature, the mixture was filtered through a celite pad, washed with tetrahydrofuran and the solvent removed under reduced pressure. The residue was purified on silica gel column eluting with pure hexane to furnish the terminal alkyne **16** as an oily liquid that solidified at lower temperature.

**Yield:** 0.7 g, 84 %; **m.p.** Oily liquid at room temperature;  $^1\text{H NMR}$  ( $\text{CDCl}_3$ ):  $\delta$  = 7.44 (d, 2H,  $J = 8.98$  Hz), 6.85 (d, 2H,  $J = 8.98$  Hz), 3.95 (t, 2H,  $J = 6.64$  Hz), 3.00 (s, 1H), 1.81 (qui, 2H,  $J = 8.01$  Hz), 1.32 (m, 16H), 0.94 (t, 3H,  $J = 7.03$  Hz);  $^{13}\text{C NMR}$  ( $\text{CDCl}_3$ , 50 MHz):  $\delta$  = 160.1, 134.0, 115.0, 114.7, 84.3, 76.2, 68.5, 32.6, 30.3, 30.0, 29.8, 26.6, 23.3, 14.6; **FT-IR** ( $\text{KBr}$ ,  $\text{cm}^{-1}$ ): 3318, 2923, 2854, 2109, 1887, 1607, 1506, 1469, 1289, 1249, 1170, 1108, 1026, 831.

*1,2-Bis(dodecyloxy)benzene (30a)*

In a flame dried 3-necked flask (1000 mL) connected to argon, a mixture of catechol i.e. 1,2-dihydroxybenzene **29** (14.80 g, 134.4 mmol),  $K_2CO_3$  (46.37 g, 336 mmol) and  $DMF_{dry}$  (100 mL) was stirred at 65 °C for 30 min. 1-Bromododecane (77.26 g, 310 mmol) was added and the reaction mixture was further stirred at 90-95 °C for 24 h. The reaction mixture was cooled to room temperature and the base removed by suction filtration. Distilled water (300 mL) was added to the filtrate and the product was extracted with  $CH_2Cl_2$  (3 x 100 mL) and dried over  $MgSO_4$ . The solvent was removed under reduced pressure and the resulting residue was recrystallized from ethanol to yield the alkylated compound **30a** as white needle like crystals.

**Yield:** 51.6 g, 86 %; **m. p.** 45.2 - 46.3 °C;  $^1H$  NMR ( $CDCl_3$ ):  $\delta$  = 6.89 (s, 4H), 3.99 (t, 4H,  $J$  = 6.64 Hz), 1.82 (qui, 4H,  $J$  = 8.01 Hz), 1.47 (qui, 4H,  $J$  = 7.81), 1.27 (m, 32H), 0.89 (t, 6H,  $J$  = 7.03 Hz);  $^{13}C$  NMR ( $CDCl_3$ ):  $\delta$  = 149.44, 121.20, 114.30, 69.49, 32.16, 29.95, 29.90, 29.88, 29.69, 29.61, 29.57, 26.29, 22.93, 14.36; **FT-IR (KBr,  $cm^{-1}$ ):** 2925, 2853, 1594, 1510, 1465, 1258, 1217, 1128, 747, 723.

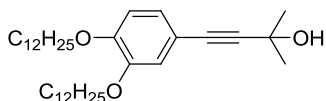
*4-Bromo-1,2-bis(dodecyloxy)benzene (28)*

In a 250 mL round bottom flask, a mixture of 1,2-bis(dodecyloxy)benzene **30a** (8.57 g, 19.18 mmol), NBS (3.42 g, 19.2 mmol), silica gel (8.5 g) in dichloromethane (80 mL) was stirred at room temperature for 20 h. After TLC indicated reaction completion, the mixture was filtered under suction. The filtrate was washed with aqueous  $Na_2S_2O_3 \cdot 5H_2O$  (to consume excess of  $Br_2$ ) followed by drying with  $Na_2SO_4$ . The solvent was removed by rotary evaporator and the

resulting residue was recrystallized from ethanol to get compound **28** as ultra white fine crystals.

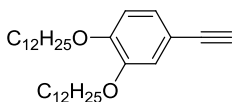
**Yield:** 8.06 g, 80 %; **m. p.** 48.0 - 49.5 °C (lit. 47.0 °C); <sup>1</sup>H NMR (CDCl<sub>3</sub>): δ = 6,99 (m, 2 H), 6,74 (d, 1 H), 3,97 (m, 4 H), 1,81 (m, 4 H), 1,46 (s, 4H), 1,28 (s, 32 H), 0,90 (t, 6 H); **FT-IR (KBr, cm<sup>-1</sup>):** 2921, 2848, 1507, 1466, 1257, 1218, 1134, 802, 723.

*4-(3,4-Bis(dodecyloxy)phenyl)-2-methylbut-3-yn-2-ol (37)*



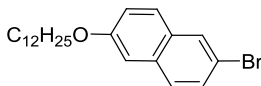
In a schlenk flask (250 mL) fitted with a dropping funnel under argon, a mixture of the 4-bromo-1,2-bis(dodecyloxy)benzene **28** (5.0 g, 9.51 mmol), Pd(PPh<sub>3</sub>)<sub>2</sub>Cl<sub>2</sub> (0.33 g, 0.48 mmol), PPh<sub>3</sub> (0.13 g, 0.48 mmol) and CuI (0.48 mmol) in Et<sub>3</sub>N (50 mL) was stirred at 50 °C for 30 minutes. A solution of 2-methyl-3-butyn-2-ol (1.2 g, 14.27 mmol) in triethylamine (10 mL) was added drop-wise. After complete addition, the reaction mixture was stirred overnight at 80 °C. The reaction mixture was cooled to room temperature, filtered through a celite pad and washed with tetrahydrofuran. After vacuum evaporation of the solvent, the crude product was purified on silica gel column (2 - 5 % ethyl acetate : hexane) to furnish the target compound **37** as an off-white solid.

**Yield:** 3.62 g, 72 %; **m. p.** 61.2 - 63.7 °C; <sup>1</sup>H NMR (CDCl<sub>3</sub>): δ = 6.97 (dd, 1H, <sup>3</sup>J = 8.20 Hz, <sup>4</sup>J = 1.95 Hz), 6.92 (d, 1H, <sup>4</sup>J = 1.95), 6.77 (d, 1H, <sup>3</sup>J = 8.20 Hz) 3.97 (2 overlapping t appearing as q, 4H), 2.03 (broad s, 1H, -OH) 1.80 (qui, 4H, J = 7.22 Hz), 1.45 (m), 1.26 (m, 32H), 0.88 (t, 6H, J = 7.03 Hz); <sup>13</sup>C NMR (CDCl<sub>3</sub>): δ = 149.82, 148.86, 125.12, 116.95, 114.96, 113.37, 92.23, 82.54, 69.44, 69.35, 65.88, 32.16, 29.93 - 29.85, 29.59 - 29.40, 26.23, 22.93, 14.35; **FT-IR (KBr, cm<sup>-1</sup>):** 3287, 2919, 2849, 1597, 1515, 1468, 1415, 1246, 1213, 1132, 854, 815, 721.

*1,2-Bis(dodecyloxy)-4-ethynylbenzene (17)*

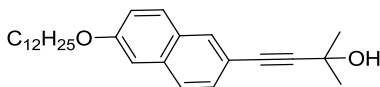
Prepared by a procedure similar to that described for the formation of compound **16** using 4-(3,4-bis(dodecyloxy)phenyl)-2-methylbut-3-yn-2-ol **37** (6.75 g, 12.76 mmol), NaOH (1.02 g, 25.5 mmol), toluene (50 mL) and stirred at 70 °C to yield compound **17** as yellowish crystals that changed to a bluish green color after 3 days.

**Yield:** 5.62 g, 93.7 %; **m. p.** 37.0 - 39.5 °C; **<sup>1</sup>H NMR (CDCl<sub>3</sub>):** δ = 7.06 (dd, 1H, <sup>3</sup>J = 8.20 Hz, <sup>4</sup>J = 1.95 Hz), 7.00 (d, 1H, <sup>4</sup>J = 1.95), 6.80 (d, 1H, <sup>3</sup>J = 8.40 Hz) 3.99 (2 overlapping t appearing as q, 4Hz), 2.99 (s, 1H), 1.82 (qui, J = 7.61 Hz), 1.47 (m), 1.27 (m, 32H), 0.89 (t, 6H, J = 7.03 Hz); **<sup>13</sup>C NMR (CDCl<sub>3</sub>):** δ = 150.27, 148.85, 125.72, 117.30, 114.26, 113.28, 84.20, 75.62, 69.46, 69.32, 32.17, 29.94 - 29.86, 29.64 - 29.61, 29.41 - 29.38, 26.23, 22.94, 14.36; **FT-IR (KBr, cm<sup>-1</sup>):** 3315, 2925, 2854, 2108, 1599, 1511, 1469, 1416, 1262, 1135, 1022, 853, 805.

*2-Bromo-6-(dodecyloxy)naphthalene (53)*

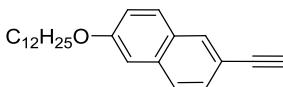
Prepared by using the same procedure as used for the synthesis of compound **27** using 6-bromonaphthalen-2-ol (10.0 g, 44.84 mmol), K<sub>2</sub>CO<sub>3</sub> (18.56 g, 134.52 mmol), 1-bromododecane (12.3 g, 49.32 mmol) and butanone (70 mL). The product recrystallized from ethanol as an off-white powder.

**Yield:** 14.57 g, 83 %; **m. p.** 62.0 - 64.5 °C; **<sup>1</sup>H NMR (CDCl<sub>3</sub>):** δ = 7.91 (d, 1H, <sup>4</sup>J = 1.95 Hz), 7.65 (d, 1H, J = 8.99 Hz), 7.58 (d, 1H, J = 8.60 Hz), 7.48 (dd, 1H, <sup>3</sup>J = 8.60 Hz, <sup>4</sup>J = 1.95 Hz), 7.16 (dd, 1H, <sup>3</sup>J = 8.99 Hz, <sup>4</sup>J = 2.34 Hz), 7.08 (d, 1H, <sup>4</sup>J = 2.34 Hz), 4.05 (t, 2H, J = 6.64 Hz), 1.84 (qui, 2H, J = 8.21 Hz), 1.50 (qui, 2H, J = 7.82 Hz), 1.27 (m, 16H), 0.88 (t, 3H, J = 7.03 Hz); **FT-IR (KBr, cm<sup>-1</sup>):** 2918, 2851, 1916, 1765, 1624, 1587, 1498, 1466, 1389, 1263, 1211, 851.

4-(6-(Dodecyloxy)naphthalen-2-yl)-2-methylbut-3-yn-2-ol (**54**)

Prepared by following the standard Sonogashira coupling procedure as used for preparing compound **37**. **Amounts used**; 2-bromo-6-(dodecyloxy)naphthalene **53** (5.0 g, 12.8 mmol), Pd(PPh<sub>3</sub>)<sub>2</sub>Cl<sub>2</sub> (0.45 g, 0.64 mmol), PPh<sub>3</sub> (0.17 g, 0.64 mmol), CuI (0.64 mmol), 2-methyl-3-butyn-2-ol (1.62 g, 19.2 mmol), THF : Et<sub>3</sub>N 50 % each (50 mL). The 2-methyl-3-butyn-2-ol was added drop-wise at 55 - 60 °C and then the reaction mixture was stirred at 80 °C for 6 h. The crude product was purified using a silica gel column (eluent 2 - 4 % ethyl acetate/hexane) to get the desired compound **54** as pale yellow solid.

**Yield**: 3.32 g, 65.7 %; **m. p.** 78 - 79 °C; **<sup>1</sup>H NMR (CDCl<sub>3</sub>) 200 MHz** : δ = 7.87 (broadened s, 1H), 7.68 (d, 1H, J = 8.84 Hz), 7.64 (d, 1H, J = 8.34 Hz), 7.43 (dd, 1H, <sup>3</sup>J = 8.34 Hz, <sup>4</sup>J = 1.77 Hz), 7.16 (dd, 1H, <sup>3</sup>J = 8.84 Hz, <sup>4</sup>J = 2.53 Hz), 7.09 (d, 1H, <sup>4</sup>J = 2.53 Hz), 4.07 (t, 2H, J = 6.57 Hz), 1.85 (qui, 2H, J = 7.58 Hz), 1.67 (s, 6H), 1.53 (m, 2H), 1.28 (m, 16H), 0.90 (t, 3H, J = 6.82 Hz); **FT-IR (KBr, cm<sup>-1</sup>)**: 3348, 2915, 2850, 1599, 1251, 1171, 857

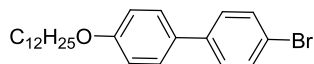
2-(Dodecyloxy)-6-ethynynaphthalene (**39**)

NaOH (0.2 g, 5.1 mmol) was added to a solution of the 4-(6-(dodecyloxy)naphthalen-2-yl)-2-methylbut-3-yn-2-ol **54** (1.0 g, 2.53 mmol) in toluene (10 mL) at 80 °C. The temperature was further raised and the mixture stirred under reflux (115 °C) for 3 h. After cooling to room temperature, the NaOH was filtered off, the solvent removed under reduced pressure and the resulting residue chromatographed over silica gel column, eluted with 100 % hexane, to furnish compound **39**.

As a white powder **Yield**: 0.44 g, 52 %; **m. p.** 55 -56 °C; **<sup>1</sup>H NMR (CDCl<sub>3</sub>)**: δ = 7.96 (broadened s, 1H), 7.69 (d, 1H, J = 8.99 Hz), 7.66 (d, 1H, J = 8.60 Hz), 7.50 (dd, 1H, <sup>3</sup>J = 8.21 Hz, <sup>4</sup>J = 1.56 Hz), 7.18 (dd,

1H,  $^3J = 8.99$  Hz,  $^4J = 2.34$  Hz), 7.10 (d, 1H,  $^4J = 2.34$  Hz), 4.06 (t, 2H,  $J = 6.64$  Hz), 3.13 (s, 1H), 1.85 (qui, 2H,  $J = 7.82$  Hz), 1.51 (m, 2H), 1.29 (m, 16H), 0.91 (t, 3H,  $J = 7.03$  Hz);  $^{13}\text{C NMR (CDCl}_3\text{)}$ :  $\delta = 158.01, 134.46, 132.08, 129.08, 129.24, 129.07, 128.19, 128.78, 119.82, 116.77, 106.47, 84.29, 76.66, 68.08, 31.97, 29.72 - 29.63, 29.46, 29.41, 29.22, 26.13, 22.74, 14.17$ ; **FT-IR (KBr,  $\text{cm}^{-1}$ )**: 3299, 3063, 2920, 2849, 1925, 1794, 1718, 1626, 1597, 1469, 1387, 1229, 1021, 860.

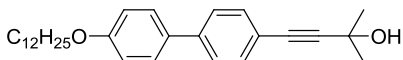
*4-Bromo-4'-(dodecyloxy)biphenyl (41)*



In a 125 mL flask, the available 4-bromo-[1,1'-biphenyl]-4-ol acetate (4.0 g, 13.7 mmol), NaOH (1.8 g, 45 mmol) in a mixture of butanone (60 mL), ethanol (10 mL) and H<sub>2</sub>O (3 mL) was stirred under reflux (85 - 90 °C). After the TLC indicated (5 h) full conversion of the starting substrate to 4'-bromobiphenyl-4-ol, 1-bromododecane (4.1 g, 16.44 mmol) was added and the reaction was further stirred under reflux for overnight. Next day, the formation of a white solid was observed. After cooling to room temperature, the organic solvents were evaporated under vacuum, the precipitate was triturated with H<sub>2</sub>O for 20 minutes, filtered under suction and successively washed with water and cold ethanol to give 4-bromo-4'-(dodecyloxy)biphenyl as a bright white solid in one step.

**Yield:** 4.5 g, 78.5 %; **m. p.** 112.6 - 113.1 °C (lit. 114.0 - 115.0 °C);  $^{176}\text{H NMR (CDCl}_3\text{)}$ :  $\delta = 7.53$  (d, 2H,  $J = 8.60$  Hz), 7.48 (d, 2H,  $J = 8.99$  Hz), 7.41 (d, 2H,  $J = 8.99$  Hz), 6.96 (d, 2H,  $J = 8.60$  Hz), 3.99 (t, 2H,  $J = 6.64$  Hz), 1.81 (qui, 2H,  $J = 7.82$  Hz), 1.47 (m, 2H), 1.27 (m, 16H), 0.89 (t, 3H,  $J = 7.03$  Hz);  $^{13}\text{C NMR (CDCl}_3\text{)}$ :  $\delta = 139.77, 132.18, 131.74, 128.24, 127.90, 120.67, 114.85, 104.98, 68.09, 31.91, 29.66 - 29.58, 29.39, 29.35, 29.25, 26.04, 22.69, 14.13$ ; **FT-IR (KBr,  $\text{cm}^{-1}$ )**: 2961, 2918, 2849, 1897, 1659, 1607.

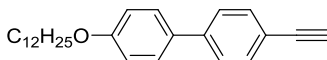
## 4-(4'-(Dodecyloxy)biphenyl-4-yl)-2-methylbut-3-yn-2-ol (42)



Prepared by following the same procedure as used for analogous reactions. **Amounts of reagents used:** 4-bromo-4'-(dodecyloxy)biphenyl **41** (4.0 g, 9.58 mmol), Pd(PPh<sub>3</sub>)<sub>2</sub>Cl<sub>2</sub> (0.34 g, 0.48 mmol), PPh<sub>3</sub> (0.12 g, 0.48 mmol), CuI (0.48 mmol), 2-methyl-3-butyn-2-ol (0.97 g, 11.5 mmol), THF : Et<sub>3</sub>N 50 % each (50 mL). The reaction mixture was stirred at 80 °C for 15 h and after reaction work up, the product was purified on a silica gel column eluted with 3-5 % ethyl acetate/hexane to get the target compound **42**.

A pale yellow solid. **Yield:** 1.6 g, 40 %; **m. p.** 127.5 - 130 °C; **<sup>1</sup>H NMR (CDCl<sub>3</sub>):** δ = 7.51 (overlapped d, 2H), 7.49 (overlapped d, 2H), 7.45 (d, 2H, J = 8.60 Hz), 6.96 (d, 2H, J = 8.60 Hz), 3.99 (t, 2H, J = 6.64 Hz), 2.07 (broad s, 1H), 1.80 (qui, 2H, J = 7.82 Hz), 1.63 (s, 6H), 1.46 (m, 2H), 1.26 (m, 16H), 0.88 (t, 3H, J = 7.03 Hz); **<sup>13</sup>C NMR (CDCl<sub>3</sub>):** δ = 158.99, 140.64, 132.52, 132.0, 127.97, 126.37, 120.80, 114.83, 94.08, 82.13, 68.11, 65.69, 31.91, 31.53, 29.66 - 29.58, 29.40, 29.35, 29.26, 26.04, 22.69, 14.12; **FT-IR (KBr, cm<sup>-1</sup>):** 3444, 2987, 2959, 2920, 2849, 1608, 1578, 1528, 1497.

## 4-(Dodecyloxy)-4'-ethynylbiphenyl (40)

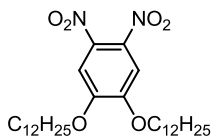


Prepared by procedure as followed for preparing the compound **39**. Amounts of reagents used: 4-(4'-(dodecyloxy)biphenyl-4-yl)-2-methylbut-3-yn-2-ol **42** (1.47 g, 3.5 mmol), NaOH (0.42 g, 10.5 mmol), toluene (30 mL). Purification on silica gel column eluted with pure hexane to furnish compound **40** as a white solid.

**Yield:** 0.7 g, 55 %; **m. p.** 97.0 - 98.5 °C; **<sup>1</sup>H NMR (CDCl<sub>3</sub>):** δ = 7.55 - 7.50 (m, 6H), 6.97 (d, 2H, J = 8.60 Hz), 3.99 (t, 2H, J = 6.64 Hz), 3.12 (s, 1H), 1.80 (qui, 2H, J = 7.82 Hz), 1.47 (m, 2H), 1.27 (m, 16H), 0.89 (t, 3H, J = 7.03 Hz); **<sup>13</sup>C NMR (CDCl<sub>3</sub>):** δ = 159.05, 141.12, 132.49, 128.02, 126.43, 120.12, 114.83, 83.67, 77.45, 68.09, 31.91, 29.66 - 29.58, 29.39 - 29.25, 26.04, 22.69, 14.13; **FT-IR (KBr, cm<sup>-1</sup>):**

3288, 3092, 3038, 2955, 2919, 2872, 2850, 2106, 1919, 1896, 1875, 1665, 1608, 1581, 1529.

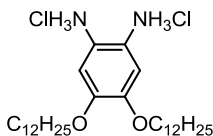
*1,2-Bis(dodecyloxy)-4,5-dinitrobenzene (31a)*



A solution of **30a** (14.0 g, 31.36 mmol) in dichloromethane (150 ml) was added drop-wise to vigorously stirred concentrated HNO<sub>3</sub> (80 ml) over a period of 30 min. After stirring for 2 h at room temperature, concentrated sulfuric acid (40 ml) was added in portions and stirred overnight at room temperature. The reaction mixture was next poured onto crushed ice and the resultant suspension was extracted with dichloromethane (3 x 50 ml). The organic layer was washed thoroughly with saturated aqueous sodium carbonate, then with water, and finally dried over anhydrous MgSO<sub>4</sub>. The solvent was evaporated to give a crude product which was crystallized from ethanol to give compound **31a** as a bright yellow crystalline solid.

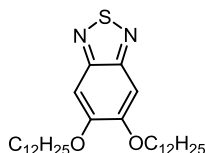
**Yield:** 14.76 g, 88 %; **m. p.** 79.0 -80.0 °C; **<sup>1</sup>H NMR (CDCl<sub>3</sub>):** δ = 7.26 (s, 2H), 4.09 (t, 4H, J = 6.44 Hz), 1.87 (qui, 4H, J = 8.01 Hz), 1.48 (qui, 4H, J = 8.01), 1.26 (m, 32H), 0.88 (t, 6H, J = 7.03 Hz); **<sup>13</sup>C NMR (CDCl<sub>3</sub>):** δ = 151.98, 136.68, 108.03, 70.40, 32.16, 29.91, 29.47, 28.91, 26.04, 22.93, 14.37; **FT-IR (KBr, cm<sup>-1</sup>):** 2123, 3070, 2917, 2850, 1727, 1586, 1529, 1465, 1372, 1334, 1289, 1225, 1070, 1041, 987, 949, 909, 872, 823.

*4,5-Bis(dodecyloxy)benzene-1,2-diammonium chloride (33)<sup>177</sup>*



A mixture of 1,2-bis(dodecyloxy)-4,5-dinitrobenzene **31a** (1.0 g, 1.86 mmol) and Sn(II)Cl<sub>2</sub> (3.36 g, 14.9 mmol) in ethanol (30 ml) and concentrated HCl (10 ml) was heated to 90 °C over the night. After cooling to room temperature the product was filtered, washed with water and methanol and dried under argon for 2 h before using directly in the next step.

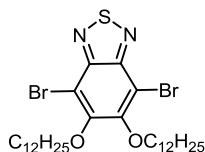
*5,6-Bis(dodecyloxy)-2,1,3-benzothiadiazole (34)*<sup>177</sup>



To a mixture of 4,5-bis(dodecyloxy)benzene-1,2-diammonium chloride **33** (0.64 g, 1.16 mmol) and triethylamine (1.17 g/1.62 mL, 11.6 mmol) in dichloromethane (35 mL) in a schlenk flask under argon, a solution of thionyl chloride (0.427 g/0.26 mL, 3.48 mmol) in dichloromethane (10 mL) was slowly added and then stirred under reflux (50 - 55 °C) for 6 h. The cooled solution was concentrated in vacuum, the solid residue was triturated with water for 30 minutes, filtered and then recrystallized from ethanol to get compound **34** as an off-white solid.

**Yield:** 0.43 g, 73 %; **m. p.** 95 - 96.7 °C; **<sup>1</sup>H NMR (CDCl<sub>3</sub>):** δ = 7.13 (s, 2H), 4.09 (t, 4H, J = 6.64 Hz), 1.91 (qui, 4H, J = 7.61 Hz), 1.51 (m, 4H), 1.26 (m, 32H), 0.88 (t, 6H, J = 7.03 Hz); **<sup>13</sup>C NMR (CDCl<sub>3</sub>):** δ = 154.0, 151.32, 98.30, 69.13, 31.92, 29.68, 29.65, 29.32, 28.75, 25.09, 22.56, 14.14; **FT-IR (KBr, cm<sup>-1</sup>):** 2910, 2850, 1497, 1467, 1321, 1197, 855.

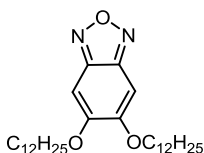
*4,7-Dibromo-5,6-bis(dodecyloxy)-2,1,3-benzothiadiazole (13)*<sup>177</sup>



Bromine (0.56 g/0.18 mL, 3.5 mmol) was added to a solution of 5,6-bis(dodecyloxy)-2,1,3-benzothiadiazole **34** (0.26 g, 0.52 mmol) in dichloromethane (15 mL) and acetic acid (7 mL) in a 125 mL flask and the resulting mixture was stirred in the dark (covered with aluminum foil) for 48 h at room temperature. The reaction mixture was then poured into water (50 mL) and extracted with dichloromethane (3 x 30 mL). The organic phase was sequentially washed with saturated NaHCO<sub>3</sub> (30 mL), saturated Na<sub>2</sub>SO<sub>3</sub> (50 mL) and water (2 x 50 mL) and dried over Na<sub>2</sub>SO<sub>4</sub>. The solvent was evaporated under reduced pressure and the residue purified by recrystallization from ethanol to get 4,7-dibromo-5,6-bis(dodecyloxy)-2,1,3-benzothiadiazole **13** as off-white fluffy crystals.

**Yield:** 0.25 g, 73 %; **m. p.** 60.4 - 61.0 °C; **<sup>1</sup>H NMR (CDCl<sub>3</sub>):** δ = 4.09 (t, 4H, J = 6.64 Hz), 1.89 (qui, 4H, J = 7.61 Hz), 1.28 (m, 32H), 0.89 (t, 6H, J = 7.03 Hz); **<sup>13</sup>C NMR (CDCl<sub>3</sub>):** δ = 154.5, 150.3, 106.2, 75.1, 31.9, 29.68, 29.65, 29.62, 29.60, 29.4, 29.3 25.9, 22.6, 14.1; **FT-IR (KBr, cm<sup>-1</sup>):** 2958, 2903, 2845, 1471, 1384, 1292, 985, 946.

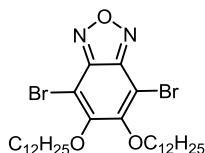
*5,6-Bis(dodecyloxy)-2,1,3-benzoxadiazole (32a)*<sup>127</sup>



To a solution of 1,2-bis(dodecyloxy)-4,5-dinitrobenzene **31a** (1.07 g, 2.0 mmol) in dry toluene (15 mL) in a flame dried flask (125 mL), was added sodium azide (0.65 g, 10 mmol), tetra - *n* -butylammonium bromide (0.13 g, 0.4 mmol) and the resulting mixture was stirred under refluxing conditions (110 - 115 °C). After stirring for 5 h, the TLC indicated complete consumption of the substrate. Subsequently triphenylphosphine (0.63 g, 2.4 mmol) was added and the mixture was further refluxed for 3 h. After cooling to room temperature, the reaction mixture was filtered on a short silica pad and rinsed with dichloromethane. The solvent was evaporated under vacuum and the resulting solid was purified by recrystallization from ethanol to afford 5,6-bis(dodecyloxy)-2,1,3-benzoxadiazole as an off-white solid.

**Yield:** 0.75 g, 77 %; **m. p.** 107.3 - 108.8 °C;  $^1\text{H NMR}$  ( $\text{CDCl}_3$ ):  $\delta$  = 6.81 (s, 2H), 4.07 (t, 4H,  $J$  = 6.64 Hz), 1.90 (qui, 4H,  $J$  = 7.62 Hz), 1.51 (m, 4H), 1.27 (m, 32H), 0.88 (t, 6H,  $J$  = 7.03 Hz); **FT-IR** (**KBr**,  $\text{cm}^{-1}$ ): 2913, 2847, 1502, 1471, 1318, 1202, 848; **CHN:** Expected  $\text{C}_{30}\text{H}_{52}\text{N}_2\text{O}_3$ : C 73.72, H 10.72, N 5.73. Found: C 73.72, H 10.69, N 5.70.

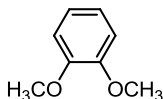
*4,7-Dibromo-5,6-bis(dodecyloxy)-2,1,3-benzoxadiazole (14)*<sup>127</sup>



To a solution of compound **32a** (0.3g, 0.61 mmol) in dichloromethane (10 mL), was added acetic acid (2 mL) and then bromine (0.48 g, 3.0 mmol). The flask was covered with aluminum foil and stirred at room temperature for 72 h in dark. A solution of 20 % NaOH (20 mL) was added and the resulting yellowish suspension was extracted with dichloromethane (3 x 50 mL). The organic phase was washed with brine (30 mL) followed water (30 mL), dried over  $\text{Na}_2\text{SO}_4$  and the solvent evaporated on vacuum rotary evaporator to furnish compound **14** as an off-white solid that was characterized without any further purification.

**Yield:** (0.36g, 91 %; **m. p.** 55.1 - 56.0 °C;  $^1\text{H NMR}$  ( $\text{CDCl}_3$ ):  $\delta$  = 4.15 (t, 4H,  $J$  = 6.64 Hz), 1.86 (qui, 4H,  $J$  = 7.81 Hz), 1.52 (m, 4H), 1.27 (m, 32H), 0.89 (t, 6H,  $J$  = 7.03 Hz); **FT-IR** (**KBr**,  $\text{cm}^{-1}$ ): 2954, 2919, 2851, 2331, 1734, 1612, 1473, 1380, 1296, 1187, 1072, 1014, 996, 948, 883, 723. **CHN:** Expected  $\text{C}_{30}\text{H}_{50}\text{Br}_2\text{N}_2\text{O}_3$ : C 55.73, H 7.79, N 4.33. Found: C 55.72, H 7.80, N 4.30.

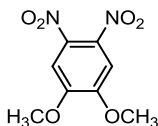
*1,2-Dimethoxybenzene/veratrol (30b)*



A mixture of catechol **29** (11.95 g, 108.57 mmol) and  $K_2CO_3$  (37.45 g, 271.4 mmol) in acetone was stirred under argon for 10 min. at room temperature. Iodomethane (14.2 mL, 228 mmol) was added, stirred for 2 h at room temperature and then refluxed overnight at 60 °C. The reaction mixture was cooled to room temperature, vacuum filtered to remove  $K_2CO_3$ . The remaining  $K_2CO_3$  was removed by washing the filtrate with water. The organic phase was dried over  $Na_2SO_4$  and the solvent removed under reduced pressure to furnish compound **30b** as an oily liquid.

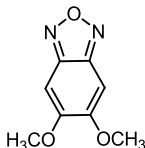
**Yield:** 14.7 g, 98 %; **m. p.** oily liquid;  $^1H$  NMR ( $CDCl_3$ ):  $\delta$  = 6.8 (m, 4H), 3.7 (s, 6H); **FT-IR (KBr,  $cm^{-1}$ ):** 3103, 3055, 3000, 2853, 1610, 1494, 1476, 1322, 1253, 1152, 1120, 1004, 753.

*1,2-Dimethoxy-4,5-dinitrobenzene (31b)*<sup>148</sup>



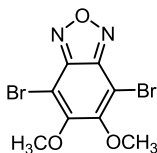
1,2-Dimethoxybenzene **30b** (14.6 g, 105.67 mmol) was added drop-wise and slowly via addition funnel to vigorously stirred 70 %  $HNO_3$  (100 mL). The temperature was kept around 20 - 25 °C during addition period by placing the reaction flask in ice - water. The formation of a yellow solid was observed during the addition. After complete addition of **30b**, the reaction mixture was stirred at 60 °C for 3 h and subsequently at 80 °C for 1 h. The mixture was cooled to room temperature and poured into ice. The precipitate was filtered off and washed with water (70 mL) and then slurried in saturated  $K_2CO_3$  solution to neutralize any  $HNO_3$  left. After filtering under suction and washing with water, the dark yellow solid was triturated with hot ethanol (100 mL) to give the target compound **31b** as brightly yellow fine crystals.

**Yield:** 17.24 g, 72 %; **m. p.** 128.2 - 129.5 °C (lit. 129.0 - 131.0 °C)<sup>148</sup>;  $^1H$  NMR ( $CDCl_3$ ):  $\delta$  = 7.33 (s, 4H), 4.0 (s, 6H); **FT-IR (KBr,  $cm^{-1}$ ):** 3067, 2986, 1585, 1522, 1370, 1325, 1287, 1234, 1045, 875, 789.

*5,6-Dimethoxy-2,1,3-benzoxadiazole (32b)*

Prepared by the cyclization of compound **31b** by the same procedure as followed for preparing compound **32a**. **Amounts used;** 1,2-dimethoxy-4,5-dinitrobenzene **31b** (5 g, 21.91 mmol),  $\text{NaN}_3$  (7.12 g, 109.57 mmol), tetra-*n*-butylammonium bromide (1.41 g, 4.38 mmol), triphenylphosphine (6.9 g, 26.28 mmol), toluene (70 mL). After complete work-up and solvent evaporation, the resulting solid was purified by recrystallization in methanol to give the target compound **32b** as golden-yellow fine crystalline solid.

**Yield:** 3.2 g, 81 %; **m. p.** 195 - 197 °C;  $^1\text{H NMR}$  ( $\text{CDCl}_3$ ):  $\delta$  = 6.88 (s, 4H), 3.99 (s, 6H);  $^{13}\text{C NMR}$  ( $\text{CDCl}_3$ ):  $\delta$  = 155.36, 146.69, 90.67, 56.58; **FT-IR** ( $\text{KBr}$ ,  $\text{cm}^{-1}$ ): 3146, 3082, 3069, 2995, 2943, 2847, 2442, 1635, 1544, 1521, 1447, 1368, 1244, 1224, 1178, 1001, 854; **CHN:** Expected  $\text{C}_8\text{H}_8\text{N}_2\text{O}_3$ : C 53.33, H 4.48, N 15.55. Found: C 53.30, H 4.50, N 15.56.

*4,7-Dibromo-5,6-dimethoxy-2,1,3-benzoxadiazole (15)*

Prepared by the bromination of the compound **32b** by the same procedure as followed for preparation of the compound **14**. **Amounts used;** 5,6-dimethoxy-2,1,3-benzoxadiazole (0.4 g, 2.22 mmol), bromine (1.77 g/0.57 mL, 11.1 mmol), dichloromethane (25 mL), acetic acid (4 mL). The product **15** was recrystallized from methanol (0.37 g, 49.3 %) as an off-white crystalline solid.

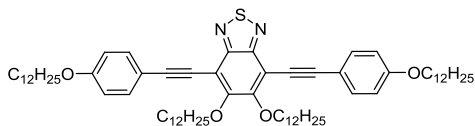
**Yield:** 0.37 g, 49.3 %; **m. p.** 128.5 - 131.0 °C;  $^1\text{H NMR}$  ( $\text{CDCl}_3$ ):  $\delta$  = 4.03 (s); **FT-IR** ( $\text{KBr}$ ,  $\text{cm}^{-1}$ ): 3010, 2952, 2847, 2363, 2136, 1608,

1530, 1477, 1382, 1310, 1075, 1010, 973, 879, 844, 732; CHN: Expected  $C_8H_6Br_2N_2O_3$ : C 28.43, H 1.79, N 8.29. Found: C 28.41, H 1.80, N 8.29.

### General Procedure For The Final Cross-Coupling Reactions

In a flame dried Schlenk flask under argon, a mixture of the heterocycle (**13-15**, **43**)  $Pd(PPh_3)_2Cl_2$ ,  $PPh_3$  and  $CuI$  in  $Et_3N$  (or THF:  $Et_3N$  if the compound is not completely soluble in  $Et_3N$ ) was stirred at  $50\text{ }^\circ C$  for 20-30 minutes. A solution of the aryl terminal alkyne (**16**, **17**, **39**, **40**) in triethylamine was added drop-wise. After complete addition of the alkyne, the reaction mixture was stirred at  $80-85\text{ }^\circ C$  for 12-14h. The reaction mixture was cooled to room temperature, filtered through a celite pad and washed with tetrahydrofuran. After vacuum evaporation of the solvent, the crude product was purified by column chromatography on flash silica gel (eluent 0.5-2 % ethyl acetate: hexane) to furnish the respective final compound.

### 4,7-Bis((4-(dodecyloxy)phenyl)ethynyl)-5,6-bis(dodecyloxy)-2,1,3-benzothiadiazole (**18**)

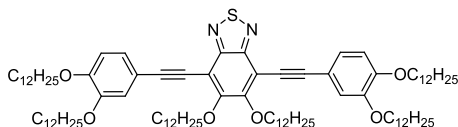


**Amounts of reagents used:** 4,7-dibromo-5,6-bis(dodecyloxy)-2,1,3-benzothiadiazole **13** (0.32 g, 0.483 mmol),  $Pd(PPh_3)_2Cl_2$  (0.024 g, 0.034 mmol),  $PPh_3$  (0.01g, 0.034 mmol),  $CuI$  (0.0065 g, 0.034 mmol), 1-(dodecyloxy)-4-ethynylbenzene **16** (0.29 g, 1.014 mmol),  $Et_3N$  (50 mL).

The product is a yellow-green solid; **yield:** 249 mg, 48%, **m.p.** =  $98.5-100.3\text{ }^\circ C$ ;  **$^1H$  NMR ( $CDCl_3$ , 400 MHz):**  $\delta$  = 7.6 (d, 4H,  $J$  = 8.8 Hz), 6.9 (d, 4H,  $J$  = 8.8 Hz), 4.4 (t, 4H,  $J$  = 6.4 Hz), 4.0 (t, 4H,  $J$  = 6.6 Hz), 1.9 (qui), 1.8 (qui), 1.3 (b), 0.9 (t);  **$^{13}C$  NMR ( $CDCl_3$ , 100.6 MHz):**  $\delta$  = 160.0, 157.6, 152.2, 135.5, 115.1, 114.7, 108.5, 101.4, 81.2, 75.2, 68.2, 32.2, 29.7, 26.5, 26.3, 23.0, 14.3; **FT-IR (KBr,  $cm^{-1}$ ):** 2924, 2854, 2201, 1605, 1513, 1467, 1289, 1247; **CI-MS [ $M+H$ ] $^+$**  calculated for

$C_{70}H_{108}N_2O_4S$  m/z: 1072.8; Found: 1073.9. **CHN**: Expected: C 78.31, H 10.14, N 2.61. Found: C 78.26, H 10.14, N 2.57.

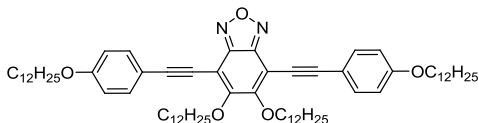
*4,7-Bis((3,4-bis(dodecyloxy)phenyl)ethynyl)-5,6-bis(dodecyloxy)-2,1,3-benzothiadiazole (19)*



**Amounts of reagents used:** 4,7-dibromo-5,6-bis(dodecyloxy)-2,1,3-benzothiadiazole **13** (0.21 g, 0.317 mmol),  $Pd(PPh_3)_2Cl_2$  (0.022 g, 0.031 mmol),  $PPh_3$  (0.01 g, 0.031 mmol),  $CuI$  (0.0061 g, 0.031 mmol), 1,2-bis(dodecyloxy)-4-ethynylbenzene **17** (0.376 g, 0.8 mmol),  $Et_3N$  (50 mL).

The product is a lime colored solid; **yield:** 233.2 mg, 51 %, **m.p.** = 80.0-81.7°C;  $^1H$  NMR ( $CDCl_3$ , 400 MHz):  $\delta$  = 7.23 (dd, 2H,  $J$  = 8.2 Hz,  $J^t$  = 2.0 Hz), 7.15 (d, 2H,  $J^t$  = 2.0 Hz), 6.86 (d, 2H,  $J$  = 8.4 Hz), 4.36 (t, 4H,  $J$  = 6.6 Hz), 4.0 (ot, 8H), 1.9 (qui), 1.8 (qui), 1.3 (b), 0.9 (t);  $^{13}C$  NMR ( $CDCl_3$ , 100.6 MHz):  $\delta$  = 157.7, 152.1, 150.5, 149.0, 125.6, 116.8, 115.1, 113.2, 108.5, 101.6, 80.8, 75.3, 69.5, 69.3, 32.2, 30.0, 29.9, 29.6, 29.4, 26.3, 23.0, 14.1; **FT-IR (KBr,  $cm^{-1}$ ):** 2922, 2852, 2205, 1605, 1505, 1468, 1290, 1246; **CHN**: Expected: C 78.28, H 10.90, N 1.94. Found: C 78.29, H 10.80, N 1.90.

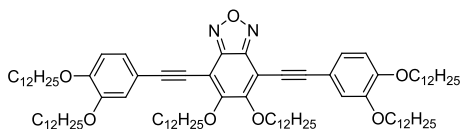
*4,7-Bis((4-(dodecyloxy)phenyl)ethynyl)-5,6-bis(dodecyloxy)-2,1,3-benzoxadiazole (20)*



**Amounts of reagents used:** 4,7-dibromo-5,6-bis(dodecyloxy)-2,1,3-benzoxadiazole **14** (0.65 g, 1.0 mmol),  $Pd(PPh_3)_2Cl_2$  (0.05 g, 0.07 mmol),  $PPh_3$  (0.02 g, 0.07 mmol),  $CuI$  (0.013 g, 0.07 mmol), 1-(dodecyloxy)-4-ethynylbenzene **16** (0.6 g, 2.1 mmol),  $Et_3N$  (50 mL).

The product is a greenish-yellow solid; **yield:** 496.8 mg, 47%; **m.p.** = 40.0-41.6 °C; **<sup>1</sup>H NMR (CDCl<sub>3</sub>, 400 MHz):** δ = 7.5 (d, 4H, *J* = 8.8 Hz), 6.9 (d, 4H, *J* = 9.0 Hz), 4.4 (t, 4H, *J* = 6.4 Hz), 4.0 (t, 4H, *J* = 6.4 Hz), 1.9 (qui), 1.8 (qui), 1.3 (b), 0.9 (t, 12H); **<sup>13</sup>C NMR (CDCl<sub>3</sub>, 100.6 MHz):** δ = 160.0, 157.6, 152.2, 133.5, 115.1, 114.7, 108.5, 101.4, 81.2, 75.2, 68.2, 32.2, 29.7, 26.5, 23.0, 14.3; **FT-IR (KBr, cm<sup>-1</sup>):** 2923, 2852, 2205, 1604, 1508, 1464, 1291, 1247; **CI-MS [M+H]<sup>+</sup>** calculated for C<sub>70</sub>H<sub>108</sub>N<sub>2</sub>O<sub>5</sub> m/z: 1056.8; Found: 1058.0. **CHN:** Expected: C 79.49, H 10.29, N 2.65. Found: C 79.47, H 10.28, N 2.63.

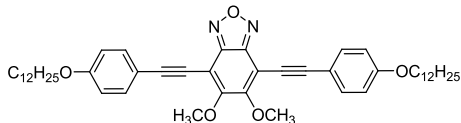
*4,7-Bis((3,4-bis(dodecyloxy)phenyl)ethynyl)-5,6-bis(dodecyloxy)-2,1,3-benzoxadiazole (21)*



**Amounts of reagents used:** 4,7-dibromo-5,6-bis(dodecyloxy)-2,1,3-benzoxadiazole **14** (0.34 g, 0.526 mmol), Pd(PPh<sub>3</sub>)<sub>2</sub>Cl<sub>2</sub> (0.026 g, 0.037 mmol), PPh<sub>3</sub> (0.01 g, 0.037 mmol), CuI (0.007 g, 0.037 mmol), 1,2-bis(dodecyloxy)-4-ethynylbenzene **17** (0.52 g, 1.10 mmol), Et<sub>3</sub>N (50 mL).

A bright orange colored solid; **yield:** 225 mg, 30%; **m.p.** = 60.0-61.5 °C; **<sup>1</sup>H NMR (CDCl<sub>3</sub>, 400 MHz):** δ = 7.2 (dd, 2H, *J* = 8.4 Hz, *J*<sup>*f*</sup> = 2.0 Hz), 7.1 (d, 2H, *J*<sup>*f*</sup> = 2.0 Hz), 6.8 (d, 2H, *J* = 8.4 Hz), 4.4 (t, 4H), 4.0 (ot, 8H), 1.8 (b), 1.3 (b), 0.9 (ot); **<sup>13</sup>C NMR (CDCl<sub>3</sub>, 100.6 MHz):** δ = 158.3, 150.5, 148.8, 147.8, 125.3, 116.6, 114.5, 113.1, 102.2, 101.1, 79.4, 75.0, 69.3, 69.1, 31.9, 30.4, 29.7, 29.7, 29.4, 26.1, 26.0, 22.7, 14.1; **FT-IR (KBr, cm<sup>-1</sup>):** 2918, 2860, 2204, 1597, 1514, 1467, 1301, 1265; **CI-MS [M+H]<sup>+</sup>** calculated for C<sub>94</sub>H<sub>156</sub>N<sub>2</sub>O<sub>7</sub> m/z: 1426.2; Found: 1427.3. **CHN:** Expected: C 79.16, H 11.02, N 1.96. Found: C 79.13, H 10.98, N 1.99.

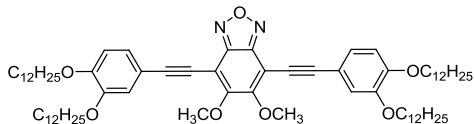
*4,7-Bis((4-(dodecyloxy)phenyl)ethynyl)-5,6-dimethoxy-2,1,3-benzoxadiazole (22)*



**Amounts of reagents used:** 4,7-dibromo-5,6-dimethoxy-2,1,3-benzoxadiazole **15** (0.22 g, 0.67 mmol), Pd(PPh<sub>3</sub>)<sub>2</sub>Cl<sub>2</sub> (0.023 g, 0.033 mmol), PPh<sub>3</sub> (0.01 g, 0.033 mmol), CuI (0.006 g, 0.033 mmol), 1-(dodecyloxy)-4-ethynylbenzene **16** (0.42 g, 1.47 mmol), Et<sub>3</sub>N (50 mL).

A yellow colored solid; **yield:** 260.9 mg, 52 %; **m.p.** = 55.5–58.0 °C; **<sup>1</sup>H NMR (CDCl<sub>3</sub>, 400 MHz):** δ = 7.6 (d, 4H, *J* = 8.6 Hz), 6.9 (d, 4H, *J* = 8.6 Hz), 4.3 (s, 6H), 4.0 (t, 4H), 1.8 (qui), 1.3 (b), 0.9 (t); **<sup>13</sup>C NMR (CDCl<sub>3</sub>, 100.6 MHz):** δ = 160.0, 158.2, 147.8, 133.3, 114.7, 114.2, 105.0, 102.4, 100.3, 79.3, 68.2, 61.6, 31.9, 29.7, 29.6, 29.6, 29.3, 29.1, 26.0, 22.7, 14.1; **FT-IR (KBr, cm<sup>-1</sup>):** 2923, 2849, 2207, 1730, 1604, 1508, 1466, 1306, 1251; **CI-MS [M+H]<sup>+</sup>** calculated for C<sub>48</sub>H<sub>64</sub>N<sub>2</sub>O<sub>5</sub> *m/z*: 748.5; Found: 749.5. **CHN:** Expected: C 76.97, H 8.61, N 3.74. Found: C 76.98, H 8.59, N 3.75.

*4,7-Bis((3,4-bis(dodecyloxy)phenyl)ethynyl)-5,6-dimethoxy-2,1,3-benzoxadiazole (23)*

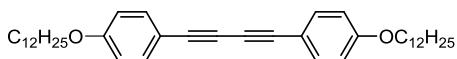


**Amounts of reagents used:** 4,7-dibromo-5,6-dimethoxy-2,1,3-benzoxadiazole **15** (0.157 g, 0.45 mmol), Pd(PPh<sub>3</sub>)<sub>2</sub>Cl<sub>2</sub> (0.016 g, 0.022 mmol), PPh<sub>3</sub> (0.006 g, 0.022 mmol), CuI (0.004 g, 0.022 mmol), 1,2-bis(dodecyloxy)-4-ethynylbenzene **17** (0.46 g, 0.97 mmol), Et<sub>3</sub>N (50 mL).

As bright orange colored solid; **yield:** 176 mg, 35 %, **m.p.** = 61.0–63.0 °C; **<sup>1</sup>H NMR (CDCl<sub>3</sub>, 400 MHz):** δ = 7.2 (dd, 2H, *J* = 8.2 Hz, *J*<sup>*f*</sup> = 2.0 Hz), 7.1 (d, 2H, *J*<sup>*f*</sup> = 2.0 Hz), 6.9 (d, 2H, *J* = 8.2 Hz), 4.3 (s, 6H), 4.0

(ot 8H), 1.8 (quint), 1.3 (br), 0.9 (t);  $^{13}\text{C}$  NMR ( $\text{CDCl}_3$ , 100.6 MHz):  $\delta = 158.3, 150.6, 148.8, 147.8, 125.4, 116.5, 114.3, 113.0, 105.0, 102.7, 100.3, 79.0, 69.4, 69.1, 61.7, 31.9, 29.4, 26.0, 22.7, 14.1$ ; FT-IR (KBr,  $\text{cm}^{-1}$ ): 2919, 2848, 2209, 1730, 1515, 1467, 1313, 1270; CI-MS  $[\text{M}+\text{H}]^+$  calculated for  $\text{C}_{72}\text{H}_{112}\text{N}_2\text{O}_7$  m/z: 1116.8; Found: 1117.9. CHN: Expected: C 77.37, H 10.10, N 2.51. Found: C 77.30, H 10.11, N 2.51.

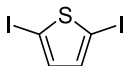
*1,4-bis(4-(dodecyloxy)phenyl)buta-1,3-diyne (38)*



The homocoupling product **38** was isolated as by-product during the synthesis of compound **22**.

$^1\text{H}$  NMR ( $\text{CDCl}_3$ ):  $\delta = 7.45$  (d, 4H,  $J = 8.79$  Hz),  $6.84$  (d, 4H,  $J = 8.79$  Hz),  $3.97$  (t, 4H,  $J = 6.64$  Hz),  $1.79$  (qui, 4H,  $J = 7.81$  Hz),  $1.45$  (m, 4H),  $1.27$  (br, 32H),  $0.89$  (t, 6H,  $J = 7.03$  Hz).

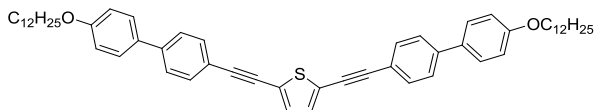
*2,5-Diiodothiophene (44)*



In a 125 mL flask, a mixture of thiophene (10 g, 118.9 mmol), Iodine (30.18 g, 118.9 mmol) and chloroform (50 mL) was stirred at room temperature till dissolution. Then 20 mL of 50%  $\text{HNO}_3$  was added slowly and drop wise with vigorous stirring. After complete addition of the acid, the reaction mixture was refluxed for 24 hours. After cooling to room temperature, the reaction mixture was extracted with dichloromethane (3 x 50 mL). The organic phase was successively washed with saturated  $\text{Na}_2\text{SO}_3$  (2 x 25 mL), 10 % NaOH (2 x 10 mL), water (2 x 10 mL) and then dried over  $\text{Na}_2\text{SO}_4$ . The solvent was evaporated under reduced pressure and the residue was purified through silica gel column eluted with hexane to furnish the 2,5-diiodothiophene.

**Yield:** 31.15 g, 78 % ;  $^1\text{H}$  NMR ( $\text{CDCl}_3$ ):  $\delta = 6.94$  (s);  $^{13}\text{C}$  NMR ( $\text{CDCl}_3$ ):  $\delta = 138.75, 76.19$ .

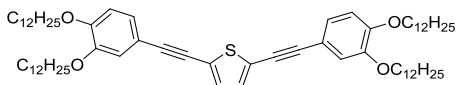
*2,5-bis((4'-(dodecyloxy)biphenyl-4-yl)ethynyl)thiophene (45)*



**Amounts of reagents used:** 2,5-Diiodothiophene **44** (0.25 g, 0.75 mmol), Pd(PPh<sub>3</sub>)<sub>2</sub>Cl<sub>2</sub> (0.052 g, 0.075 mmol), PPh<sub>3</sub> (0.02 g, 0.075 mmol), CuI (approximately 0.075 mmol), 4-(dodecyloxy)-4'-ethynylbiphenyl **40** (0.6 g, 1.65 mmol), Et<sub>3</sub>N : THF (15 : 15 mL).

As yellow colored solid; **isolated yield:** 321 mg, 53 %; <sup>1</sup>H NMR (CDCl<sub>3</sub>): δ = 7.58-7.51 (m, 14 H), 6.97 (d, 4H, *J* = 7.03 Hz), 4.00 (t, 4H, *J* = 7.03 Hz), 1.8 (qui, 4H), 1.26 (br, 32 H), 0.88 (t, 6H, *J* = 7.03 Hz); <sup>13</sup>C NMR (CDCl<sub>3</sub>): δ = Unfortunately, the solubility in solvents such as chloroform-d or dimethyl-d sulfoxide was not high enough to measure <sup>13</sup>C NMR spectra for further structural characterization. **FT-IR (KBr, cm<sup>-1</sup>):** 3040, 2954, 2934, 2918, 2874, 2848, 2189, 1920, 1896, 1664, 1606, 1580, 1528.

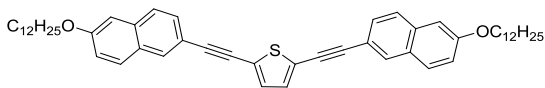
*2,5-bis((3,4-bis(dodecyloxy)phenyl)ethynyl)thiophene (46)*



**Amounts of reagents used:** 2,5-Diiodothiophene **44** (0.2 g, 0.6 mmol), Pd(PPh<sub>3</sub>)<sub>2</sub>Cl<sub>2</sub> (0.042 g, 0.06 mmol), PPh<sub>3</sub> (0.016 g, 0.06 mmol), CuI (0.06 mmol), 1,2-bis(dodecyloxy)-4-ethynylbenzene **17** (0.71 g, 1.5 mmol), Et<sub>3</sub>N : THF (25 : 25 mL).

As yellow colored solid; **isolated yield:** 153 mg, 25 %, **m.p.** = 83.0 - 85.3 °C; <sup>1</sup>H NMR (CDCl<sub>3</sub>): δ = 7.10 (s, 2H), 7.08 (dd, 2H, *J*<sup>3</sup> = 8.21 Hz, *J*<sup>4</sup> = 1.56 Hz), 7.02 (d, 2H, *J* = 1.56), 6.82 (d, 2H, *J* = 8.21 Hz), 4.01 (m, 8H), 1.82 (qui, 8H, *J* = 7.42 Hz), 1.47 (m, 8H), 1.26 (br), 0.88 (t, 12 H, *J* = 7.03 Hz); <sup>13</sup>C NMR (CDCl<sub>3</sub>): δ = 149.98, 148.69, 131.34, 124.95, 116.30, 114.55, 113.08, 94.29, 87.38, 80.29, 69.22, 69.08, 31.94, 29.71, 29.67, 29.64, 29.63, 29.42, 29.38, 29.19, 25.99, 22.70, 14.13; **FT-IR (KBr, cm<sup>-1</sup>):** 2954, 2917, 2872, 2850, 2200, 1734, 1597, 1575.

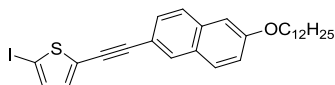
## 2,5-bis((6-(dodecyloxy)naphthalen-2-yl)ethynyl)thiophene (47)



**Amounts of reagents used:** 2,5-Diiodothiophene **44** (0.25 g, 0.74 mmol), Pd(PPh<sub>3</sub>)<sub>2</sub>Cl<sub>2</sub> (0.05 g, 0.074 mmol), PPh<sub>3</sub> (0.02 g, 0.074 mmol), CuI (approximately 0.074 mmol), 2-(dodecyloxy)-6-ethynynaphthalene **39** (0.54 g, 1.6 mmol), Et<sub>3</sub>N : THF (15 : 15 mL).

As cream color solid; **isolated yield:** 303 mg, 54 %; **<sup>1</sup>H NMR (CDCl<sub>3</sub>):** δ = 7.97 (broad singlet, 2H), 7.71 (d, 2H, J = 9.38 Hz), 7.68 (d, 2H, J = 8.60 Hz), 7.52 (dd, 2H, J<sup>3</sup> = 8.60 Hz, J<sup>4</sup> = 1.56 Hz), 7.19 (s, 2H), 7.17 (dd, 2H, J<sup>3</sup> = 9.38 Hz, J<sup>4</sup> = 2.74 Hz), 7.10 (d, 2H, J = 1.95 Hz), 4.01 (t, 4H, J = 6.64 Hz), 1.85 (qui, 4H, J = 7.42 Hz), 1.5 (m), 1.27 (broad peak, 32 H), 0.89 (t, 6H, J = 7.03 Hz); **<sup>13</sup>C NMR (CDCl<sub>3</sub>):** δ = 158.05, 134.38, 131.67, 131.34, 129.34, 128.56, 128.32, 126.86, 124.73, 119.85, 117.28, 106.56, 94.80, 82.01, 68.12, 31.93, 29.68, 29.65, 29.65, 29.60, 29.42, 29.36, 29.20, 26.10, 22.70, 14.14; **FT-IR (KBr, cm<sup>-1</sup>):** 3058, 2954, 2918, 2871, 2849, 2205, 2141, 1923, 1781, 1718, 1623, 1600.

## 2-((6-(dodecyloxy)naphthalen-2-yl)ethynyl)-5-iodothiophene (48)

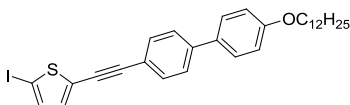


**Amounts of reagents used:** 2,5-Diiodothiophene **44** (3.0 g, 8.93 mmol), Pd(PPh<sub>3</sub>)<sub>2</sub>Cl<sub>2</sub> (0.1 g, 0.15 mmol), PPh<sub>3</sub> (0.04 g, 0.15 mmol), CuI (0.15 mmol), 2-(dodecyloxy)-6-ethynynaphthalene **39** (g, mmol), Et<sub>3</sub>N : THF (25 : 25 mL).

As cream colored solid; **Isolated yield:** 1.18 g, 73.3 %, **m.p.** = 86.7 - 87.5 °C; **<sup>1</sup>H NMR (CDCl<sub>3</sub>):** δ = 7.94 (broad singlet, 1H), 7.70 (d, 1H, J = 8.99 Hz), 7.67 (d, 1H, J = 8.60 Hz), 7.49 (dd, 1H, J<sup>3</sup> = 8.21 Hz, J<sup>4</sup> = 1.56 Hz), 7.18 (d, 1H, J = 2.74 Hz), 7.16 (d, 1H, J = 3.91 Hz), 7.10 (d, 1H, J = 1.95 Hz), 6.95 (d, 1H, J = 3.91 Hz), 4.07 (t, 2H, J = 6.64 Hz), 1.85 (qui, 2H, J = 7.82), 1.5 (m, 2H), 1.27 (broad peak, 16 H), 0.89 (t, 3H, J = 7.03 Hz); **<sup>13</sup>C NMR (CDCl<sub>3</sub>):** δ = 158.07, 137.08, 134.39,

132.93, 131.30, 129.78, 129.34, 128.50, 128.29, 126.86, 119.85, 117.14, 106.55, 95.66, 81.02, 74.34, 68.11, 31.94, 29.69, 29.66, 29.63, 29.61, 29.42, 29.37, 29.20, 26.10, 22.71, 14.15; **FT-IR (KBr,  $\text{cm}^{-1}$ )**: 3060, 2954, 2915, 2873, 2848, 1927, 1782, 1756, 1719, 1624, 1601, 1497.

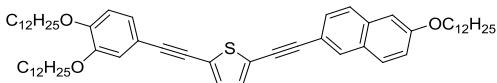
*2-((4'-(dodecyloxy)biphenyl-4-yl)ethynyl)-5-iodothiophene (49)*



**Amounts of reagents used:** 2,5-Diiodothiophene **44** (3.8 g, 11.5 mmol),  $\text{Pd}(\text{PPh}_3)_2\text{Cl}_2$  (0.13 g, 0.19 mmol),  $\text{PPh}_3$  (0.05 g, 0.19 mmol),  $\text{CuI}$  (g, 0.19 mmol), 4-(dodecyloxy)-4'-ethynylbiphenyl **40** (0.036 g, 0.19 mmol),  $\text{Et}_3\text{N}$ : THF (25 : 25 mL).

As almond colored solid; **Isolated yield:** 1.65 g, 75 %, **m.p.** = 176.0 -178.5 °C;  **$^1\text{H NMR}$  ( $\text{CDCl}_3$ )**:  $\delta$  = 7.56-7.52 (overlapped peaks, 6H), 7.16 (d, 1H,  $J$  = 3.91 Hz), 6.97 (d, 2H,  $J$  = 8.60 Hz), 6.94 (d, 1H,  $J$  = 3.52 Hz), 4.0 (t, 2H,  $J$  = 6.64 Hz), 1.80 (qui, 2H,  $J$  = 7.42 Hz), 1.47 (m, 2H), 1.27 (broad, 16H), 0.88 (t, 3H,  $J$  = 7.42 Hz);  **$^{13}\text{C NMR}$  ( $\text{CDCl}_3$ )**:  $\delta$  = Unfortunately, the solubility in solvents such as chloroform-d or dimethyl-d sulfoxide was not high enough to measure  $^{13}\text{C NMR}$  spectra for further structural characterization. **FT-IR (KBr,  $\text{cm}^{-1}$ )**: 2954, 2935, 2919, 2873, 2849, 2200, 1919, 1896, 1757, 1664, 1608, 1579.

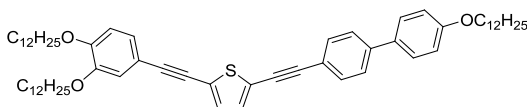
*2-((3,4-bis(dodecyloxy)phenyl)ethynyl)-5-((6(dodecyloxy)naphthalen-2-yl)ethynyl)thiophene (50)*



**Amounts of reagents used:** 2-((6-(dodecyloxy)naphthalen-2-yl)ethynyl)-5-iodothiophene **48** (0.4 g, 0.73 mmol),  $\text{Pd}(\text{PPh}_3)_2\text{Cl}_2$  (0.026 g, 0.036 mmol),  $\text{PPh}_3$  (0.01 g, 0.036 mmol),  $\text{CuI}$  (approximately 0.036 mmol), 1,2-bis(dodecyloxy)-4-ethynylbenzene **17** (0.45 g, 0.95 mmol),  $\text{Et}_3\text{N}$ : THF (25 : 25 mL).

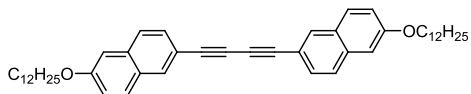
As yellow colored solid; **Isolated yield:** 250 mg, 38.3 %, **m.p.** = 73.0 - 74.5 °C; **<sup>1</sup>H NMR (CDCl<sub>3</sub>):** δ = 7.98 (s, 1H), 7.73 (d, 1H, J = 6.06 Hz), 7.69 (d, 1H, J = 5.56 Hz), 7.53 (dd, 1H, J<sup>3</sup> = 8.59 Hz, J<sup>4</sup> = 2.02 Hz), 7.20 (m, 1H), 7.16 (m, 2H), 7.13 (m, 1H), 7.09 (d, 1H, J = 2.02 Hz), 7.05 (d, 1H, J = 2.02 Hz), 6.84 (d, 1H, J = 8.59 Hz), 4.07 (t, 2H, J = 6.57 Hz), 4.02 (t, 4H, J = 6.57 Hz) 1.84 (m, 6H), 1.29 (broad, 48 H), 0.90 (t, 9H, J = 7.03 Hz); **<sup>13</sup>C NMR (CDCl<sub>3</sub>): FT-IR (KBr, cm<sup>-1</sup>):** 2955, 2919, 2873, 2849, 2200, 1850, 1776, 1627, 1598, 1574, 1521.

2-((3,4-bis(dodecyloxy)phenyl)ethynyl)-5-((4'-(dodecyloxy)biphenyl-4-yl)ethynyl)thiophene (**51**)



**Amounts of reagents used:** 2-((4'-(dodecyloxy)biphenyl-4-yl)ethynyl)-5-iodothiophene **49** (0.44 g, 0.76 mmol), Pd(PPh<sub>3</sub>)<sub>2</sub>Cl<sub>2</sub> (0.027 g, 0.038 mmol), PPh<sub>3</sub> (0.01 g, 0.038 mmol), CuI (approximately 0.038 mmol), 1,2-bis(dodecyloxy)-4-ethynylbenzene **17** (g, mmol), Et<sub>3</sub>N : THF (25 : 25 mL).

As bright yellow solid; **isolated yield:** 110 mg, 15.7 %; **<sup>1</sup>H NMR (CDCl<sub>3</sub>):** δ = 7.55-7.52 (overlapped peaks, 6H), 7.16 (d, 1H, J = 3.91 Hz), 7.13 (d, 1H, J = 3.52 Hz), 7.09 (dd, 1H, J<sub>3</sub> = 8.21 Hz, J<sub>4</sub> = 1.56 Hz), 7.03 (d, 1H, J = 1.56 Hz), 6.97 (d, 2H, J = 8.60 Hz), 6.83 (d, 1H, J = 8.21 Hz), 4.02-3.98 (m, 6H), 1.82 (m), 1.47 (m), 1.26 (m), 0.88 (t, 9H, J = 7.03 Hz); **<sup>13</sup>C NMR (CDCl<sub>3</sub>):** δ = 159.11, 148.75, 140.99, 131.85, 131.72, 131.36, 128.0, 126.50, 125.04, 125.0, 124.27, 120.70, 116.40, 114.88, 114.55, 113.16, 94.51, 94.04, 86.22, 80.75, 69.26, 68.12, 59.52, 38.14, 31.93, 31.23, 29.70-29.63 (overlapped), 29.41, 29.37, 29.27, 29.20, 29.17, 26.0, 22.69, 14.11; **FT-IR (KBr, cm<sup>-1</sup>):** 2954, 2919, 2872, 2848, 2197, 2140, 1597, 1575, 1518, 1495.

*1,4-bis(6-(dodecyloxy)naphthalen-2-yl)buta-1,3-diyne (52)*

The homocoupling product **52** was isolated as by-product during the synthesis of compound **47**.

**<sup>1</sup>H NMR (CDCl<sub>3</sub>):**  $\delta$  = 8.0 (s, 2H), 6.7 (d, 2H,  $J$  = 8.99 Hz), 7.66 (d, 2H,  $J$  = 8.60 Hz), 7.51 (dd, 2H,  $J^3$  = 8.60 Hz,  $J^4$  = 1.56 Hz), 7.17 (dd, 2H,  $J^3$  = 8.99 Hz,  $J^4$  = 2.74 Hz), 7.10 (d, 2H,  $J$  = 1.95 Hz), 4.07 (t, 4H,  $J$  = 6.64 Hz), 1.85 (qui, 4H,  $J$  = 7.82 Hz), 1.5 (m, 4H), 1.27 (br, 32H), 0.88 (t, 6H,  $J$  = 7.03 Hz); **FT-IR (KBr, cm<sup>-1</sup>):** 2957, 2921, 2870, 2848, 2141, 1917, 1781, 1622, 1600, 1498.



## **6. APPENDIX**

## A.1. CYCLIC VOLTAMMETRY

Cyclic voltammetry (CV) is a simple, rapid and a dynamic electrochemical technique that is most widely used for the fundamental studies of oxidation and reduction processes. Important parameters to analyze the electrical properties of organic materials such as ionization potential (IP), electron affinity (EA) and energy gap ( $E_g$ ) can be determined from the cyclic voltammogram. This technique is based on varying the applied potential at a working electrode (at some scan rate) and monitoring any resulting changes in cell current. The initial scan can be in either direction (negative or positive) and then reversed to run in the opposite direction to complete a potential sweep cycle, hence, the name cyclic voltammetry. The applied potential forces a change in the concentration of an electroactive species at the electrode surface by reducing or oxidizing it. Advantages of the cyclic voltammetry include excellent sensitivity for both inorganic and organic species, rapid analysis times (seconds) and the ease with which small currents are measured.

### A.1.1. The Electrochemical Cell

The CV experiment is carried out in the electrochemical cell which consists of the sample dissolved in a solvent, an electrochemically inactive ionic electrolyte, a working electrode, a reference electrode, and usually a counter (auxiliary) electrode. The material of the cell (glass, teflon, polyethylene) is selected to minimize reaction with the sample.

**Working Electrodes:** The working electrodes are of various geometries and materials, ranging from small Hg drops to flat Pt disks. Other commonly used electrode materials are gold, graphite and glassy carbon. **Reference Electrodes:** The voltage measured is that of the working electrode relative to the reference electrode. In most cases, the reference electrode should be as close as possible to the working electrode without touching it. The most commonly used reference electrodes are the calomel electrode and the silver/silver chloride electrode. **Counter Electrodes:** The counter electrode plays no part in redox reaction but completes the circuit. Most often, it consists of a thin

Pt wire, although other inert material like Au and sometimes graphite are also used.

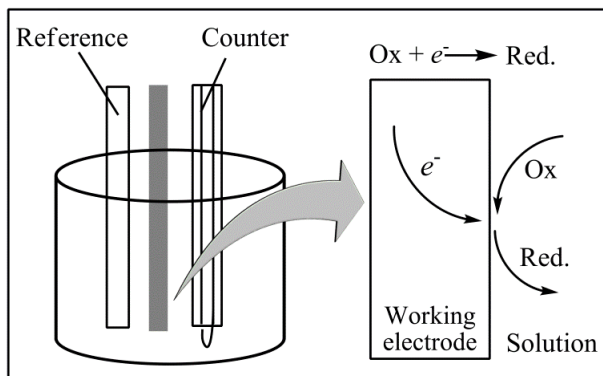


**Figure 56.** Schematic diagram of a three electrode electrochemical cell.

In aqueous solutions, the redox potentials are measured versus the universally accepted and reliable reference electrodes such as the normal hydrogen electrode (SHE) or the saturated calomel electrode (SCE). However, measurements in water are not possible in many instances due to insolubility or instability of the compound in water. Unlike for aqueous solutions, no universal reference electrode exists for the measurements in non aqueous solutions. The potentials measured versus different reference electrode systems cannot be directly related to each other, and are occasionally difficult to be reproduced. A practical approach to this problem is the use of a redox couple (e.g.  $\text{Fc}^+/\text{Fc}$ )<sup>173</sup> as an internal standard in the same fashion as the use of internal standards in NMR spectroscopy. In such cases, the measured potentials are reported relative to the (common) internal reference rather the different reference electrodes. An important advantage of this approach is that the effects of variables (i.e. type of reference electrode, solvents, electrode degradation etc.) in different measurements are eliminated. The formal potentials relative to the internal standard remain unchanged and are reproducible.

### A.1.2. Practical Considerations In Cyclic Voltammetry

During a CV experiment, considerations are given to the effects of the solvent, the electrolytes and the electrodes. For accurate measurement, the solvent must resist oxidation or reduction at the applied potentials. Usually the solvents with high dielectric constants (e.g. water or acetonitrile) are used to enable the electrolyte to dissolve and aid the passage of current. Furthermore, the electrodes and the supporting electrolyte also must not react with the sample. The combination of solvent, electrolyte and specific working electrode material determines the range of the potential that can be applied. Prior to experiment, any dissolved oxygen is removed from the solution by bubbling an inert gas. A potentiostat applies a known potential between the working and the reference electrodes. Potential of the reference electrode is usually fixed and only potential of the working electrode is varied. At a certain potential, the oxidation or reduction of a substance takes place on the surface of the working electrode (**Fig. 56**). This results in the mass transport of new material from bulk solution to the electrode surface, which in turn generates a current that flows between the working and counter electrodes. When the scan is reversed, the reaction moves back through the equilibrium position gradually converting electrolysis product back to reactant. The current flow is now in the direction opposite to that of the forward step, i.e. from the solution species back to the electrode.

### A.1.3. Mass Transport

The current is a quantitative measure of how fast a species is being reduced or oxidized at the electrode surface. For a fixed electrode area, the reaction can be controlled by two factors i.e. the rate constant and the surface concentration of the reactant. If the rate constant is large such that any reactant close to the interface is immediately converted into products, then the current will be controlled by the amount of fresh reactant reaching the interface from the bulk solution. Thus movement of reactant in and out of the electrode-solution interface (mass transport) is important in predicting the current flowing.

There are three forms of mass transport which can influence an electrolysis reaction. **Diffusion:** Diffusion arises from the local uneven concentrations of reagents and is often found to be the most significant transport process for many electrolysis reactions. Since the reaction only occurs at the electrode surface, there exist a lower reactant concentration at the electrode than in bulk solution. Similarly a higher concentration of product will exist near the electrode than further out into solution. Entropic forces act to smooth out these uneven distributions of concentration and are therefore the main driving force for the diffusion process. **Migration:** Migration is the movement of a charged ion in the presence of an electric field. In the bulk solution, concentration gradients are generally small and ionic migration carries most of the current. The relative contributions of diffusion and migration to the flux of a species differs for different locations in solution. Near the electrode, in general, the mass transport is mainly by the diffusion. In the bulk solution (away from the electrode), concentration gradients are usually small and the current is carried mainly by migration. **Convection:** Convection is the mass transfer of the electroactive species by thermal currents, by density gradients present in the solution, or by some form of mechanical movement like stirring the solution or rotating the electrode. In many voltammetric experiments, there is no stirring and the only form of mass transport is diffusion. These are referred to as *stationary solution* techniques. In other experiments referred to as *hydrodynamic* techniques, the solution is stirred either by a stir bar or preferably (due to the more precise control of the rate of rotation) by a rotating electrode.

#### A.1.4. The Role of Supporting Electrolyte

The shape of the voltammogram depends on the rate of reaction and the rate of the mass transport. If the rate of reaction is very slow or the transport is migration controlled, a wave instead of a peak is observed. Addition of an excess of a supporting electrolyte (non-electroactive ions) nearly eliminates the contribution of migration to the mass transfer and the flux of electroactive species to the electrode is almost completely due to diffusion.<sup>178</sup> The choice of supporting electrolyte depends on the solvent used and electrode process of interest. Many acids, bases, and salts are available for aqueous solutions. For organic solvents with high dielectric constants, e.g. acetonitrile and

DMF, usually tetra-*n*-alkylammonium salts such as tetrabutylammonium tetrafluoroborate (TBABF<sub>4</sub>), tetra-*n*-butylammonium hexafluorophosphate (TBAPF<sub>6</sub>) and tetraethylammonium perchlorate (Et<sub>4</sub>NClO<sub>4</sub>) are employed. In addition to minimizing the contribution of migration, the supporting electrolyte serves other important functions as well. The presence of a high concentration of ions decreases the solution resistance between the working and reference electrodes. Consequently, the supporting electrolyte allows an improvement in the accuracy with which the working electrode's potential is measured. It also establishes a uniform ionic strength throughout the solution, even when ions are produced or consumed at the electrodes. Besides these physical benefits, the supporting electrolyte may also contribute chemically by establishing the solution composition (pH, ionic strength, ligand concentration) that controls the reaction conditions.<sup>179</sup>

## A.2. Vacuum Level and Its Relationship With The IP, EA and E<sub>gap</sub>

When an isolated electron is at rest in a vacuum, it is said to be at the vacuum level (VL)<sup>180</sup> and this level is often taken as an invariant energy reference. Ionization potential (IP) is the energy required to remove an electron from the HOMO to an infinite distance in vacuum and the energy required to bring an electron from an infinite distance in vacuum to the LUMO is called the electron affinity (EA). The difference between IP and EA is equivalent to the band gap energy E<sub>g</sub> i.e. difference between HOMO and LUMO energy levels (**Fig. 57**). These parameters are very important to understand the electrical properties of materials and can be determined from the cyclic voltammogram. The graphical and mathematical procedures for estimating the positions of HOMO and LUMO levels from electrochemical data are described in the results and discussions section.

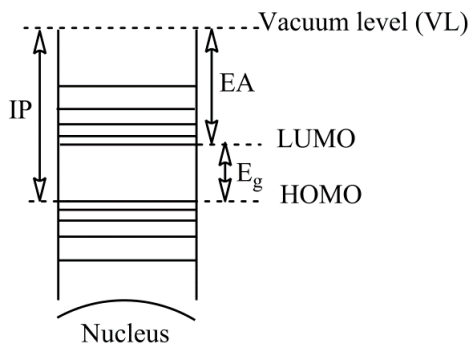


**Figure 57.** Schematic diagram representing the HOMO, LUMO levels and their relationship with the vacuum level (VL).

### A.3. IDENTIFICATION OF THE MESOPHASES

No single method of identification is conclusive in determining the mesophase and a set of optical, spectroscopic and calorimetric methods are used. The most commonly used techniques for the identification of liquid crystal phases are differential scanning calorimetry, polarizing optical microscopy and X-ray diffraction analysis. Before performing DSC, thermal stability of the sample is determined thermogravimetrically to find the safe temperature limit up to which it can be repeatedly heated without any decomposition.

#### A.3.1. Polarizing Optical Microscopy

Polarizing optical microscopy (POM) is often the method of first choice for the identification of different types of mesophases formed and to note their respective transition temperatures. In this technique, a small amount of the test sample taken on a glass slide and covered with a cover slip is placed on a temperature controlled hot stage between the polarizer and analyzer which are crossed at  $90^\circ$  to each other. The compound is gradually heated first at a controlled rate and then cooled at a slow rate, usually from  $0.5$  to  $2^\circ\text{C}/\text{min}$ . Interactions of the resulting phases with the polarized light are observed through the analyzer. Polarized light remains unaffected by isotropic liquid and the field of view appears dark. However, for the mesophases, being anisotropic and hence birefringent, light is not extinguished and an optical texture

develops that gives information about the arrangement of molecules within the mesophase. The term texture refers to the orientation of liquid crystal molecules in the vicinity of a surface. Regions with the same color have the same orientation of their constituent molecules. Each liquid crystal mesophase can form its own characteristic textures, which are useful in identification.<sup>66</sup>

### A.3.2. Differential Scanning Calorimetry

Differential scanning calorimetry (DSC) is a preliminary technique used for determining the transition temperatures and complements optical methods in the study of liquid crystal phase transitions. It proves useful to determine the occurrence, magnitude and temperatures of transitions, however, it is not a tool for identification of the mesophases. This technique involves measurement of heat changes of the sample in comparison to some reference. Any material having constant heat capacity for the temperature range may be used as a reference. A sample pan containing the material to be analyzed and another pan containing a reference material are heated or cooled simultaneously at a particular rate, usually 5-10°C/min. During heating (or cooling) any chemical or physical event in which the sample absorbs or releases energy must be offset by the reference so that the balance is maintained through a displacement of the base line.<sup>181</sup> An endothermic transition in the sample demands more heat to flow to it as compared to the heat that flows to the reference compound to ensure that the temperature of the two ovens remain the same. Similarly, any exothermic change causes diminution of heat flow to the sample to maintain the uniform temperature rise for both the sample and the reference. This difference in heat flux between the two pans is recorded and plotted versus temperature to give a DSC thermogram (**Fig. 58**).

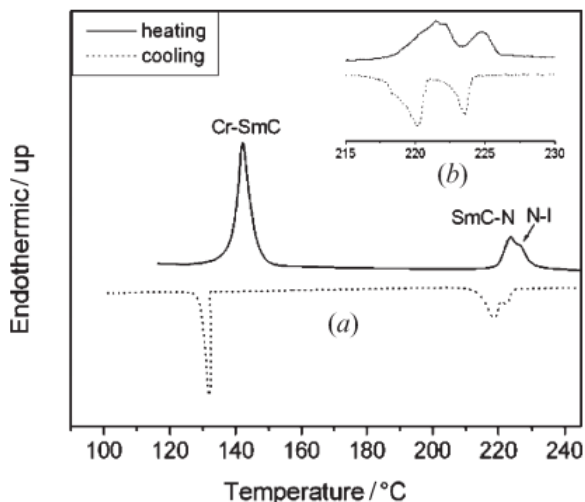


**Figure 58.** A DSC thermogram of a liquid crystalline compound showing the thermal transitions.<sup>182</sup>

From a DSC curve, two valuable information are obtained: the peak position gives the temperature at which the transition occur and the area under the peak is directly proportional to the heat absorbed or released by the reaction. The heat flux during a transition is, in turn, proportional to change in molecular arrangement during the phase transition. The higher the amount of energy involved in a transition, the greater will be the change in molecular order of the material. Thus, the transitions from solid to the mesophase tend to have high energy values due to large structural changes. However, for transitions between different LC phases and from LC phase to an isotropic liquid, the energy involved is much smaller.<sup>183</sup>

### A.3.3. X-Ray Diffraction Analysis

Due to the presence of partial molecular organization in mesophases, the liquid crystals possess a periodicity which permits the use of X-ray technique for this type of compounds. The X-ray diffraction analysis (XRD) with variable temperature complements the POM and DSC and furnishes important information about the molecular organization in mesophase. The technique used is similar to that employed for crystals. However, unlike crystals, where the technique is

based on the distance between the periodically repeating atomic planes, in liquid crystals, the technique is based on the distance between the molecular planes of a mesophase. Due to their relatively low scattering power, LCs require the use of more intense X-ray beams than the solids.<sup>184</sup> The sample is placed on top of a controlled heating plate, and then irradiated by a beam of X-ray from the source. The irradiated X-ray beam undergoes diffraction. Meanwhile, the detector moves in order to measure the intensity of diffracted radiation at different angles.

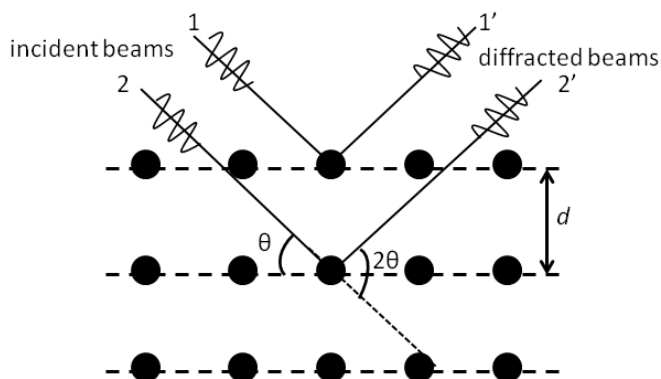


**Figure 59.** Bragg diffraction by crystal plane.

Bragg's law visualizes the scattering of X-rays as the result of reflections from sets of lattice planes (**Fig. 59**). Note that the phases of the incident X-rays change by  $180^\circ$  upon scattering. The various scattered wavelets from the different atomic sites combine and undergo constructive or destructive interference, depending on the relative phases of the different wavelets. According to Bragg's law, for a particular set of planes, constructive interference between the rays reflected by successive planes occurs only when the path difference between the reflected rays ( $2d \sin \theta$ ) equals an integral number of the wavelength.<sup>185</sup>

$$2d \sin \theta = n\lambda \quad (8)$$

where:  $n$  is an integral number,  $\lambda$  is the wavelength of the X-ray beam,  $d$  is the distance between periodic atomic planes and  $\theta$  the angle between the incident beam and the scattering plane. The diffraction angle, i.e. the

angle between the incident and scattered waves, is assumed to be  $2\theta$  (**Fig. 59**) and it depends on the wavelength of the x-ray as well as the periodic distance between atomic planes of the material. To observe a particular diffraction peak (Bragg's peak), the Bragg's conditions must be satisfied i.e. the scattering planes, apart at a distance  $d$ , must be aligned to the incident beam (of wavelength  $\lambda$ ) at an angle  $\theta$ . The resulting graph of diffraction intensity  $I(Q)$  versus diffraction angle  $2\theta$  (i.e. the angle between the incident and the diffracted beams) gives information about the state of the sample (solid, liquid-crystalline or liquid) and in the case of mesophases, even the type of molecular organization present in the mesophase.

Interpretation of the obtained diffractogram begins by looking at the number of diffraction peaks, their precise positions and looking for a relation between them. The position of a diffraction peak in the XRD diffractogram provides information, qualitatively, about the type of molecular organization and is reciprocally related to the separation between molecules (or groups of molecules) within the liquid crystalline phase. The low angle peaks relate to the translational order over long distances, for example the spacing between layers of the smectic phases. The wide angle peaks relate to the translational order over short distances (or having short periodicities), for example the lateral (in plane) order in the various smectic phases.<sup>185</sup> Similarly the sharpness of the diffraction peaks is also a measure of the extent of positional order. In general, the sharp peaks indicate existence of some long distance positional order whereas the diffuse scattering points to local orders.<sup>186</sup>

Usually, diffraction patterns of the different mesophases considerably differ from each other. A geometric relationship exists between the respective peaks and the ratio of the peak positions reveals the type of mesophase. In the case of the low-angle peaks, ratios of 1, 2, 3... indicate a smectic phase; ratios of 1,  $\sqrt{3}$ , 2,  $\sqrt{7}$ , 3. indicate a hexagonal phase; ratios of 1,  $\sqrt{2}$ ,  $\sqrt{3}$ , 2,  $\sqrt{5}$ ,  $\sqrt{6}$ ,  $\sqrt{8}$ , 3. indicate a cubic phase (**Fig. 60**). For the nematic phases, due to their more distorted and imperfect liquid-like organization, diffuse scattering peaks spread over a large angular range are seen in both the low and wide angle regions. The peaks are diffuse because these positional orders are only short range. In fact, such short range correlations usually also exist in the isotropic phase because, in real liquids, each selected molecule "feels" its nearest neighbors and forms the so-called coordination spheres i.e. there is a

short-range positional order.<sup>93</sup> So it may be difficult to distinguish the powder patterns of the nematic from that of the isotropic phase.<sup>185</sup>

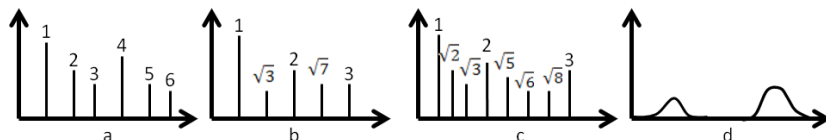


**Figure 60.** Characteristic relationship between low angle diffraction patterns of more structured (a) 1-D layer (smectic) phases, (b) 2-D hexagonal phases, (c) 3-D cubic phases, and (d) of the un-aligned nematic phases.

#### A.4. BANANA LIQUID CRYSTALS

Some bent shaped (e.g. v-shaped, hockey stick) compounds that are neither perfectly linear nor discotic can also form mesophases. In addition to the formation of conventional smectic and nematic phases, the distinguishing and characteristic feature of some bent-core LCs is the formation of polar smectic or the so called “banana phases” (B). The banana mesophases are polar and chiral (shows ferroelectricity, antiferroelectricity) even if the molecules are achiral in nature.<sup>187</sup> However, not all the bent shaped LCs are banana LCs and the term banana liquid crystals is used specifically in cases when a chiral mesophase (banana mesophase) is generated by achiral bent shaped molecules. Once grouped into the non-conventional LCs, they are now established as the third class of thermotropic LCs.<sup>188</sup> Typically, their molecular structure consists of three units: an angular central core, usually 1,3-phenylene with a bent angle of  $120^\circ$  that is changed in case of nearby substituents,<sup>188</sup> two linear rigid cores and terminal flexible chains (**Fig. 61**). Most of the banana LCs contain at least five aromatic rings. Compounds with six or seven aromatic rings<sup>189,190</sup> including six membered heteroaromatic systems as angular central core<sup>191</sup> have also been reported. Whether banana or conventional smectic (or both) phases will be formed, depends both on conformation and size of the bent core and on the structure and length of the terminal chains.

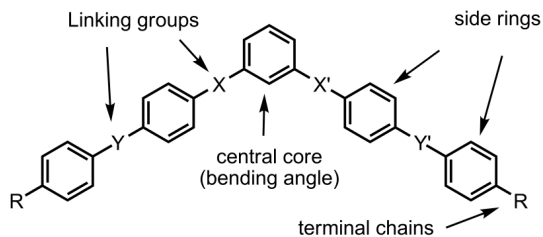


**Figure 61.** General template for banana mesogen.

The occurrence of polar order and chiral properties (optical activity, ferroelectricity) from achiral molecule is attributed to steric packing effects of the molecules.<sup>192</sup> According to this hypothesis, incorporation of bend angle in the molecule reduces the molecular symmetry. The bent shape molecules are preferably packed in certain directions (directed stacking) resulting in macroscopic polarization of the smectic layers and produce polar smectic phases (**Fig. 62**) usually SmAP, SmCP where P means polar.<sup>193</sup>

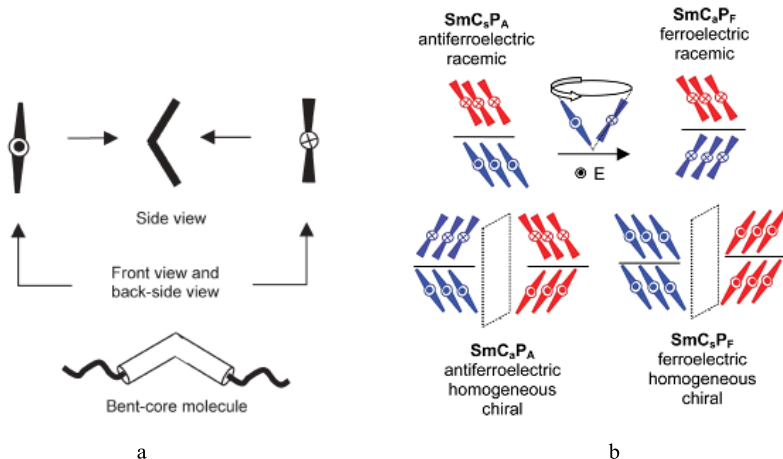


**Figure 62.** Schematic representation of (a) bent core molecule from different angles (b) Formation of polar ferroelectric, antiferroelectric and chiral phases due to directional packing of the bent core molecules in layers.<sup>194</sup>

Macroscopic polar structures are unstable and in order to escape from macroscopic polarization, the layer structures are rearranged in various ways (**Fig. 63**) that leads to chiral superstructures. Such systems

manifest superstructural chirality even though the constituent molecules are achiral.<sup>194</sup> Moreover in polar SmC (SmCP) with polarized tilted layers, combination of director tilt and polar order leads to the chirality of smectic layers although the constituent molecules are achiral.<sup>195</sup>

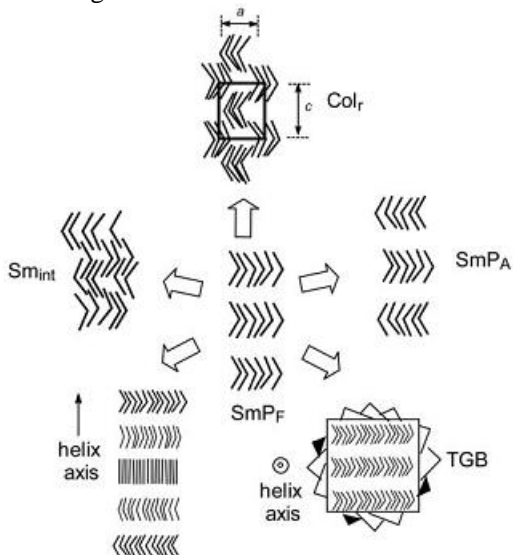


**Figure 63.** Different ways to release macroscopic polarization of the polarized layers.

## **7. BIBLIOGRAPHY**

1. Geffroy B.; Le Roy P.; Prat C. Organic light-emitting diode (OLED) technology: materials, devices and display technologies. *Polym. Int.* **2006**, 55(6), 572 - 82.
2. Maria V.; Dimitra G.; George P.; Panagiotis A. Tuning the Emitting Color of Organic Light-Emitting Diodes Through Photochemically Induced Transformations: Towards Single-Layer, Patterned, Full-Color Displays and White-Lighting Applications. *Adv. Funct. Mater.* **2007**, 17, 3477–3485.
3. Su, S. Y.; Lin, H. H.; Chang, C. C. Dual optical responses of phenothiazine derivatives: near-IR chromophore and water-soluble fluorescent organic nanoparticles. *J. Mater. Chem.* **2010**, 20 (39), 8653-8658.
4. Xiong, L.; Yu, M.; Cheng, M.; Zhang, M.; Zhang, X.; Xu, C.; et al. A photostable fluorescent probe for targeted imaging of tumor cells possessing integrin  $\alpha(v)\beta(3)$ . *Mol. BioSyst.* **2009**, 5 (3), 241-243.
5. Kajiyama, S.; Uemura, Y.; Miura, H.; Hara, K.; Koumura, N. Organic dyes with oligo-n-hexylthiophene for dye-sensitized solar cells. Relation between chemical structure of donor and photovoltaic performance. *Dyes Pigment.* **2012**, 92 (3), 1250-1260.
6. Monnier, V.; Dubuisson, E.; Sanz-Menez, N.; Boury, B.; Rouessac, V.; Ayrat, A.; et al. Selective chemical sensors based on fluorescent organic nanocrystals confined in sol-gel coatings of controlled porosity. *Microporous Mesoporous Mater.* **2010**, 132 (3), 531-537.
7. Akio, Tsuji.; Masakatsu, M.; Masako, M.; Larry, J. K.; Philip, E. S. Proceedings of the 13th International Symposium on bioluminescence and chemiluminescence progress and Perspectives. *World Scientific Publishing Co.* **2005**.
8. Fung, E. Y.; Olmstead, M. M.; Vickery, J. C.; Balch, A. L. Glowing gold rings: solvoluminescence from planar trigold (I) complexes. *Coord. Chem. Rev.* **1998**, 171, 151-159.
9. Eddingsaas, N. C.; Suslick, K. S. Intense mechanoluminescence and gas phase reactions from the sonication of an organic slurry. *J. Am. Chem. Soc.* **2007**, 129 (21), 6718-6719.
10. Gilbert, A.; Baggott, J. *Essentials of Molecular Photochemistry, 1st ed.*, Blackwell Science, Oxford, **1991**.

11. Lakowicz, J. R. *Principles of Fluorescence Spectroscopy*, 2nd ed., Kluwer Academic Plenum Publishers, New York, **1999**.
12. Kasha, M. Characterization of electronic transitions in complex molecules. *Disc. Faraday Soc.* **1950**, 9, 14-19.
13. Korolkova, N. V.; Klimenko, V. G.; Kir'yanova, T. A.; Serov, S. A.; Gastilovich, E. A. Internal heavy-atom effect on spin orbit and vibronic-spin-orbit coupling:  $n\pi^*$  phosphorescence of 9,10-anthraquinone haloderivatives. *Chem. Phys.* **1999**, 248, 233-246.
14. Parson, W. W. *Modern Optical Spectroscopy*. Springer, **2007**.
15. Schenk, G. H. *Absorption of Light and Ultraviolet Radiation Fluorescence and Phosphorescence Emission*. Ally and Bacon Inc., Boston, **1973**.
16. Rendell, D. *Fluorescence and Phosphorescence Spectroscopy*. John Wiley & Sons, **1987**.
17. Yersin, H.; Finkenzeller, W. J. Triplet Emitters for Organic Light-Emitting Diodes: Basic Properties. In Highly Efficient OLEDs with Phosphorescent Materials; Yersin, H., Ed.; Wiley-VCH: Weinheim, **2008**, p 1.
18. Baleizão, C.; Berberan-Santos, M. N. Thermally activated delayed fluorescence as a cycling process between excited singlet and triplet states: Application to the fullerenes. *J. Chem. Phys.* **2007**, 126 (20), 204510/1-204510/8.
19. Turro, N. J. *Modern Molecular Photochemistry, 1st ed.*, University Science Books, **1991**.
20. Wilson, J. S.; Chawdhury, N.; Al-Mandhary, M. R. A.; Younus, M.; Khan, M. S.; Raithby, P. R.; Köhler, A.; Friend, R. H. The Energy Gap Law for Triplet States in Pt-Containing Conjugated Polymers and Monomers. *J. Am. Chem. Soc.* **2001**, 123 (38), 9412-9417.
21. Valeur, Bernard. *Molecular Fluorescence: Principles and Applications*. Wiley-VCH, 2001.
22. Birks, J. B. *Photochemistry of Aromatic Molecules*. John Wiley, New York, **1970**.
23. Förster, T. Intermolecular energy transference and fluorescence. *Ann. Physik.* **1948**, 2, 55-75.
24. Lakowicz, J. R. *Principles of Fluorescence Spectroscopy, 3rd ed.* Springer, New York, **2006**.

25. Pauluth, Detlef; Tarumi, Kazuaki. Advanced liquid crystals for television. *J. Mater. Chem.* **2004**, 14 (8), 1219-1227.
26. Kelly, S. M. *Flat panel displays: Advanced Organic Materials*. RSC Materials Monographs, R.S.C, **2000**.
27. Vernon, F.; Khakoo, A. N. Comparison of Bentone and liquid-crystal stationary phases for the gas chromatographic separation of isomers. *J. Chromatogr.* **1978**, 157, 412-41.
28. Weiss, R. G. Thermotropic liquid crystals as reaction media for mechanistic investigations. *Tetrahedron.* **1988**, 44 (12), 3413-75.
29. Fukunaga, K.; Kansui, H.; Taniguchi, T.; Kunieda, T. Liquid Crystal Control of Regio- and Diastereoselectivity in the Acid-Catalyzed Elimination of Alkyl Phosphates to Alkenes. *Tetrahedron Lett.* **1997**, 38 (50), 8731-8734.
30. Fukunaga, K. Kunieda, T. Liquid Crystal Control: A remarkable enhancement of both efficiency and diastereoselectivity of intramolecular thermal cycloadditions in smectic solvents. *Tetrahedron Lett.* **1999**, 40, 6041-6044.
31. Lounila, J.; Jokisaari, J. Anisotropies in spin-spin coupling constants and chemical shifts as determined from the NMR spectra of molecules oriented by liquid-crystal solvents. *Progress in NMR Spectroscopy.* **1982**, 15, (3), 249-90.
32. Meddour, A. ; Berdague, P.; Hedli, A.; Courtieu, J.; Lesot, P. Proton-decoupled carbon-13 NMR spectroscopy in a lyotropic chiral nematic solvent as an analytical tool for the measurement of the enantiomeric excess. *J. Am. Chem. Soc.* **1997**, 119, 4502-4508.
33. Eichhorn, H. Mesomorphic phthalocyanines, tetraazaporphyrins, porphyrins and triphenyl-enes as charge-transporting materials. *J. Porphyrins Phthalocyanines.* **2000**, 4 (1), 88-102.
34. Eidenschink, R.; Hager, A. M. Reduction of friction through presmectic lubricants. *Mol. Cryst. Liq. Cryst. Sci. Technol. Sect. A.* **1997**, 304, 513-517.
35. Hussain, A.; Pina, A. S.; Roque, A. C. A. Bio-recognition and detection using liquid crystals. *Biosens. bioelectron.* **2009**, 25 (1), 1-8.
36. Matharu, A. S.; Shehzad, J.; Ramanujam, P. S. Liquid crystals for holographic optical data storage. *Chem. Soc. Rev.* **2007**, 36 (12), 1868-80.

37. Lehmann, O. Über fließende Kristalle. *Zeitschrift für Physikalische Chemie*. **1889**, 4, 462-72.
38. Lehmann, O. *Die flüssige Kristalle*. Leipzig, Wilhelm Engelmann, **1904**.
39. Gray, G. W. Introduction and historical development. In: Demus.; Goodby, D. J.; Gray, G.W.; Spiess, H.W.; Vill, V. (Ed.). *Handbook of Liquid Crystals*. Wiley-VCH, **1998**, Vol. 1, page 3-4.
40. G. Tammann, *Ann. Physik*. **1901**, 4, 524. **1902**, 8, 103. **1906**, 19,421.
41. W. Nernst, *Z. Elektrochem*. **1906**, 12, 43.
42. Friedel. G. The mesomorphic states of matter. *Ann. phys.* **1922**, 18, 273-474.
43. Collings, P. J. *Nature's Delicate Phase of Matter*. Princeton U. P. **1990**.
44. Baron1, M.; Stepto, R. F. T. *Pure Appl. Chem*. **2002**, 74 (3), 493-509.
45. Singh, S. Phase transitions in liquid crystals. *Phys. Rep.* **2000**, 324(2-4), 107-269.
46. Guittard, F.; Taffin de Givenchy, E.; Geribaldi, S.; Cambon, A. Highly fluorinated thermotropic liquid crystals: an update. *J. Fluorine Chem.* **1999**, 100 (1-2), 85-96.
47. Binnemans, K. Ionic liquid crystals. *Chem. Rev.* **2005**, 105 (11), 4148-204.
48. Cook, A. G.; Baumeister, U.; Tschierske, C. Supramolecular dendrimers: Unusual mesophases of ionic liquid crystals derived from protonation of DAB dendrimers with facial amphiphilic carboxylic acids. *J. Mater. Chem.* **2005**, 15 (17), 1708-1721.
49. Hudson, S. A.; Maitlis, P. M. Calamitic metallomesogens: metal-containing liquid crystals with rodlike shapes. *Chem. Rev.* **1993**, 93 (3), 861-85.
50. Giroudgodquin, A. M.; Maitlis, P. M. Metallomesogens: Metal Complexes in Organized Fluid Phases. *Angew. Chem. Int. Ed. Engl.* **1991**, 30 (4), 375-402.
51. *Metallomesogens: Synthesis, Properties, and Applications*. Edited by Jose Luis Serrano, VCH, **1996**.
52. Ishihara, S.; Furuki, Y.; Takeoka, S. A hydrogen-bonded supramolecular hexagonal columnar liquid crystal composed of

- a tricarboxylic triphenylene and monopyridyl dendrons. *Chem. Lett.* **2007**, 36 (2), 282-283.
53. Ciferri, Alberto. Assembling nano and macrostructures and the supramolecular liquid crystal. *Prog. Polym. Sci.* **1995**, 20 (6), 1081-120.
54. Taylor, R. A.; Ellis, H. A. Polymorphism, crystal-crystal and liquid crystalline thermotropic phase transition behaviour of even chain length zinc(II) n-alkanoates. *Liq. Cryst.* **2009**, 36 (3), 257-268.
55. Ray, A. Micelle formation in pure ethylene glycol. *J. Amer. Chem. Soc.* **1969**, 91 (23), 6511-6512.
56. Nakamura, Y.; Koori, M.; Li, Y.; Norisuye, T. Lyotropic liquid crystal formation of polystyrene polymacromonomers in dichloromethane. *Polymer* **2008**, 49 (22), 4877-4881.
57. Albayrak, C.; Oezkan, N.; Dag, O. Origin of Lyotropic Liquid Crystalline Mesophase Formation and Liquid Crystalline to Mesostuctured Solid Transformation in the Metal Nitrate Salt-Surfactant Systems. *Langmuir* **2011**, 27 (3), 870-873.
58. Greaves, T. L.; Drummond, C. J. Ionic liquids as amphiphile self-assembly media. *Chem. Soc. Rev.* **2008**, 37 (8), 1709-1726.
59. Fairhurst, C. E.; Fuller, S.; Gray, J.; Holmes, M.C.; Tiddy, G. J. T. Lyotropic surfactant liquid crystals. In: Demus, D.; Goodby, J.; Gray, G.W.; Spiess, H.-W.; Vill, V. (Ed.). *Handbook of Liquid Crystals*. Wiley-VCH, **1998**, Vol. 3, 346.
60. Orisch, K.; Tschierske, C.; Goring, P.; Diele, Siegm. Molecular design of thermotropic liquid crystalline polyhydroxy amphiphiles exhibiting columnar and cubic mesophases of the normal type. *Chem. Commun.* **1998**, (24), 2711-2712.
61. Stephen T. H. Identification of lyotropic liquid crystalline mesophases. In: Holmberg, K. (Ed.). *Handbook of applied surface and colloid chemistry*. John Wiley & sons **2001**.
62. Hamley, I.W.; Krysmann, M. J.; Castelletto, V.; Noirez, L. Multiple lyotropic polymorphism of a poly(ethylene glycol)-peptide conjugate in aqueous solution. *Adv. Mater.* **2008**, 20 (23), 4394-4397.
63. Fuller, S.; Hopwood, J.; Rahman, A.; Shinde, N.; Tiddy, G. J.; Attard, G. S.; Howell, O.; Sproston, S. Amphitropic liquid crystals: two lamellar phases in a surfactant containing

- thermotropic and lyotropic mesogenic groups. *Liq. Cryst.* **1992**, 12 (3), 521-529.
64. Corcoran, J.; Fuller, S.; Rahman, A.; Shinde, N.; Tiddy, G. T.; Attard, G. S. Amphitropic liquid crystals. Part 1. Effect of a thermotropic mesogen on lyotropic mesomorphism, and of a surfactant on thermotropic mesomorphism. The C16EO8-5-CB-water system. *J. Mater. Chem.* **1992**, 2 (7), 695-702.
65. Joshi, L.; Kang, S. W.; Agra, K.; Dena, Mae.; Kumar, S. Concentration, temperature, and pH dependence of sunset-yellow aggregates in aqueous solutions: An x-ray investigation. *Phys. Rev. E: Stat., Nonlin. Soft Matter Phys.* **2009**, 80, 041703/1-041703/8.
66. Dierking, I. *Textures of Liquid Crystals*. WILEY-VCH Verlag GmbH & Co. KGaA, Weinheim, **2003**.
67. Goodby, G.W. Phase structures of calamitic liquid crystals. In: Demus, D.; Goodby, J.; Gray, G.W.; Spiess, H-W.; Vill, V. (Ed.). *Handbook of Liquid Crystals*. Wiley-VCH, **1998**, Vol. 2A, 3-20.
68. Osipov, M. A.; Kuball, H. G. Helical twisting power and circular dichroism in nematic liquid crystals doped with chiral molecules. *Eur. Phys. J. E: Soft Matter* **2001**, 5 (5), 589-598.
69. Gray, G. W.; Goodby, J. W. *Smectic Liquid Crystals: Textures and Structures*. Leonard Hill, Glasgow, UK, **1984**.
70. Lagerwall, J. P. F.; Giesselmann, F. Current topics in smectic liquid crystal research. *ChemPhyschem: A European journal of chemical physics and physical chemistry* **2006**, 7 (1), 20-45.
71. Chandrasekhar, S.; Sadashiva, B. K.; Suresh, K. A. Liquid crystals of disc-like molecules. *Pramana* **1977**, 9 (5), 471-480.
72. Vorlander, D. Influence of Molecular form on the Liquid Crystalline State. *Ber. Dtsch. Chem. Ges.* **1907**, 40, 1970-1972.
73. Cammidge, A. N.; Bushby, R. J. Synthesis and structural features. In: Demus, D.; Goodby, J.; Gray, G.W.; Spiess, H-W.; Vill, V. (Ed.). *Handbook of Liquid Crystals*. Wiley-VCH, **1998**, Vol. 2B, 693-747.
74. Dolores, P.; Enrique, G. Selected strategies for the synthesis of triphenylenes. *Chem. Soc. Rev.* **2004**, 33 (5), 274-283.

75. Roussel, O.; Kestemont, G.; Tant, J.; Halleux, V. Discotic liquid crystals as electron carrier materials. *Molec. Cryst. Liq. Cryst.* **2003**, 396, 35-39.
76. Cristiano, R.; Gallardo, H.; Bortoluzzi, A. J.; Bechtold, I. H.; Carlos, E. M. Longo, R. L. Tristriazolotriazines: a core for luminescent discotic liquid crystals. *Chem. Commun.* **2008**, 5134-5136.
77. Qi, M-H.; Liu, G-F. Synthesis and properties of transition metal benzoporphyrin compound liquid crystals. *J. Mater. Chem.* **2003**, 13 (10), 2479-2484.
78. Sergeev, S.; Pisula, W.; Geerts, Y. H. Discotic liquid crystals: A new generation of organic semiconductors. *Chem. Soc. Rev.* **2007**, 36 (12), 1902-1929.
79. Msayib, K.; Makhseed, S.; McKeown, N. B. Synthetic strategies towards macrodiscotic materials. Can a new dimension be added to liquid crystal polymers? *J. Mater. Chem.* **2001**, 11(11), 2784-2789.
80. Kumar, S. *Chemistry of Discotic Liquid Crystals: From Monomers to Polymers*. CRC Press, Taylor and Francis Group **2011**.
81. Ichihara, M.; Suzuki, A.; Hatsusaka, K.; Ohta, K. Discotic liquid crystals of transition metal complexes 37\*: A thermotropic cubic mesophase having  $pn\bar{3}m$  symmetry exhibited by phthalocyanine based derivatives. *Liq. Cryst.* **2007**, 34 (5), 555-567.
82. Alameddine, B.; Aebischer, O. F.; Deschenaux, R.; Guillon, D.; Titus, A. Mesomorphic Hexabenzocoronenes Bearing Perfluorinated Chains. *Chem. Mater.* **2005**, 17 (19), 4798-4807.
83. Kumar, S. Playing with discs. *Liq. Cryst.* **2009**, 36 (6-7), 607-638.
84. Madhusudana, N. V. Recent advances in thermotropic liquid crystals. *Current Science* **2001**, 80 (8), 1018-1025.
85. Kohne, B.; Praefcke, Klaus. Liquid crystal compounds. Part 43. Hexaalkynylbenzene derivatives, first hydrocarbons as new columnar or nematic discotic liquid crystals. *Chimia* **1987**, 41(6), 196-198.
86. Langne, M.; Praefcke, K.; Krueerke, D.; Heppke, G. Chiral radial pentaynes exhibiting cholesteric discotic phases. *J. Mater. Chem.* **1995**, 5 (4), 693-699.

87. Praefcke, K.; Singer, D.; Kohne, B.; Ebert, M.; Liebmann, A.; Wendorff, J. H. Liquid crystalline compounds. 63. Charge transfer induced nematic columnar phase in low molecular weight disk-like systems. *Liq. Cryst.* **1991**, 10 (2), 147-159.
88. Kouwer, P. H. J.; Jager, W. F.; Mijs, W.; Picken, S. J. The Nematic Lateral Phase: A Novel Phase in Discotic Supramolecular Assemblies. *Macromolecules* **2001**, 34 (22), 7582-7584.
89. Kouwer, P. H. J.; Van den Berg, O.; Jager, W. F.; Mijs, W. J.; Picken, S. J. Induced Liquid Crystalline Diversity in Molecular and Polymeric Charge-Transfer Complexes of Discotic Mesogens. *Macromolecules* **2002**, 35 (7), 2576-2582.
90. Imrie, C. T.; Karasz, F. E.; Attard, G. S. Comparison of the mesogenic properties of monomeric, dimeric, and side-chain polymeric liquid crystals. *Macromolecules* **1993**, 26 (3), 545-50.
91. Blumstein, A.; Sivaramakrishnan, K. N.; Clough, S. B.; Blumstein, R. B. Polymeric thermotropic liquid crystals: polymers with mesogenic elements and flexible spacers in the main chain. *Mol. Cryst. Liq. Cryst.* **1979**, 49 (8), 255-8.
92. Blumstein, R. B.; Blumstein, A. Inherently flexible thermotropic main chain polymeric liquid crystals. *Mol. Cryst. Liq. Cryst.* **1988**, 165, 361-87.
93. Blinov, L. M. *Structure and Properties of Liquid Crystals*. Springer Science, **2011**.
94. Demus, D. One century liquid crystal chemistry: From Vorlander's rods to disks, stars and dendrites. *Mol. Cryst. Liq. Cryst. Sci. Technol., Sect. A* **2001**, 364 25-91.
95. Tschierske, C. Non-conventional liquid crystals: the importance of micro-segregation for self-organization. *J. Mater. Chem.* **1998**, 8 (7), 1485-1508.
96. Tschierske, C. Micro-segregation, molecular shape and molecular topology-partners for the design of liquid crystalline materials with complex mesophase morphologies. *J. Mater. Chem.* **2001**, 11 (11), 2647-2671.
97. Goodby, J. W.; Bruce, D. W.; Hird, M.; Imrie, C.; Neal, M. An introduction to Materials Discussion No. 4: Molecular topology in liquid crystals. *J. Mater. Chem.* **2001**, 11, 2631-2636.

98. Lehmann, M.; Jahr, M.; Grozema, F. C.; Abellon, R. D.; Siebbeles, L. D. A.; Mueller, M. Columnar mesophases with 3D order from new functional nonconventional star-shaped mesogens. *Adv. Mater.* **2008**, 20 (23), 4414-4418.
99. Lehmann, M.s; Gearba, R. I.; Koch, M. H. J.; Ivanov, D. A. Semiflexible Star-Shaped Mesogens as Nonconventional Columnar Liquid Crystals. *Chem. Mater.* **2004**, 16(3), 374-376.
100. Artal, M. C.; Toyne, K. J.; Goodby, J. W.; Barbera, J.; Photinos, D. J. Synthesis and mesogenic properties of novel board-like liquid crystals. *J. Mater. Chem.* **2001**, 11(11), 2801-2807.
101. Sultana, N. H.; Kelly, S. M.; Mansoor, B.; O'Neill, M. Polycatenar oligophenylene liquid crystals. *Liq. Cryst.* **2007**, 34 (11), 1307-1316.
102. Gharbia, M.; Gharbi, A.; Nguyen, H. T.; Malthete, J. Polycatenar liquid crystals with long rigid aromatic cores: a review of recent works. *Curr. Opin. Colloid Interface Sci.* **2002**, 7 (5,6), 312-325.
103. Yutaka, M.; Ayako, M.; Ryo, H.; Norihiro, M.; Takashi, K.; Eiichi, N. Stacking of molecules possessing a fullerene apex and a cup-shaped cavity connected by a silicon connection. *J. Amer. Chem. Soc.* **2004**, 126 (2), 432-433.
104. Zhong, Y-W; Matsuo, Y.; Eiichi, N. Lamellar Assembly of Conical Molecules Possessing a Fullerene Apex in Crystals and Liquid Crystals. *J. Amer. Chem. Soc.* **2007**, 129 (11), 3052-3053.
105. Komori, T.; Shinkai, S. Novel columnar liquid crystals designed from cone-shaped calix[4]arenes. The rigid bowl is essential for the formation of the liquid crystal phase. *Chem. Lett.*(1993), (8), 1455-8.
106. Mindyuk, O.; Stetzer, M. R.; Heiney, Paul, A.; Nelson, J. C.; Moore, J. S. High-resolution x-ray diffraction study of a tubular liquid crystal. *Adv. Mater.* **1998**, 10 (16), 1363-1366.
107. Kato, T.; Mizoshita, N.; Kishimoto, K. Functional liquid-crystalline assemblies: Self-organized soft materials. *Angew. Chem. Int. Ed.* **2006**, 45 (1), 38-68.
108. Tabushi, I.; Yamamura, K.; Kominami, K. Electric stimulus-response behavior of liquid-crystalline viologen. *J. Amer. Chem. Soc.* **1986**, 108 (20), 6409-10.

109. Aprahamian, I.; Yasuda, T.; Ikeda, T.; Saha, S.; Dichtel, W. R.; Isoda, K.; Kato, T.; Stoddart, J. Fraser. A liquid-crystalline bistable [2]rotaxane. *Angew. Chem. Int. Ed.* **2007**, 46 (25), 4675-4679.
110. Westphal, E.; Bechtold, I. H.; Gallardo, H. Synthesis and Optical/Thermal Behavior of New Azo Photoisomerizable Discotic Liquid Crystals. *Macromolecules* **2010**, 43, 1319-1328.
111. Broer, D. J.; Cees, M. W.; Bastiaansen, M. G. Debije, Albertus P. H.; Schenning, J. Functional Organic Materials based on Polymerized Liquid-Crystal Monomers: Supramolecular Hydrogen-Bonded Systems. *Angew. Chem. Int. Ed.* **2012**, 51, 7102-7109.
112. Kato, T.; Kihara, H.; Kumar, U.; Uryu, T.; Fréchet, J. M. J. A Liquid-Crystalline Polymer Network Built by Molecular Self-Assembly through Intermolecular Hydrogen Bonding. *Angew. Chem. Int. Ed. Engl.* **1994**, 33, 1644-1645.
113. Kanie, K.; Yasuda, T.; Nishii, M.; Ujiie, S.; Kato, T. Hydrogen-bonded lyotropic liquid crystals of folic acids: responses to environment by exhibiting different complex patterns. *Chem. Lett.* **2001**, (6), 480-481.
114. Berkovic, G.; Krongauz, V.; Weiss, V. Spiropyran and Spirooxazines for Memories and Switches. *Chem. Rev.* **2000**, 100, 174.
115. Irie, M. Diarylethenes for Memories and Switches. *Chem. Rev.* **2000**, 100, 1685.
116. Yokoyama, Y. Fulgides for Memories and Switches. *Chem. Rev.* **2000**, 100, 1717.
117. Dinescu, L.; Lemieux, R.P. Photomodulation of the Spontaneous Polarization of a Ferroelectric Liquid Crystal: Harnessing the Transverse Dipole Modulation of a Chiral Thioindigo Dopant. *J. Amer. Chem. Soc.* **1997**, 119, 8111.
118. Nobuyuki, T.; Takashi, K. Reversible photo-regulation of the properties of liquid crystals doped with photochromic compounds. *J. Photochem. Photobio. C: Photochem. Rev.* **2010**, 11, 47-61.
119. Neto, B. A. S.; Lopes, A. S. A.; Ebeling, G.; Goncalves, R. S.; Costa, V. E. U.; Quina, F. H.; Dupont, J. Photophysical and

- electrochemical properties of  $\pi$ -extended molecular 2,1,3-benzothiadiazoles. *Tetrahedron* **2005**, 61 (46), 10975-10982.
120. Ku, S-Y.; Chi, L-C.; Hung, W-Y.; Yang, S-W.; Tsai, T.C.; Wong, K-T.; Chen, Y-H.; Wu, C-I. High-luminescence non-doped green OLEDs based on a 9,9-diarylfuorene-terminated 2,1,3-benzothiadiazole derivative. *J. Mater. Chem.* **2009**, 19 (6), 773-780.
121. Thomas, K. R. J.; Lin, J. T.; Velusamy, M.; Tao, Y-T; Chuen, C-H. Color tuning in benzo[1,2,5]thiadiazole-based small molecules by amino conjugation/deconjugation: Bright red-light-emitting diodes. *Adv. Funct. Mater.* **2004**, 14 (1), 83-90.
122. Zhang, D.; Liu, J.; Wang, L.; Liu, Y.; Ma, D. Blue amplified spontaneous emission from 2,1,3-benzothiadiazole attached polyfluorene semiconductor polymer with high photoluminescence efficiency. *J. Phys. D: Appl. Phys.* **2009**, 42 (4), 045417/1-045417/4.
123. Vieira, A. A.; Cristiano, R; Bortoluzzi, A. J.; Gallardo, H. Luminescent 2,1,3-benzothiadiazole-based liquid crystalline compounds. *J. Mol. Struct.* **2008**, 875(1-3), 364-371.
124. Gallardo, H.; Conte, G.; Tuzimoto, P. A.; Behramand, B.; Molin, F.; Eccher, J.; Bechtold, I. V. New Luminescent Liquid Crystals Based on 2,1,3-Benzothiadiazole and Bent Five-membered N-Heterocyclic Cores. *Liquid Cryst.* **2012**, 39 (9), 1099-1111.
125. Marcelo, N. F.; Vieira, A. A.; Cristiano, R.; Gallardo, H.; Bechtold, I. H. Polarized light emission from aligned luminescent liquid crystal films based on 4,7-disubstituted-2,1,3-benzothiadiazoles. *Synth. Met.* **2009**, 159 (7-8), 675-680.
126. Fu, B.; Baltazar, J.; Hu, Z.; Chien, A-T.; Kumar, S.; Henderson, C. L.; Collard, D. M.; Reichmanis, E. High Charge Carrier Mobility, Low Band Gap Donor-Acceptor Benzothiadiazole-oligothiophene based Polymeric Semiconductors. *Chem. Mater.* **2012**, 24, 4123-4133
127. Bouffard, J.; Swager, T. M. Fluorescent conjugated polymers that incorporate substituted 2,1,3-benzooxadiazole and 2,1,3-benzothiadiazole units. *Macromolecules* **2008**, 41 (15), 5559-5562.
128. Zoombelt, A. P.; Fonrodona, M.; Wienk, M. M.; Sieval, A. B.; Hummelen, J. C.; Janssen, R.A. J. Photovoltaic Performance of

- an Ultrasmall Band Gap Polymer. *Org. Lett.* **2009**, 11 (4), 903-906.
129. Subbiah, J.; Choudhury, K. R.; Ellinger, S.; Reynolds, J. R.; Franky S. Color Tunable  $\pi$ -Conjugated Polymers for Solar-Cell Applications: Engineering of Bandgap, Interface, and Charge Transport Properties. *IEEE J. Sel. Topics Quantum Electron.* **2010**, 16 (6), 1792-1800.
130. Yang, R.; Tian, R.; Yan, J.; Zhang, Y.; Yang, J.; Hou, Q.; Yang, W.; Zhang, C.; Cao, Y. Deep-Red Electroluminescent Polymers: Synthesis and Characterization of New Low Band-Gap Conjugated Copolymers for Light-Emitting Diodes and Photovoltaic Devices. *Macromolecules* **2005**, 38 (2), 244-253.
131. Fabio, S.; Assunta, M.; Mirko, S.; Choongik, K.; Tobin J. M.; Antonio, F.; Aldo, T. Solution-processable low-molecular weight extended arylacetylenes: versatile p-type semiconductors for field-effect transistors and bulk heterojunction solar cells. *J. Amer. Chem. Soc.* **2010**, 132 (17), 6108-6123.
132. Santa, T.; Takeshi, F.; Tomoko, I.; Imai, K. Recent progress in the development of derivatization reagents having a benzofurazan structure. *Biomed. Chromatogr.* **2008**, 22 (4), 343-353.
133. Song, Y.; Funatsu, T.; Tsunoda, M. Amino acids analysis using a monolithic silica column after derivatization with 4-fluoro-7-nitro-2,1,3-benzoxadiazole (NBD-F). *J. Chromatogr. B.* **2011**, 879, 335-340.
134. Toshimasa, T. Indirect enantioseparation by HPLC using chiral benzofurazan-bearing reagents. *Methods Mol. Biol.* **2004**, 243, 231-246.
135. Sumiya, S.; Sugii, T.; Shiraishi, Y.; Hirai, T. A benzoxadiazole-thiourea conjugate as a fluorescent chemodosimeter for Hg(II) in aqueous media. *J. Photochem. Photobiol., A: Chemistry* **2011**, 219, 154-158.
136. Caputo, B. J. A.; Welch, G. C.; Kamkar, D. A.; Henson, Z. B.; Nguyen, T-Q.; Bazan, G. C. A Dithienosilole Benzooxadiazole Donor-Acceptor Copolymer for Utility in Organic Solar Cells. *Small* **2011**, 7(10), 1422-1426.
137. Zeng, S.; Yin, L.; Jiang, X.; Li, Y.; Li, K. D-A-D low band gap molecule containing triphenylamine and benzoxadiazole/ben-

- zothiadiazole units: Synthesis and photophysical properties. *Dyes Pigment.* **2012**, 95, 229-235.
138. Lin, Z.; Bjorgaard, J.; Yavuz, A. G. Kose, M. E. Low Band Gap Star-Shaped Molecules Based on Benzothia(oxa)diazole for Organic Photovoltaics. *J. Phys. Chem. C* **2011**, 115, 15097-15108.
139. Chan, H. S. O.; Choon Ng, S. Synthesis, Characterization and applications of thiophene-based functional polymers. *Prog. Polym. Sci.*, **1998**, 23, 1167-1231.
140. Roncali, J. Conjugated Poly(thiophenes): Synthesis, Functionalization, and Applications. *Chem. Rev.* **1992**, 92, 711-738.
141. Mishra, A.; Ma, C-Q.; Segura, J. L.; Bauerle, P. Functional oligothiophene-based materials: Nanoarchitectures and Applications. In: *Handbook of Thiophene-based Materials: Applications in Organic Electronics and Photonics*. John Wiley & Sons **2009**.
142. Seed, A. Synthesis of self-organizing mesogenic materials containing a sulfur-based five-membered heterocyclic core. *Chem. Soc. Rev.* **2007**, 36, 2046-2069.
143. Yasuda, T.; Shimizu, T.; Liu, F.; Ungar, G.; Kato, T. Electro-functional Octupolar  $\pi$ -Conjugated Columnar Liquid Crystals. *J. Am. Chem. Soc.* **2011**, 133, 13437-13444.
144. Jie, H.; Yan-Mei, W.; Xiao-Guang, W. Synthesis, Mesogenic and Spectroscopic Properties of 2,5-Disubstituted Thiophene Derivatives. *Chin. J. Chem.* **2006**, 24, 1594-1598.
145. Huang, X.; Dong, Y.; Meng, J.; Cheng, Y.; Zhu, C. Fluorescence Polymer Incorporating Triazole and Benzo[2,1,3]thiadiazole Moieties for Ni<sup>2+</sup> Detection. *Synlett* **2010**, (12), 1841-1844.
146. Tahara, K.; Furukawa, S.; Uji-i, H; Uchino, T.; Ichikawa, T.; Zhang, J.; Mamdouh, W.; Sonoda, M.; De Schryver, F. C.; De Feyter, S.; Tobe, Y. Two-Dimensional Porous Molecular Networks of Dehydrobenzo[12]annulene Derivatives via Alkyl Chain Interdigitation. *J. Am. Chem. Soc.* **2006**, 128, 16613-16625.
147. Grolik, J.; Sieron, L.; Eilmes, J. A new liquid crystalline derivative of dibenzotetraaza[14]annulene: synthesis,

- characterization and the preliminary evaluation of mesomorphic properties. *Tetrahedron Lett.* **2006**, 47, 8209–8213.
148. Wulfman, D. S.; Cooper, C. F. Monoreduction of dinitroarenes with iron/acetic acid. *Synthesis* **1978**, 12, 924–925.
149. Melissaris, A. P.; Litt, M. H. A simple and economic route to p-ethynylaniline and ethynyl terminated substrates. *J. Org. Chem.* **1994**, 59 (19), 5818–5821.
150. Ma, L.; Hu, Q. S.; Pu, L. Synthesis of an optically active poly (aryleneethynylene) containing extended conjugation in the repeat unit. *Tetrahedron: Asymmetry* **1996**, 7 (11), 3103–3136.
151. Bleicher, L.; Cosford, N. D. P. Aryl- and heteroaryl-alkyne coupling reactions catalyzed by palladium on carbon and CuI in an aqueous medium. *Synlett* **1995**, 11, 1115–1116.
152. Malkina, A. G.; Brandsma, L.; Vasilevsky, S. F.; Trofimov, B. A. An improved procedure for the preparation of aryl- and heteroarylacetylenes. *Synthesis* **1996**, 589–590.
153. Chinchilla, R.; Najera, C. The Sonogashira Reaction: A Booming Methodology in Synthetic Organic Chemistry. *Chem. Rev.* **2007**, 107, 874–922.
154. Chinchilla, R.; Najera, C. Recent advances in Sonogashira reactions. *Chem. Soc. Rev.* **2011**, 40, 5084–5121.
155. Siemsen, P.; Livingston, R. C.; Diederich, F. Acetylenic Coupling: A powerful tool in molecular construction. *Angew. Chem. Int. Ed.* **2000**, 39, 2632–2657.
156. Li, J. H.; Liang, Y.; Zhang, X. D. Amine- and Phosphine-free Palladium(II)-Catalyzed Homocoupling Reaction of Terminal Alkynes. *Tetrahedron* **2005**, 61, 1903–1907.
157. Thorand, S.; Krause, N. Improved Procedures for the Palladium-Catalyzed Coupling of Terminal Alkynes with Aryl Bromides (Sonogashira Coupling) *J. Org. Chem.* **1998**, 63, 8551–8553.
158. Gerard P. M.; Fairlamb, I. J. S. Palladium-Catalysed Cross-Coupling and Related Processes: Some Interesting Observations that Have Been Exploited in Synthetic Chemistry. *Eur. J. Org. Chem.* **2009**, 4011–4029.
159. Marsden, J. A.; Haley, M. M. Cross-Coupling Reactions to sp Carbon Atoms. In: *Metal Catalyzed Cross-Coupling Reactions*. 2nd Ed. Volume 1, Edited by A. de Meijere, F. Diederich. WILEY-VCH, **2004**.

160. Wei, Y.; Zhang, Q.; Jiang, Y.; Yu, J. Novel Low Bandgap EDOT- Naphthalene Bisimides Conjugated Polymers: Synthesis, Redox, and Optical Properties. *Macromol. Chem. Phys.* **2009**, 210, 769-775.
161. Crespilho, F. N.; Zucolotto, V.; Siqueira Jr, J. R.; Carvalho, A. J. F.; Nart, F. C.; Oliveira Jr, O. N. Using Electrochemical Data to Obtain Energy Diagrams for Layer-By-Layer Films from Metallic Phthalocyanines. *Int. J. Electrochem. Sci.* **2006**, 151-159.
162. Wu, C-C.; Sturm, J. C.; Register, R. A.; Tian, J.; Dana, E. P.; Thompson, M. E. Efficient Organic Electroluminescent Devices Using Single- Layer Doped Polymer Thin Films with Bipolar Carrier Transport Abilities. *IEEE Trans. Electron Devices* **1997**, 4 (8), 1269-1281.
163. Micaroni, L.; Nart, F.C.; Hummelgen, I.A. Considerations about the electrochemical estimation of the ionization potential of conducting polymers. *J. Solid State Electrochem.* **2002**, 7: 55-59.
164. Hung, Y-C.; Jiang, J-C.; Chao, C-Y.; Su, W. F.; Lin, S-T. Theoretical Study on the Correlation between Band Gap, Bandwidth, and Oscillator Strength in Fluorene-Based Donor Acceptor Conjugated Copolymers. *J. Phys. Chem. B* **2009**, 113, 8268-8277.
165. Chen, X.; Liu, B.; Zou, Y.; Xiao, L.; Guo, X.; He Y.; Li, Y. A new benzo[1,2-b:4,5-b']difuran-based copolymer for efficient polymer solar cells. *J. Mater. Chem.* **2012**, 22, 17724-17731.
166. Kayaa, I.; Aydın, A. Synthesis, characterization, thermal stability, conductivity, and band gaps of substitute oligo/polyamines or polyphenol. *Polym. Adv. Technol.* **2010**, 21 337-347.
167. Gallardo, H.; Conte, G.; Tuzimoto, P.; Bortoluzzi, A.; Peralta, R. A.; Neves, A. Synthesis, crystal structure and luminescent properties of new tris-b-diketonate Eu(III) complex with thiadiazolophenanthroline derivative ligand. *Inorg. Chem. Commun.* **2008**, 11, 1292-1296.
168. Eckhardt, H.; Shacklette, L.W.; Jen, K.Y.; Elsenbaumer, R.L. The electronic and electrochemical properties of poly(phenylene vinylenes) and poly(thienylene vinylenes): An

- experimental and theoretical study. *J. Chem. Phys.* **1989**, 91(2), 1303-1315.
169. Zhang, K.; Tieke, B.; Forgie, J. C.; Vilela, F.; Skabara, P. J. Donor-Acceptor Conjugated Polymers Based on p- and o-Benzodifuranone and Thiophene Derivatives: Electrochemical Preparation and Optical and Electronic Properties. *Macromolecules* **2012**, 45, 743–750.
170. Hellstrom, S.; Zhang, F.; Ingnas, O.; Andersson, M. R. Structure-property relationships of small bandgap conjugated polymers for solar cells. *Dalton Trans.* **2009**, 10032–10039.
171. Han, J.; Wang, Y-M, Wang, X-G. Synthesis, Mesogenic and Spectroscopic Properties of 2,5-Disubstituted Thiophene Derivatives. *Chin. J. Chem.* **2006**, 24, 1594—1598.
172. Fery-Forgues, S.; Lavabre, D. Are Fluorescence Quantum Yields So Tricky to Measure? A Demonstration Using Familiar Stationery Products. *J. Chem. Educ.* **1999**, 76 (9), 1260-1264.
173. Robert, R. G.; Carl, A. K.; George, C. L. Ferrocene as an Internal Standard for Electrochemical Measurements. *Inorg. Chem.* **1980**, 19 (9), 2854-5.
174. Heck, R. F.; *Palladium Reagents in Organic Synthesis*. Academic Press: London, **1985**.
175. Kaller, M.; Tussetschlager, S.; Fischer, P.; Deck, C.; Baro, A.; Giesselmann, F.; Laschat, S. Columnar Mesophases Controlled by Counterions in Potassium Complexes of Dibenzo[18]crown-6 Derivatives. *Chem. Eur. J.* **2009**, 15 (37) 9530-9542.
176. McDonald, R.; Lacey, D.; Watson, P.; Cowling, S.; Wilson, P. Synthesis and evaluation of some novel chiral heterocyclic liquid crystalline materials exhibiting ferro- and antiferroelectric phases. *Liq. Cryst.* **2005**, 32 (3), 319-330.
177. Helgesen, M.; Gevorgyan, S. A.; Krebs, F. C.; Janssen, R. A. J. Substituted 2,1,3-Benzothiadiazole- and Thiophene-Based Polymers for Solar Cells - Introducing a New Thermocleavable Precursor. *Chem. Mater.* **2009**, 21, 4669–4675.
178. Edmund, J. F.; Dickinson, J. G. Limon, P.; Rees, N. V.; Richard, G. C. How Much Supporting Electrolyte is Required to Make a Cyclic Voltammetry Experiment Quantitatively “Diffusional”? A Theoretical and Experimental Investigation. *J. Phys Chem. C.* **2009**, 113, 11157–11171.

179. Bard, A. J.; Faulkner, L. R. *ELECTROCHEMICAL METHODS: Fundamentals and Applications*. 2nd ed. Chapter 4 © John Wiley & Sons Inc. **2001**.
180. Ishii, H.; Sugiyama, K.; Ito, E.; Seki, K. Energy Level Alignment and Interfacial Electronic Structures at Organic/Meta and Organic/Organic Interfaces. *Adv. Mater.* **1999**, 11, No. 8, 605-625.
181. Fifield, F. W.; Kealey, D. *Principles and Practice of Analytical Chemistry*. 5th ed. **2000**, Blackwell Science Ltd.
182. Cristiano, R.; Oliveira Santos, D. M. P.; Conte, G.; Gallardo, H. 1,4-Diaryl and Schiff's base [1,2,3]-triazole derivative liquid crystalline compounds. *Liq. Cryst.* **2006**, 33 (9), 997-1003.
183. Boden, N.; Movaghar, B. Applicable Properties of Columnar Discotic Liquid Crystals. In: Demus, D.; Goodby, J.; Gray, G.W.; Spiess, H.W.; Vill, V. (Ed.). *Handbook of Liquid Crystals*. Wiley-VCH, **1998**, Vol. 2b, 781-798.
184. Ternpler, R. H. X-Ray Characterization of Liquid Crystals: Instrumentation. In: Demus, D.; Goodby, J.; Gray, G.W.; Spiess, H.W.; Vill, V. (Ed.). *Handbook of Liquid Crystals*. Wiley-VCH, **1998**, Vol. 1, 619-634.
185. Seddon, J.M. Structural studies of liquid crystals by X-Ray diffraction. In: Demus, D.; Goodby, J.; Gray, G.W.; Spiess, H.W.; Vill, V. (Ed.). *Handbook of Liquid Crystals*. Wiley-VCH, **1998**, Vol. 1, 635-680.
186. Davidson, P. Selected topic in X-Ray scattering by liquid-crystalline polymers. In: *Liquid crystals II, Structure and bonding* 95, Volume Editor: Mingos, D.M.P. Springer-Verlag, **1999**.
187. Niori, T.; Sekine, T.; Watanabe, J.; Furukawa, T.; Takezoe, H. Distinct ferroelectric smectic liquid crystals consisting of banana shaped achiral molecules. *J. Mater. Chem.* **1996**, 6 (7), 1231-1233.
188. Weissflog, W.; Nadasi, H.; Dunemann, U.; Pelzl, G.; Diele, S.; Eremin, A.; Kresse, H. Influence of lateral substituents on the mesophase behaviour of banana-shaped mesogens. *J. Mater. Chem.* **2001**, 11 (11), 2748-2758.
189. Shen, D.; Pegenau, A.; Diele, S.; Wirth, I.; Tschierske, C. Molecular Design of Nonchiral Bent-Core Liquid Crystals with

- Antiferroelectric Properties. *J. Amer. Chem. Soc.* **2000**, 122 (8), 1593-1601.
190. Sadashiva, B. K.; Murthy, H. N.; Shreenivasa; Dhara, S. Effect of lateral substituents on the mesophases formed by some achiral banana-shaped molecules. *Liq. Cryst.* **2001**, 28 (3), 483-487.
191. Shen, D.; Diele, S.; Pelzl, G.; Wirth, I.; Tschierske, C. Designing banana-shaped liquid crystals without Schiff's base units: m-terphenyls, 2,6-diphenylpyridines and V-shaped tolane derivatives. *J. Mater. Chem.* **1999**, 9 (3), 661-672.
192. Link, D. R.; Natale, G.; Shao, R.; MacLennan, J. E.; Clark, N. A.; Korblova, E.; Walba, D.M. Spontaneous formation of macroscopic chiral domains in a fluid smectic phase of achiral molecules. *Science* **1997**, 278 (5345), 1924-1927.
193. Gerhard P; Wolfgang, W. Mesophase behavior at the borderline between calamitic and "banana shaped" mesogens. In: Ayyalusamy R. (Ed.) *Thermotropic Liquid Crystals recent advances*. Springer, **2007**, 1-54.
194. Reddy, R. A.; Tschierske, C. Bent-core liquid crystals: polar order, superstructural chirality and spontaneous desymmetrization in soft matter systems. *J. Mater. Chem.* **2006**, 16 (10), 907-961.
195. Heppke, G.; Moro, D. Chiral order from achiral molecules. *Science* **1998**, 279 (5358), 1872-1873.
196. Sekine, T.; Niori, T.; Sone, M.; Watanabe, J.; Choi, S-W.; Takanishi, Y.; Takezoe, H. Origin of helix in achiral banana-shaped molecular systems. *Jpn J. Appl. Phys., Part 1.* **1997**, 36 (10), 6455-6463.



## **8. PUBLISHED PAPER**



## 2,1,3-Benzoxadiazole and 2,1,3-benzothiadiazole-based fluorescent compounds: Synthesis, characterization and photophysical/electrochemical properties

Behramand Behramand, Fernando Molin, Hugo Gallardo\*

Departamento de Química, INCT Catalise, Universidade Federal de Santa Catarina, Florianópolis-SC 88040-900, Brazil

### ARTICLE INFO

#### Article history:

Received 4 May 2012  
Received in revised form  
30 May 2012  
Accepted 5 June 2012  
Available online 4 July 2012

#### Keywords:

Benzoxadiazole  
Benzothiadiazole  
Sonogashira coupling  
Fluorescence  
Cyclic voltammetry  
Band gap

### ABSTRACT

Six new fluorescent compounds derived from 2,1,3-benzoxadiazole and 2,1,3-benzothiadiazole heterocycles with varying numbers of alkoxy chains were successfully synthesized. Sonogashira cross-coupling was used as the key synthetic step to link the central and terminal aromatic units through an acetylenic linker unit which ensures molecular planarity and extension of the conjugation. All of the synthesized compounds showed UV–vis absorption in the 426–437 nm range with reasonably high molar extinction coefficients. All six compounds emit in the green region of the visible spectrum with reasonably large Stokes shifts (95–107 nm) and medium emission efficiencies ( $\phi_f = 0.27$ –0.32). Electrochemical studies showed that the compounds have closely spaced HOMO and LUMO energy levels and that they may present good electron transporting properties.

© 2012 Elsevier Ltd. All rights reserved.

### 1. Introduction

Due to their environmentally-friendly, facile and economical processing and easy modification to provide desirable properties [1], organic fluorescent compounds have important applications in diverse fields including fluorescent organic nanoparticles (FONs) [2], organic light-emitting diodes (OLEDs) for electroluminescent devices and flat panel display technology [3], as solid state light sources for sign boards and light appliances, fluorescent probes in medical science for locating tumor cells [4], photoconductors for solar cells [5] and chemical sensors [6].

In relation to the search for organic fluorescent compounds with potential applications in diverse fields, we decided to exploit the fluorophoric nature of the heterocycles 2,1,3 benzoxadiazole, more specifically known as benzofurazan [7] and its sulfur containing analogue 2,1,3-benzothiadiazole. Both of these heterocycles possess planar molecular structures and their derivatives with extended conjugation usually present intense fluorescence [8]. Due to the presence of oxygen, the benzofurazan is more electronegative than 2,1,3-benzothiadiazole and its derivatives have mainly been used as fluorescent pre-column labeling reagents for amino acids and

peptides analysis [9], as derivatization reagents for indirect HPLC enantioseparation [10] and for heavy metal detection [11].

Depending on the type of substituents, the derivatives of 2,1,3-benzothiadiazole have been shown to emit a variety of colors including red [12], blue [13] and green [14], the three fundamental colors for full color display. Due to its rigid planar structure, ability to form well-ordered crystals and efficient fluorophoric nature, we have used this system as the central core for luminescent liquid crystalline compounds [15]. More importantly, due to its electron-deficient nature, it has especially been used as an acceptor unit in many donor-acceptor conjugated copolymers with small HOMO-LUMO band gap [16] for potential application in field effect transistors [17], light emitting diodes [18] and solar cells.

In this paper, we report the synthesis and characterization of six new light-emitting compounds (**1–6**) with a variable number of flexible alkoxy chains using 5,6-alkoxy 2,1,3-benzoxadiazole and 2,1,3-benzothiadiazole fluorophores as the central cores (Fig. 1). With the presence of pendent flexible alkoxy chains there was an improvement in the solubility of compounds.

### 2. Experimental

#### 2.1. Materials and characterizations

4-Bromophenol 97%, 1-bromododecane 98%, methyl iodide and thionyl chloride 97% were purchased from Sigma–Aldrich; catechol

\* Corresponding author. Fax: +55 48 37216850.  
E-mail address: [hugo.gallardo@ufsc.br](mailto:hugo.gallardo@ufsc.br) (H. Gallardo).

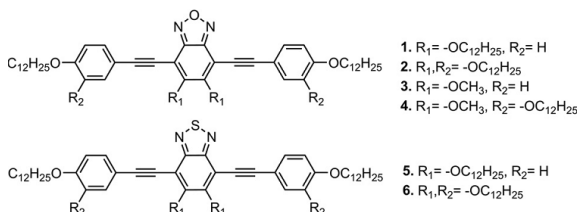


Fig. 1. Molecular structures of the newly synthesized compounds.

99%, 2-methyl-3-buten-2-ol 98% and tin (II) chloride dihydrate were purchased from Acros Organics and used as received. N-bromosuccinimide was recrystallized from water (10 mL H<sub>2</sub>O per 1 g of NBS) prior to its use. Toluene and dimethylformamide were dried over activated molecular sieves. Triethylamine was dried by heating under reflux in the presence of KOH and subsequent distillation. The intermediates were purified either by recrystallization in commercial grade solvents or via column chromatography on silica-gel 60-200 (mesh 60A). The final compounds were purified by column chromatography using flash silica gel. Preliminary purity tests were performed by developing thin layer chromatographs using silica-gel Si 60-F254 TLC plates purchased from Merck. Melting points were determined with an Olympus BX50 microscope equipped with a Mettler Toledo FP-82 hot stage. <sup>1</sup>H and <sup>13</sup>C NMR spectra were recorded on a Varian Mercury Plus spectrometer operating at 400 and 100.6 MHz, respectively. The data are reported as: chemical shift, multiplicity (s, singlet; d, doublet; t, triplet; q, quartet; qui, quintet; sep, septet; m, multiplet; br, broad; o, overlapping or as a combination of these e.g. dd, dt), coupling constant (J) and integration. Elemental analysis was carried out using a Carlo Erba model E-1110 instrument. IR and Mass spectra were obtained using Varian 3100 FT-IR Spectrometer and Bruker APCI/MS/MS Ion Trap mass spectrometer instrument respectively. Cyclic voltammetry was carried out on an Autolab PGSTAT128N potentiostat, connected to data processing software (GPES, version 4.9.007, Eco Chemie), at a scan rate of 50 mV/s.

## 2.2. General procedure for Sonogashira cross-couplings

In a flame dried Schlenk flask under argon, a mixture of the heterocycle **7-9** (0.4–0.5 mmol), Pd(PPh<sub>3</sub>)<sub>2</sub>Cl<sub>2</sub>, PPh<sub>3</sub> and CuI (7 mol % each) in Et<sub>3</sub>N (20–25 mL) was stirred at 50 °C for 20 min. A solution of the terminal aryl acetylene **10** or **11** (2.2 equivalent) in triethylamine (10 mL) was added drop-wise. After complete addition, the reaction mixture was stirred at 80–85 °C for 12–14 h. The reaction mixture was cooled to room temperature, filtered through a celite pad and washed with tetrahydrofuran. After vacuum evaporation of the solvent, the crude product was purified by column chromatography on flash silica gel (eluent 1–2% ethyl acetate: hexane) to furnish the respective final compound.

### 2.2.1. 4,7-Bis(4-(dodecyloxy)phenyl)ethynyl)-5,6-bis(dodecyloxy)-2,1,3-benzoxadiazole (**1**)

Greenish-yellow solid; yield: 47%, m.p. = 40.0–41.6 °C. <sup>1</sup>H NMR (CDCl<sub>3</sub>, 400 MHz): δ = 7.5 (d, 4H, J = 8.8 Hz), 6.9 (d, 4H, J = 9.0 Hz), 4.4 (t, 4H, J = 6.4 Hz), 4.0 (t, 4H, J = 6.4 Hz), 1.9 (qui), 1.8 (qui), 1.3 (br), 0.9 (t, 12H). <sup>13</sup>C NMR (CDCl<sub>3</sub>, 100.6 MHz): δ: 160.0, 157.6, 152.2, 133.5, 115.1, 114.7, 108.5, 101.4, 81.2, 75.2, 68.2, 32.2, 29.7, 26.5, 23.0, 14.3. FT-IR (KBr, cm<sup>-1</sup>): 2923, 2852, 2205, 1604, 1508, 1464, 1291,

1247. CI-MS [M + H]<sup>+</sup> calculated for C<sub>70</sub>H<sub>108</sub>N<sub>2</sub>O<sub>5</sub> m/z: 1056.8; Found: 1058.0. CHN: Expected: C 79.49, H 10.29, N 2.65. Found: C 79.47, H 10.28, N 2.63.

### 2.2.2. 4,7-Bis(3,4-bis(dodecyloxy)phenyl)ethynyl)-5,6-bis(dodecyloxy)-2,1,3-benzoxadiazole (**2**)

Bright orange colored solid; yield: 30%, m.p. = 60.0–61.5 °C. <sup>1</sup>H NMR (CDCl<sub>3</sub>, 400 MHz): δ = 7.2 (dd, 2H, J = 8.4 Hz, J<sup>1</sup> = 2.0 Hz), 7.1 (d, 2H, J<sup>1</sup> = 2.0 Hz), 6.8 (d, 2H, J = 8.4 Hz), 4.4 (t, 4H), 4.0 (ot, 8H), 1.8 (br), 1.3 (b), 0.9 (ot). <sup>13</sup>C NMR (CDCl<sub>3</sub>, 100.6 MHz): δ: 158.3, 150.5, 148.8, 147.8, 125.3, 116.6, 114.5, 113.1, 105.0, 102.2, 101.1, 79.4, 75.0, 69.3, 69.1, 31.9, 30.4, 29.7, 29.7, 29.4, 26.1, 26.0, 22.7, 14.1. FT-IR (KBr, cm<sup>-1</sup>): 2918, 2860, 2204, 1597, 1514, 1467, 1301, 1265. CI-MS [M + H]<sup>+</sup> calculated for C<sub>94</sub>H<sub>156</sub>N<sub>2</sub>O<sub>7</sub> m/z: 1426.2; Found: 1427.3. CHN: Expected: C 79.16, H 11.02, N 1.96. Found: C 79.13, H 10.98, N 1.99.

### 2.2.3. 4,7-Bis(4-(dodecyloxy)phenyl)ethynyl)-5,6-dimethoxy-2,1,3-benzoxadiazole (**3**)

Yellow colored solid; yield: 52%, m.p. = 55.5–58.0 °C. <sup>1</sup>H NMR (CDCl<sub>3</sub>, 400 MHz): δ = 7.6 (d, 4H, J = 8.6 Hz), 6.9 (d, 4H, J = 8.6 Hz), 4.3 (s, 6H), 4.0 (t, 4H), 1.8 (qui), 1.3 (br), 0.9 (t). <sup>13</sup>C NMR (CDCl<sub>3</sub>, 100.6 MHz): δ: 160.0, 158.2, 147.8, 133.3, 114.7, 114.2, 105.0, 102.4, 100.3, 79.3, 68.2, 61.6, 31.9, 29.7, 29.6, 29.6, 29.3, 29.1, 26.0, 22.7, 14.1. FT-IR (KBr, cm<sup>-1</sup>): 2923, 2849, 2207, 1730, 1604, 1508, 1466, 1306, 1251. CI-MS [M + H]<sup>+</sup> calculated for C<sub>68</sub>H<sub>64</sub>N<sub>2</sub>O<sub>5</sub> m/z: 748.5; Found: 749.5. CHN: Expected: C 76.97, H 8.61, N 3.74. Found: C 76.98, H 8.59, N 3.75.

### 2.2.4. 4,7-Bis(3,4-bis(dodecyloxy)phenyl)ethynyl)-5,6-dimethoxy-2,1,3-benzoxadiazole (**4**)

Bright orange colored solid; yield: 35%, m.p. = 61.0–63.0 °C. <sup>1</sup>H NMR (CDCl<sub>3</sub>, 400 MHz): δ = 7.2 (dd, 2H, J = 8.2 Hz, J<sup>1</sup> = 2.0 Hz), 7.1 (d, 2H, J<sup>1</sup> = 2.0 Hz), 6.9 (d, 2H, J = 8.2 Hz), 4.3 (s, 6H), 4.0 (ot, 8H), 1.8 (quint), 1.3 (br), 0.9 (t). <sup>13</sup>C NMR (CDCl<sub>3</sub>, 100.6 MHz): δ: 158.3, 150.6, 148.8, 147.8, 125.4, 116.5, 114.3, 113.0, 105.0, 102.7, 100.3, 79.0, 69.4, 69.1, 61.7, 31.9, 29.4, 26.0, 22.7, 14.1. FT-IR (KBr, cm<sup>-1</sup>): 2919, 2848, 2209, 1730, 1515, 1467, 1313, 1270. CI-MS [M + H]<sup>+</sup> calculated for C<sub>72</sub>H<sub>112</sub>N<sub>2</sub>O<sub>7</sub> m/z: 1116.8; Found: 1117.9. CHN: Expected: C 77.37, H 10.10, N 2.51. Found: C 77.30, H 10.11, N 2.51.

### 2.2.5. 4,7-Bis(4-(dodecyloxy)phenyl)ethynyl)-5,6-bis(dodecyloxy)-2,1,3-benzothiadiazole (**5**)

Yellow-green solid; yield: 48%, m.p. = 98.5–100.3 °C. <sup>1</sup>H NMR (CDCl<sub>3</sub>, 400 MHz): δ = 7.6 (d, 4H, J = 8.8 Hz), 6.9 (d, 4H, J = 8.8 Hz), 4.4 (t, 4H, J = 6.4 Hz), 4.0 (t, 4H, J = 6.6 Hz), 1.9 (qui), 1.8 (qui), 1.3 (br), 0.9 (t). <sup>13</sup>C NMR (CDCl<sub>3</sub>, 100.6 MHz): δ: 160.0, 157.6, 152.2, 135.5, 115.1, 114.7, 108.5, 101.4, 81.2, 75.2, 68.2, 32.2, 29.7, 26.5, 26.3, 23.0, 14.3. FT-IR (KBr, cm<sup>-1</sup>): 2924, 2854, 2201, 1605, 1513, 1467, 1289,

1247. CI-MS  $[M + H]^+$  calculated for  $C_{70}H_{108}N_2O_4S$  m/z: 1072.8; Found: 1073.9. CHN: Expected: C 78.31, H 10.14, N 2.61. Found: C 78.26, H 10.14, N 2.57.

**2.2.6. 4,7-Bis((3,4-bis(dodecyloxy)phenyl)ethynyl)-5,6-bis(dodecyloxy)-2,1,3-benzothiadiazole (6)**

Light colored solid; yield: 51%, m.p. = 80.0–81.7 °C.  $^1H$  NMR ( $CDCl_3$ , 400 MHz):  $\delta$  = 7.2 (dd, 2H,  $J$  = 8.2 Hz,  $J^H$  = 2.0 Hz), 7.2 (d, 2H,  $J^H$  = 2.0 Hz), 6.9 (d, 2H,  $J$  = 8.4 Hz), 4.4 (t, 4H,  $J$  = 6.6 Hz), 4.0 (ot, 8H), 1.9 (qui), 1.8 (qui), 1.3 (br), 0.9 (t).  $^{13}C$  NMR ( $CDCl_3$ , 100.6 MHz)  $\delta$ : 157.7, 152.1, 150.5, 149.0, 125.6, 116.8, 115.1, 113.2, 108.5, 101.6, 80.8, 75.3, 69.5, 69.3, 32.2, 30.0, 29.9, 29.6, 29.4, 26.3, 23.0, 14.1. FT-IR (KBr,  $cm^{-1}$ ): 2922, 2852, 2205, 1605, 1505, 1468, 1290, 1246. CHN: Expected: C 78.28, H 10.90, N 1.94. Found: C 78.29, H 10.80, N 1.90.

**2.2.7. 4,7-Dibromo-5,6-bis(dodecyloxy)-2,1,3-benzoxadiazole (7)**

Off-white solid; yield: 90%, m.p. = 55.0–56.1 °C.  $^1H$  NMR ( $CDCl_3$ , 400 MHz):  $\delta$  = 4.2 (t, 4H,  $J$  = 6.6 Hz), 1.9 (m, 4H), 1.5 (m, 4H), 1.3 (br), 0.9 (t, 6H,  $J$  = 0.7 Hz), FT-IR (KBr,  $cm^{-1}$ ): 2954, 2919, 2851, 2331, 1734, 1612, 1473, 1380, 1296, 1187, 1072, 1014, 996, 948, 883, 723. CHN: Expected  $C_{30}H_{50}Br_2N_2O_3$ : C 55.73, H 7.79, N 4.33. Found: C 55.72, H 7.80, N 4.30.

**2.2.8. 4,7-Dibromo-5,6-dimethoxy-2,1,3-benzoxadiazole (8)**

Recrystallized from methanol. Off-white crystalline solid; yield: 49%, m.p. = 128.5–131.0 °C.  $^1H$  NMR ( $CDCl_3$ , 400 MHz):  $\delta$  = 4.0 (s), FT-IR (KBr,  $cm^{-1}$ ): 3010, 2952, 2847, 2363, 2136, 1608, 1530, 1477, 1382, 1310, 1075, 1010, 979, 879, 844, 732. CHN: Expected  $C_8H_6Br_2N_2O_3$ : C 28.43, H 1.73, N 8.29. Found: C 28.41, H 1.80, N 8.29.

**2.2.9. 4,7-Dibromo-5,6-bis(dodecyloxy)-2,1,3-benzothiadiazole (9) [19]**

Off-white fluffy crystalline solid; yield: 73%, m.p. = 60.4–61.0 °C (lit. 64–65 °C).  $^1H$  NMR ( $CDCl_3$ , 400 MHz):  $\delta$  = 4.2 (t, 4H,  $J$  = 6.6 Hz), 1.9 (m, 4H), 1.3 (br), 0.9 (t, 6H,  $J$  = 7.0 Hz).  $^{13}C$  NMR ( $CDCl_3$ , 125 MHz)  $\delta$ : 154.5, 150.3, 106.2, 75.1, 31.9, 29.68, 29.65, 29.62, 29.60, 29.4, 29.3, 25.9, 22.6, 14.1. FT-IR (KBr,  $cm^{-1}$ ): 2958, 2903, 2845, 1471, 1384, 1292, 985, 946.

**2.2.10. 1-Dodecyloxy-4-ethynylbenzene (10) [20–22]**

Prepared according to our reported procedure. Oily liquid at room temperature; yield: 84%.  $^1H$  NMR ( $CDCl_3$ , 400 MHz):  $\delta$  = 7.4 (d, 2H,  $J$  = 9.0 Hz), 6.8 (d, 2H,  $J$  = 9.0 Hz), 4.0 (t, 2H,  $J$  = 6.6 Hz), 3.0 (s, 1H), 1.8 (m), 1.3 (m), 0.9 (t, 6H,  $J$  = 7.0 Hz).  $^{13}C$  NMR ( $CDCl_3$ , 50 MHz)  $\delta$ : 160.1, 134.0, 115.0, 114.7, 84.3, 76.2, 68.5, 32.6, 30.3, 30.0, 29.8, 26.6, 23.3, 14.6. FT-IR (KBr,  $cm^{-1}$ ): 3318, 2923, 2854, 2109, 1887, 1607, 1506, 1469, 1289, 1249, 1170, 1108, 1026, 831.

**2.2.11. 1,2-Bis(dodecyloxy)-4-ethynylbenzene (11)**

Greenish off-white crystalline solid; yield: 94%, m.p. = 37.0–39.2 °C.  $^1H$  NMR ( $CDCl_3$ , 400 MHz):  $\delta$  = 7.1 (dd, 1H,  $J$  = 8.2 Hz,  $J^H$  = 2.0 Hz), 7.0 (d, 1H,  $J^H$  = 2.0 Hz), 6.8 (d, 1H,  $J$  = 8.4 Hz), 4.0 (m, 4H), 3.0 (s, 1H), 1.8 (m, 4H), 1.3 (br), 0.9 (t, 6H,  $J$  = 7.0).  $^{13}C$  NMR ( $CDCl_3$ , 100.6 MHz)  $\delta$ : 150.3, 148.8, 125.7, 117.3, 114.3, 113.3, 84.2, 75.6, 69.5, 69.3, 32.17, 29.9, 29.6, 26.2, 22.9, 14.4. FT-IR (KBr,  $cm^{-1}$ ): 3315, 2925, 2854, 2108, 1599, 1511, 1469, 1416, 1262, 1135, 1022, 853, 805.

**2.2.12. 1,2-Bis(dodecyloxy)benzene (13a)**

The reaction mixture was heated under reflux at 90 °C overnight. Work up: The reaction mixture was first filtered under vacuum to remove  $K_2CO_3$ . Water (300 mL) was added to the filtrate to remove DMF and the product extracted with  $CH_2Cl_2$  (3  $\times$  100 mL), dried over  $MgSO_4$ , concentrated under reduced pressure and the resulting crude product was recrystallized in ethanol furnishing the pure

alkylated product **13a** as needle-like white crystals. Yield: 86%, m.p. = 45.2–46.3 °C (lit. 45.0–48.0 °C).  $^1H$  NMR ( $CDCl_3$ , 400 MHz):  $\delta$  = 6.9 (s, 4H), 4.0 (t, 4H,  $J$  = 6.6 Hz), 1.8 (m, 4H), 1.3 (br), 0.9 (t, 6H,  $J$  = 7.0 Hz).  $^{13}C$  NMR ( $CDCl_3$ , 100.6 MHz)  $\delta$ : 149.4, 121.2, 114.3, 69.5, 32.2, 29.9, 29.6, 26.3, 22.9, 14.4. FT-IR (KBr,  $cm^{-1}$ ): 2925, 2853, 1594, 1510, 1465, 1258, 1217, 1128, 747, 723.

**2.2.13. 1,2-Dimethoxybenzene/Veratrol (13b)**

A mixture of catechol (11.95 g, 108.57 mmol) and  $K_2CO_3$  (37.45 g, 271.4 mmol) in acetone was stirred under argon for 10 min at room temperature. Iodomethane (14.2 mL, 228 mmol) was added, stirred for 1.5 h at room temperature and then heated under reflux overnight at 60 °C. The reaction mixture was cooled to room temperature, vacuum filtered to remove  $K_2CO_3$  and the filtrate concentrated under reduced pressure to furnish the oily product (14.6 g, 98%).  $^1H$  NMR ( $CDCl_3$ , 400 MHz):  $\delta$  = 6.8 (m, 4H), 3.7 (s, 6H). FT-IR (KBr,  $cm^{-1}$ ): 3103, 3055, 3000, 1258, 1610, 1494, 1476, 1322, 1253, 1152, 1120, 1004, 753.

**2.2.14. 1,2-Bis(dodecyloxy)-4,5-dinitrobenzene (14a) [23]**

Prepared as reported for an analogous conversion. Bright yellow solid; yield: 88%, m.p. = 79.0–80.0 °C (lit. 81.0–82.0 °C).  $^1H$  NMR ( $CDCl_3$ , 400 MHz):  $\delta$  = 7.3 (s, 2H), 4.1 (t, 4H,  $J$  = 6.4 Hz), 1.9 (m, 4H), 1.5 (m), 1.3 (br), 0.9 (t, 6H,  $J$  = 7.0 Hz).  $^{13}C$  NMR ( $CDCl_3$ , 100.6 MHz)  $\delta$ : 152, 136.7, 108, 70.4, 32.16, 29.9, 29.5, 28.9, 22.9, 14.4. FT-IR (KBr,  $cm^{-1}$ ): 2123, 3070, 2917, 2850, 1727, 1586, 1529, 1465, 1372, 1334, 1289, 1225, 1070, 1041, 987, 949, 909, 872, 823.

**2.2.15. 1,2-Dimethoxy-4,5-dinitrobenzene (14b) [24]**

Prepared according to previously reported procedure. Bright yellow colored fine crystals; yield: 72%, m.p. = 128.2–129.5 °C (lit. 129.0–131.0 °C).  $^1H$  NMR ( $CDCl_3$ , 400 MHz):  $\delta$  = 7.3 (2H), 4.0 (s, 6H), FT-IR (KBr,  $cm^{-1}$ ): 3067, 2986, 1585, 1522, 1370, 1325, 1287, 1234, 1045, 875, 789.

**2.2.16. 5,6-Bis(dodecyloxy)-2,1,3-benzothiadiazole (16) [19]**

Recrystallized from ethanol. Off-white crystalline solid; yield: 73%, m.p. = 95.0–96.7 °C.  $^1H$  NMR ( $CDCl_3$ , 400 MHz):  $\delta$  = 7.1 (s, 2H), 4.1 (t, 4H,  $J$  = 6.6 Hz), 1.9 (m, 4H), 1.5 (m, 4H), 1.3 (br), 0.9 (t, 6H,  $J$  = 7.0).  $^{13}C$  NMR ( $CDCl_3$ , 100 MHz)  $\delta$ : 154.0, 151.3, 98.3, 69.1, 31.9, 29.68, 29.65, 29.3, 28.7, 25.9, 22.6, 14.1. FT-IR (KBr,  $cm^{-1}$ ): 2910, 2850, 1497, 1467, 1321, 1197, 855.

**2.2.17. 5,6-Bis(dodecyloxy)-2,1,3-benzoxadiazole (17a)**

Recrystallized from ethanol to furnish **17a** as off-white solid; yield: 77%, m.p. = 107.3–108.8 °C.  $^1H$  NMR ( $CDCl_3$ , 400 MHz):  $\delta$  = 6.8 (s, 2H), 4.1 (t, 4H,  $J$  = 6.6 Hz), 1.9 (m, 4H), 1.3 (br), 0.9 (t, 6H,  $J$  = 7.0 Hz), FT-IR (KBr,  $cm^{-1}$ ): 2913, 2847, 1502, 1471, 1318, 1202, 848. CHN: Expected  $C_{30}H_{52}N_2O_3$ : C 73.72, H 10.72, N 5.73. Found: C 73.72, H 10.69, N 5.70.

**2.2.18. 5,6-Dimethoxy-2,1,3-benzoxadiazole (17b)**

Recrystallized from methanol. Yellow needle-like crystals; yield: 81%, m.p. = 195.0–197.0 °C.  $^1H$  NMR ( $CDCl_3$ , 400 MHz):  $\delta$  = 6.9 (s, 2H), 4.0 (s, 6H).  $^{13}C$  NMR ( $CDCl_3$ , 100.6 MHz)  $\delta$ : 155.4, 146.7, 90.7, 56.6. FT-IR (KBr,  $cm^{-1}$ ): 3146, 3082, 3069, 2995, 2943, 2847, 2442, 1635, 1544, 1521, 1447, 1368, 1244, 1224, 1178, 1001, 854. CHN: Expected  $C_8H_8N_2O_3$ : C 53.33, H 4.48, N 15.55. Found: C 53.30, H 4.50, N 15.56.

### 3. Results and discussions

#### 3.1. Synthesis and characterization

The synthetic strategy to obtain the target compounds (**1-6**) utilized Sonogashira cross-coupling [25] of the separately prepared



**Table 1**  
Photophysical parameters of the final compounds.

Compound	$\lambda_{\text{max}}$ (nm) <sup>a</sup>	$\epsilon$ (Lmol <sup>-1</sup> cm <sup>-1</sup> )	$\lambda_{\text{exc}}$ (nm)	$\lambda_{\text{em}}$ (nm)	Stokes shifts (nm) <sup>b</sup>	$\phi_f^c$
1	429	26,400	436	535	99	0.31
2	437	25,200	449	552	103	0.28
3	426	18600	435	536	101	0.31
4	435	26,000	448	555	107	0.27
5	429	19,400	442	543	101	0.32
6	428	30,200	440	535	95	0.32

<sup>a</sup> Solutions in  $5 \times 10^{-6}$  mol L<sup>-1</sup> in CHCl<sub>3</sub>.

<sup>b</sup> Stokes shifts =  $\lambda_{\text{em}} - \lambda_{\text{exc}}$ .

<sup>c</sup> Measured in CHCl<sub>3</sub> using 4,7-bis(phenylethynyl)-2,1,3-benzothiadiazole ( $\phi_f = 0.37$ ) as the standard [8].

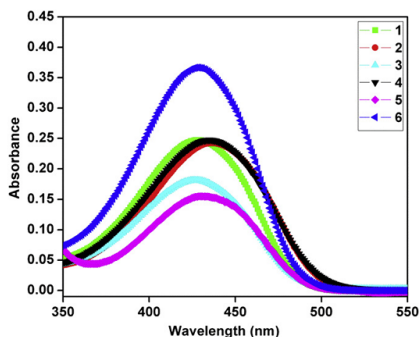


Fig. 2. UV-vis absorption spectra of the final compounds in CHCl<sub>3</sub>.

maximum absorption within a narrow range of 426–437 nm (Fig. 2) with reasonably high absorption coefficients (Table 1). Shrinking the dodecyloxy groups on the heterocyclic centers in **1** and **2** to methoxy groups resulted in slight blue shifts in the absorptions maxima of **3** and **4**. Moreover, the presence of an additional terminal dodecyloxy chain in **2** and **4**, compared to **1** and **3**, caused a reasonable red shift in the absorption maxima. In the case of 2,1,3-benzothiadiazoles, an

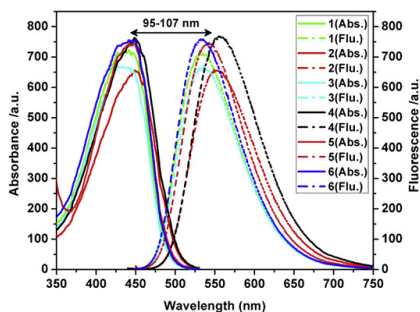


Fig. 3. The emission spectra of target compounds in CHCl<sub>3</sub>.

**Table 2**  
Electrochemical data and molecular orbital energies for final compounds.

Compounds	$E_{\text{ox}}^a$ (vs. Fc/Fc <sup>+</sup> )	$E_{\text{red}}^a$ (vs. Fc/Fc <sup>+</sup> )	$E_{\text{HOMO}}^b$ (eV vs. vacuum)	$E_{\text{LUMO}}^b$ (eV vs. vacuum)	$E_{\text{gap}}^c$ (eV)	$E_{\text{gap}}^c$ (eV)
1	0.70	-1.24	-5.50	-3.56	1.94	2.56
2	0.80	-1.27	-5.60	-3.53	2.07	2.50
3	0.76	-1.22	-5.56	-3.58	1.98	2.55
4	0.64	-1.27	-5.44	-3.53	1.91	2.50
5	0.85	-1.72	-5.65	-3.08	2.57	2.54
6	0.93	-1.21	-5.73	-3.59	2.14	2.55

<sup>a</sup>  $E_{\text{ox}}$  (vs. Fc/Fc<sup>+</sup>) =  $E_{\text{ox}}$  (vs. Ag/Ag<sup>+</sup>) - 0.43,  $E_{\text{red}}$  (vs. Fc/Fc<sup>+</sup>) =  $E_{\text{red}}$  (vs. Ag/Ag<sup>+</sup>) - 0.43.

<sup>b</sup>  $E_{\text{HOMO}} = (-4.8 - E_{\text{ox}})$ ,  $E_{\text{LUMO}} = (-4.8 - E_{\text{red}})$ .

<sup>c</sup>  $E_{\text{gap}} = E_{\text{ox}} - E_{\text{red}}$  or  $E_{\text{gap}} = E_{\text{HOMO}} - E_{\text{LUMO}}$ .

additional chain results in a slight blue shift. Compared to the benzoxadiazoles **1** and **2**, their sulfur-containing analogues **5** and **6** absorb at slightly shorter wavelengths. This blue shift in the absorption may be attributed to a slightly diminished delocalization of the lone pair on sulfur towards nitrogen due to the difference in the sizes of the participant orbitals and more polarizable nature of the sulfur.

The fluorescence spectra of the compounds show emission maxima  $\lambda_{\text{em}}$  between 535 and 555 nm. The Stokes shifts presented are in the range of 95–107 nm, which indicates only a small region of coincidence between the absorption and emission (Fig. 3). This finding indicates that re-absorption of the emitted light is almost negligible, which is very important in order to avoid undesired losses in the LED performance. The relative fluorescence efficiencies were determined in CHCl<sub>3</sub> solutions using 4,7-bis(phenylethynyl)-2,1,3-benzothiadiazole ( $\phi_f = 0.37$ ) as the standard [8]. All compounds showed moderate quantum yields ( $\phi_f = 0.27$ – $0.32$ ) with the sulfur-based compounds (**5**, **6**) being slightly more efficient.

### 3.3. Electrochemical properties

Cyclic voltammetry (CV) experiments were performed in solutions of 0.1 M tetra-*n*-butylammonium hexafluorophosphate (TBAF<sub>6</sub>) in CH<sub>2</sub>Cl<sub>2</sub> as the supporting electrolyte and the ferrocene/ferrocenium (Fc/Fc<sup>+</sup>) redox couple as an internal reference. A three-electrode cell was used, comprised of a glassy carbon electrode (GCE) as the working electrode, a platinum wire as the counter electrode and an Ag–AgCl electrode as the reference. Prior to each measurement, the cell was deoxygenated by purging with nitrogen.

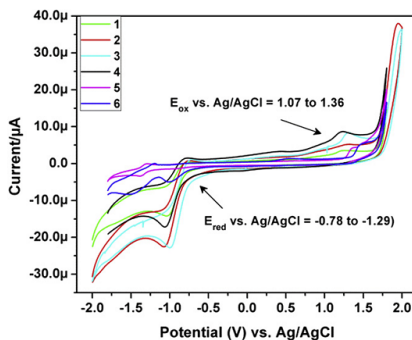


Fig. 4. Cyclic voltammograms of the target compounds vs. Ag/AgCl.

The CV results were used to investigate the redox behavior of the final compounds and to assess the HOMO and LUMO energy levels. The data are summarized in Table 2.

As can be seen in Fig. 4, all of the final compounds show single irreversible oxidation peaks between 1.07 and 1.36V vs. Ag/AgCl (0.64–0.93 vs. Fc/Fc<sup>+</sup> couple) and reduction peaks between –0.78 and –1.29 V vs. Ag/AgCl (–1.21 to –1.72 vs. Fc/Fc<sup>+</sup> couple). The potential values obtained with respect to the Fc/Fc<sup>+</sup> redox couple were converted to the vacuum scale using the standard approximation that the Fc/Fc<sup>+</sup> HOMO level is –4.8 eV [17,32]. The HOMO and LUMO energy levels of the final compounds were calculated as –5.44 to –5.73 eV and –3.08 to –3.59 eV, respectively. The electrochemical and optical band gaps were calculated as 1.91–2.57 eV and from 2.50 to 2.56 eV, respectively.

#### 4. Conclusions

In summary, six new highly conjugated compounds bearing either the 2,1,3-benzoxadiazole or 2,1,3-benzothiadiazole fluorophores as the central cores, with varying numbers of terminal alkoxy chains and alkoxy chains of different lengths on the central rings, were synthesized using Sonogashira cross-coupling as the key synthetic step. All compounds emitted in the green region of the visible spectrum and their photophysical parameters were measured. The type of central heterocycle and the alkoxy chains attached to it showed a slight influence on the absorption and emission characteristics. However, the number of terminal alkoxy chains showed a moderate effect on the absorption characteristics. These compounds possess medium fluorescence-emitting abilities with  $\phi_f$  values of 0.27–0.32 and reasonable Stokes shifts (95–107 nm). Electrochemical measurements revealed that the target compounds possess small band gaps between 1.91 and 2.57 eV.

#### Acknowledgments

We thank the following institutions for financial support: CAPES/PNPD, CNPq/PRONEX/FAPESC, INCT-Catalise and TWAS, the Academy of Sciences for the Developing World. The authors thank Dr. Haidi Fiedler from Universidade Federal de Santa Catarina (UFSC) for providing free access to the photophysical equipments and to Jorge A. Pedro for assistance in photophysical characterizations and prof. Dr. Hernán Terenzi for free access to Ion Trap mass spectrometer instrument at CEBIME-UFSC.

#### References

- Vasilopoulou M, Georgiadou D, Pistoris G, Argitis P. Tuning the emitting color of organic light emitting diodes through photochemically induced transformations: towards single layer, patterned, full color displays and white lighting applications. *Adv Func Mater* 2007;17:3477–85.
- Su SY, Lin HH, Chang CC. Dual optical responses of phenothiazine derivatives: near-IR chromophore and water-soluble fluorescent organic nanoparticles. *J Mater Chem* 2010;20:8653–8.
- Geffroy B, le Roy P, Prat C. Organic light-emitting diode (OLED) technology: materials, devices and display technologies. *Polym Int* 2006;55(6):572–82.
- Xiong L, Yu M, Cheng M, Zhang M, Zhang X, Xu C, et al. A photostable fluorescent probe for targeted imaging of tumour cells possessing integrin  $\alpha$ v $\beta$ 3. *Mol Biosyst* 2009;5(3):241–3.
- Kajiyama S, Uemura Y, Miura H, Hara K, Koumura N. Organic dyes with oligo-n-hexylthiophene for dye-sensitized solar cells. Relation between chemical structure of donor and photovoltaic performance. *Dyes Pigment* 2012;92(3):1250–6.
- Monnier V, Dubuisson E, Sanz-Mener N, Boury B, Rouessac V, Ayral A, et al. Selective chemical sensors based on fluorescent organic nanocrystals confined in sol-gel coatings of controlled porosity. *Microporous Mesoporous Mater* 2010;132(3):531–7.

- Gaughran RJ, Picard JP, Kaufman JVR. Contribution to the chemistry of benzofuran and benzofuran derivatives. *J Am Chem Soc* 1954;76(8):2233–6.
- Da Silveira Neto BA, Sant'Ana Lopes A, Ebeling G, Goncalves RS, Costa VEU, Quina FH, et al. Photophysical and electrochemical properties of  $\pi$ -extended molecular 2,1,3-benzothiadiazole. *Tetrahedron* 2005;61(46):10975–82.
- Santa T, Takeshi Fukushima, Ichibangase T, Imai K. Recent progress in the development of derivatization reagents having a benzofuran structure. *Biomed Chromatogr* 2008;22(4):343–53.
- Toyo'oka T. Indirect antiseperation by HPLC using chiral benzofuran-bearing reagents. *Methods Mol Biol* 2004;243:231–46.
- Sunmya S, Sugii T, Shiraishi Y, Hirai T. A benzoxadiazole-thiourea conjugate as a fluorescent chemodosimeter for Hg(II) in aqueous media. *J Photochem Photobiol A* 2011;219:154–8.
- Thomas KRJ, Lin JT, Velusamy M, Tao YT, Chuen CH. Color tuning in benzo [1,2,5]thiadiazole-based small molecules by amino conjugation/deconjugation: bright red-light-emitting diodes. *Adv Func Mater* 2004;14(1):83–90.
- Zhang L, Liu J, Wang L, Liu Y, Ma D. Blue amplified spontaneous emission from 2,1,3-benzothiadiazole attached polyfluorene semiconductor polymer with high photoluminescence efficiency. *J Phys D Appl Phys* 2009;42(4):045417/1–045417/4.
- Ku SY, Chi LC, Hung WY, Yang SW, Tsai TC, Wong KT, et al. High-luminescence non-doped green OLEDs based on a 9,9-diarylfuorene-terminated 2,1,3-benzothiadiazole derivative. *J Mater Chem* 2009;19(6):773–80.
- Veitza AA, Cristiano R, Bortoluzzi AJ, Gallardo H. Luminescent 2,1,3-benzothiadiazole-based liquid crystalline compounds. *J Mol Struct* 2008; 875:364–71.
- Zoombelt AP, Fonrodona M, Wienk MM, Sieval AB, Hummelin JC, Janssen RAJ. Photovoltaic performance of an Ultrasmall band gap polymer. *Org Lett* 2009; 11(4):903–6.
- Silvestri F, Marrocchi A, Serri M, Kim C, Marks TJ, Facchetti A, et al. Solution-processable low-molecular weight extended arylacetylenes: versatile p-type semiconductors for field-effect transistors and bulk heterojunction solar cells. *J Am Chem Soc* 2010;132(17):6108–23.
- Yang R, Tian R, Yan J, Zhang Y, Yang J, Hou Q, et al. Deep-red electroluminescent polymers: synthesis and characterization of new low band-gap conjugated copolymers for light-emitting diodes and photovoltaic devices. *Macromolecules* 2005;38(2):244–53.
- Sung-Yu K, Christopher DL, Daniel JB, Neil DT, Justin EC, Elizabeth A, et al. A facile synthesis of low-band-gap donor-acceptor copolymers based on dithieno[3,2-b:2'-d']thiophene. *Macromolecules* 2011;44:9533–8.
- Gallardo H, Cristiano R, Veitza AA, Neves Filho RAW, Srivastava RM, Sonogashira coupling applied in the synthesis of 1,2,4-oxadiazole based non-symmetrical liquid crystals. *Synthesis* 2008;8:605–9.
- Cristiano R, Veitza AA, Ely F, Gallardo H. Synthesis and characterization of luminescent hockey stick-shaped liquid crystalline compounds. *Liq Cryst* 2006;33(4):381–90.
- Merlo AA, Braun JE, Vasconcelos U, Ely F, Gallardo H. Chiral liquid crystalline n-nitroarols and tolans: synthesis and mesomorphic properties. *Liq Cryst* 2000;27(5):657–63.
- Grolik J, Sieron L, Eilmes J. A new liquid crystalline derivative of dibenzotetraaza[14]annulene: synthesis, characterization and the preliminary evaluation of mesomorphic properties. *Tetrahedron Lett* 2006;47:8209–13.
- Wuifman DS, Cooper CE. Monoreduction of dinitroaroes with iron/acetic acid. *Synthesis* 1978;12:924–5.
- Sonogashira K, Tohda Y, Hagihara N. A convenient synthesis of acetylenes: catalytic substitutions of acetylenic hydrogens with bromoalkenes, iodoarenes and bromopyridines. *Tetrahedron Lett* 1975;50:4467–70.
- Cui W, Zhao Y, Tian H, Xie Z, Geng Y, Wang F. Synthesis and characterizations of poly(9,10-bisarylethynyl-2,6-anthrylene)s and poly(9,10-bisalkynyl-2,6-anthrylene). *Macromolecules* 2009;42:8021–7.
- Melissaris AP, Litt MH. A simple and economic route to p-phenylaniline and ethynyl terminated substrates. *J Org Chem* 1994;59(19):5818–21.
- Bleicher L, Cosford NDP. Aryl- and heteroaryl-alkyne coupling reactions catalyzed by palladium on carbon and CuI in an aqueous medium. *Synlett* 1995;11:1115–6.
- Ma L, Hu QS, Pu L. Synthesis of an optically active poly(aryleneethynylene) containing extended conjugation in the repeat unit. *Tetrahedron, Asymmetry* 1996;7(11):3103–6.
- Tahara K, Furukawa S, Uji H, Uchino T, Ichikawa T, Zhang J, et al. Two-dimensional porous molecular networks of dehydrobenzo [12] annulene derivatives via alkyl chain interdigitation. *J Am Chem Soc* 2006;128: 16613–25.
- Bouffard J, Swager TM. Fluorescent conjugated polymers that incorporate substituted 2,1,3-benzoxadiazole and 2,1,3-benzothiadiazole units. *Macromolecules* 2008;41:5510–62.
- Wu CC, Sturm JG, Register RA, Tian J, Dana EP, Thompson ME. Efficient organic electroluminescent devices using single-layer doped polymer thin films with bipolar carrier transport abilities. *IEEE Trans Electron Devices* 1997;44(8): 1269–81.